IMPROVEMENTS TO FLUORESCENT AFFINITY LABELS AND THE RIBONUCLEASE S SYSTEM

AND

GENE EXPRESSION RESPONSE TO CLINICALLY RELEVANT RIBONUCLEASES

by

Rex Wayne Watkins

A dissertation submitted in partial fulfillment

of the requirements for the degree of

Doctor of Philosophy

(Biochemistry)

at the

UNIVERSITY OF WISCONSIN–MADISON

2010

IMPROVEMENTS TO FLUORESCENT AFFINITY LABELS AND THE RIBONUCLEASE S SYSTEM AND GENE EXPRESSION RESPONSE TO CLINICALLY RELEVANT RIBONUCLEASES

submitted to the Graduate School of the
University of Wisconsin-Madison
in partial fulfillment of the requirements for the
degree of Doctor of Philosophy

By

Rex Wayne Watkins

Date of final oral examination: 18 August 2010
Month and year degree to be awarded: August 2010

The dissertation is approved by the following members of the Final Oral Committee:
Ronald T. Raines, Professor, Biochemistry
Aseem Z. Ansari, Professor, Biochemistry
Laura L. Kiessling, Professor, Biochemistry
Douglas B. Weibel, Professor, Biochemistry
Jon S. Thorson, Professor, Pharmaceutical Sciences

IMPROVEMENTS TO FLUORESCENT AFFINITY LABELS AND THE RIBONUCLEASE S SYSTEM AND GENE EXPRESSION RESPONSE TO CLINICALLY RELEVANT RIBONUCLEASES

Rex Wayne Watkins

Under the supervision of Professor Ronald T. Raines

at the University of Wisconsin–Madison

An effective toolkit is essential in the quest to comprehend the remarkable complexities of nature and develop knowledge-based theories, models, and designs that lead to innovation and improved human conditions. Countless advances—including the development of novel chemical probes, the manipulation of model systems, and the rise of multiplex assays—have enabled important scientific discoveries. Many important scientific discoveries were made with the toolkit of the past. Increasingly, however, the frontiers of science are unexplored due to an inadequate armamentarium.

CHAPTER 1 serves as an introduction to the tools (affinity labels and protein-fragment complementation systems) and primary scientific question (cellular response to ribonuclease chemotherapeutics) addressed in this thesis.

CHAPTER 2 describes the synthesis and use of a novel fluorogenic affinity label to visualize a targeted protein in live cells. Unique features of the urea–rhodamine profluorophore facilitate rapid and specific labeling. Such fluorogenic affinity labels, which enlist catalysis by two cellular enzymes, may find utility in pulse-chase experiments, high-content screening, and other protocols.

In CHAPTER 3, we revisit the historic ribonuclease S protein-fragment complementation system. We avail ourselves of decades of experimental knowledge and technological improvements to overcome two limitations of the venerable system: the heterogeneous mixture of subtilisin-generated products and the loss of catalytic activity at low concentrations.

The gene-expression response of cancerous cells to a novel class of therapeutics is examined in CHAPTER 4. Certain pancreatic-type ribonucleases that evade the cytosolic ribonuclease inhibitor protein enter cancerous cells and destroy intracellular RNA, leading to cell death. The effects of two clinically investigated ribonucleases, onconase and QBI-139, on cancerous cells are observed by microarray analysis. The data show that the cellular response is likely due to RNA degradation. Interestingly, onconase and QBI-139 elicit remarkably different transcriptional responses, strongly suggesting that there are important differences in their mechanism of action. Furthermore, the most striking response to QBI-139 is an increase in polyadenylated histone mRNA perhaps due to an increase in *trans*-splicing.

In CHAPTER 5, I highlight several possible directions for future research. In particular I note several applications in which urea–rhodamine probes may be advantageous in labeling technologies. I also describe follow-up experiments from CHAPTER 4 that are designed help illuminate the connection between chemotherapeutic ribonucleases and chimeric RNA molecules.

Finally, in the appendix, I outline efforts to identify protein interaction partners with ribonuclease inhibitor protein.

Acknowledgements

Understandest thou what thou readest?

And he said, How can I, except some man should guide me? (Acts 8:30-31)

Mentoring is a brain to pick, an ear to listen, and a push in the right direction.

—John C. Crosby

I begin my acknowledgements with those who've been with me from the beginning—my parents—Wayne and Lynn Watkins. They have always been, and continue to be, sources of wisdom, love, encouragement, and support. They have fostered my love of learning and have demonstrated by example how to live life to the fullest.

I thank a myriad of neighbors, educators, friends, leaders, missionary companions, and family members who patiently endured me during my pre-college years and taught me invaluable skills such as optimism, hard work, diligence, and laughter.

My undergraduate advisor at Utah State University, Lisa Berreau, deserves special recognition. She is a model mentor and a wonderful friend. I count myself fortunate to begin laboratory research with someone of her enthusiasm, patience, and talent.

It has been a privilege to work in the laboratory of Ron Raines. I have benefitted greatly from his insight, experience, guidance, and professionalism. Additionally, he has assembled a fantastic scientific team. These fellow Raines lab members have become good friends and indispensable mentors. Greg Ellis deserves special recognition for tolerating me as a "baymate" on days when my experiments failed and my irritability increased.

My thesis committee—Aseem Ansari, Laura Kiessling, Doug Weibel, and Jon Thorson—has provided constructive criticism, new ideas, and encouragement.

The best science generally results from a team effort, and I certainly have had excellent collaborators and colleagues. Luke Lavis developed the synthetic methodology for the profluorescent ligand described in CHAPTER 2. He also gave excellent experimental guidance. Randy Dimond and Georgyi Los from Promega provided additional help on the same project. Uli Arnold pioneered the introduction of an enterokinase cleavage site for RNase S (CHAPTER 3). Darrell McCaslin and Gary Case assisted with instrumentation. Additionally, members from both Marv Wickens' and Sam Butcher's labs have provided technical assistance not available in our own.

Echelon Biosciences Inc. sponsored a ten-week internship for me in Salt Lake City, Utah. I greatly appreciate their kindness and the opportunity to experience research in a commercial setting.

I thank the taxpayers of the United States. I am well aware that significant federal funding has enabled both my research and stipend.

Last, and most importantly, I thank Natalie. Together we've laughed and cried. We've experienced profound joy and irksome uncertainty. She has been my best friend and confidant, and I'm lucky to be married to her. While in graduate school, our family has expanded to include two delightful little girls, Emilyn and Camilla. Natalie has sacrificed much for our family and my career. For this I will be forever grateful. I look forward to the road ahead with my best friend.

Table of Contents

List of Figures

List of Schemes and Tables

List of Abbreviations

3AT	3-Amino-1,2,4-triazole
Ala (A)	alanine
ANOVA	analysis of variance
Asp (D)	aspartic acid
Arg (R)	arginine
Boc (*t*-Boc)	*tert*-butoxycarbonyl
cDNA	complementary DNA
Cys (C)	cysteine
DEPC	diethylpyrocarbonate
DIPEA	diisopropylethylamine (Hünig's base)
DMF	dimethylformamide
DMSO	dimethylsulfoxide
DNA	deoxyribonucleic acid
dNTP	deoxyribonucleotide triphosphate
DTNB	5,5′-dithiobis(2-nitrobenzoic acid)
DTT	dithiothreitol
ε	extinction coefficient or dielectric constant
EDC	1-ethyl-3-(3-dimethylaminopropyl)carbodiimide hydrochloride
EDTA	ethylenediaminetetraacetic acid
ESI	electrospray ionization
EtOAC	ethyl acetate
FBS	fetal bovine serum

FPLC	fast performance liquid chromatography
h	hour
HCl	hydrochloric acid
HD	haloalkane dehalogenase
His (H)	histidine
HPLC	high performance (pressure) liquid chromatography
HRMS	high-resolution mass spectrometry
IC_{50}	half maximal inhibitory concentration
IPTG	isopropyl-1-thio-β-D-galactopyranoside
k_{cat}	first-order enzymatic rate constant
K_d	equilibrium dissociation constant
kDa	kilodalton
K_M	Michaelis constant
λ_{max}	maximum wavelength
LB	Luria–Bertani medium
log*D*	log of the distribution coefficient
Lys (K)	lysine
MALDI–TOF	matrix-assisted laser desorption/ionization time-of-flight
min	minute
mRNA	messenger RNA
NaCl	sodium chloride
NHS	*N*-hydroxysuccinimide
NLS	nuclear localization signal

NMR	nuclear magnetic resonance
NTB	2-nitro-5-thiobenzoate
OD	optical density
PAGE	polyacrylamide gel electrophoresis
PBS	phosphate-buffered saline
PCR	polymerase chain reaction
PDB	protein data bank
p*I*	isoelectric point
pK_a	negative log of the acid dissociation constant
qPCR	quantitative real-time PCR
RI	ribonuclease inhibitor
RMA	robust multichip average
RNA	ribonucleic acid
RNase A	bovine pancreatic ribonuclease
RNase 1	human pancreatic ribonuclease
s	second
SDS–PAGE	sodium dodecyl sulfate poly(acrylamide) gel electrophoresis
TFA	trifluoroacetic acid
THF	tetrahydrofuran
T_m	temperature at the midpoint of the denaturation curve
Tris	2-amino-2-(hydroxymethyl)-1,3-propanediol
tRNA	transfer RNA
UV	ultraviolet

Y2H	yeast two-hybrid
Z	net molecular charge (Arg + Lys – Asp – Glu for proteins)

CHAPTER 1

Introduction:

Improvements to Fluorescent Affinity Labels

and the Ribonuclease S System

and

Gene Expression Response to Clinically Relevant Ribonucleases

1.1 Overview

Life on earth is astonishingly complex. For instance, a single human cell contains approximately 10,000 unique proteins (Morón and Devi, 2007) and 300,000 mRNA molecules (Velculescu *et al.*, 1999). Making sense of this complexity requires suitable tools.

In CHAPTER 2, I present a urea–rhodamine affinity label as an important tool for the facile, rapid imaging of proteins in live cells. This fluorogenic label, together with an enzymic fusion tag, enables the specific labeling of a single protein from among the ~10,000 unique proteins in a cell. Detection instruments, such as confocal microscopy enable the investigation of protein localization, turnover, and function in a cellular context. We envision that this probe will be useful in pulse-chase experiments, and find utility in high throughput technologies such as high-content screening.

CHAPTER 3 describes improvements to a historic protein-fragment complementation system. A detailed understanding of protein structure and function requires an accessible, easily manipulable system that allows for perturbations that are not very accessible using the tools of molecular biology. The RNase S protein-fragment complementation system has for decades been the model system of choice in protein chemistry. Our improvements to this protein-fragment complementation system simplify the isolation of RNase S components and overcome difficulties inherent in studying a non-covalent complex.

Lastly, we use microarrays and amplification techniques as tools to investigate the response of cancerous cells to ribonucleases that show promise as cancer therapeutics. This multiplex experiment provides an important glimpse of the ribonuclease-induced changes that occur to the ~300,000 mRNA molecules within a cell.

In this chapter, I summarize the background that led me to each of these initiatives.

1.2 Affinity Labeling

In the 1990's, Douglas Prasher and Martin Chalfie cloned green fluorescent protein (Prasher *et al.*, 1992) from the jellyfish *Aequorea victoria* and demonstrated its use in fusion protein systems (Chalfie *et al.*, 1994). This work precipitated a rapid rise in the use of autofluorescent proteins that has revolutionized cell imaging. Common autofluorescent proteins have several advantageous features—genetic encodability for the facile generation of fusion proteins, relatively small size, high stability, and very low phototoxicity (Chalfie and Kain, 2006). These features have led to widespread adoption of autofluorescent proteins as gene reporters, and in determining the subcellular localization, dynamics, and chemical environment of many proteins (Chalfie and Kain, 2006).

Still, the use of autofluorescent proteins is limited in several respects. First, autofluorescent proteins are perpetually "on". The inability to initiate fluorescence with acute temporal control can obscure important information. Second, a single genetic construct generates only one fluorescent output. Cloning or mutagenesis is required to overcome this "one clone–one color" limitation. Furthermore, the spectral properties of autofluorescent proteins are limited, and many autofluorescent proteins suffer from other complications (Shaner *et al.*, 2005).

More recently, a variety of site-specific labeling methods have been developed for fusion tags. For instance, Roger Tsien's group has developed a system in which biarsenical membrane-permeable non-fluorescent dyes bind to and create a fluorescent

complex with proteins that have been genetically fused to the CCPGCC tetracysteine motif (Griffin *et al.*, 2000; Machleidt *et al.*, 2006).

Still others, noting the high reactivity that has evolved in enzyme active sites, have modified two-step enzyme-catalyzed reactions such that turnover is prevented due to the formation of a non-labile covalent enzyme-substrate adduct (Johnsson and Johnsson, 2007; Los and Wood, 2007). These affinity labels react rapidly and specifically with the target proteins. By appending variously ligands to the core affinity label, a single genetic construct can be used to attach the fusion protein to a solid surface or conjugate it to affinity handles or fluorescent probes.

Haloalkane dehalogenase (HD; EC 3.8.1.5) is perhaps the most oft-used enzymic fusion tag. The enzyme catalyzes the hydrolysis of haloalkanes via a covalent enzyme-substrate intermediate that undergoes hydrolysis (Figure 1.1). An HD variant that cannot perform the second, hydrolysis step (HaloTag®, Promega) reacts rapidly and specifically with a wide variety of haloalkanes to form a covalent adduct (Los *et al.*, 2008). Suitable haloalkanes include affinity handles (*e.g.*, biotin), solid supports, and fluorophores with varied spectral and physiochemical properties.

One important advantage of fluorescent affinity labeling over autofluorescent proteins is the ability to control spatially and temporally the addition of the affinity label, and thus the onset of fluorescence. This attribute is crucial for pulse-chase experiments in which temporally disparate pools of protein must be differentially labeled.

Rapid labeling permits researchers to study processes that occur on short timescales. For many labeling technologies, the chemistry between the probe and the target are primarily responsible for slow labeling. Nonetheless, for HD (with a second-order rate

constant of approximately 2.7×10^6 M^{-1} s^{-1}) (Los *et al.*, 2008), the ability of the probe to cross the membrane is often the rate-limiting step.

Many extant probes lack the membrane permeance needed for rapid labeling. In CHAPTER 2, we describe a urea–rhodamine fluorgenic affinity label with desirable membrane permeance that enables the rapid, facile labeling of fusion proteins in live cells.

We envision that this probe will provide increased temporal resolution in pulse-chase experiments and may find use in high throughput technologies, such as high-content screening.

1.3 Ribonuclease A as a model protein

Bovine pancreatic ribonuclease (RNase A, EC 3.1.27.5) is perhaps the most studied enzyme of the twentieth century. Discovered in 1920 (Jones, 1920), and first isolated in 1938 (Dubos and Thompson, 1938), RNase A attracted the attention of early protein scientists. During a hiatus of ribonuclease research due to World War II, Edwin J. Cohn of Harvard University convinced the research group at Armour, Inc. (a slaughterhouse and meatpacking company with an abundant supply of bovine pancreata) that a large quantity of purified protein was necessary for detailed study (Richards, 1997). In the early 1950's, using Moses Kunitz's procedure (Kunitz, 1939), Armour purified over 1 kg of RNase A and distributed it freely to interested scientists throughout the world.

The accessibility, purity, and remarkable stability of RNase A were a great boon to protein chemists and spawned important research in enzymology, protein structure, protein stability, and protein chemistry. In 1972, the Nobel Prize selection committee

recognized this historic work by awarding the Nobel Prize in chemistry to Chris Anfinsen (Anfinsen, 1973), Stanford Moore (Moore and Stein, 1973), and William Stein (Moore and Stein, 1973) for work on RNase A. Later, in 1984, another Nobel Prize would be awarded to Bruce Merrifield for work that also featured RNase A prominently (Merrifield, 1984).

RNase A catalyzes the cleavage of the P–$O^{5'}$ bond of RNA, preferentially cleaving RNA on the 3′-side of pyrimidine residues (Raines, 1998). The rate of cleavage of the dinucleotide UpA is maximal at pH 6.0, where $k_{cat} = 1.4 \times 10^3\ s^{-1}$ and $k_{cat}/K_M = 2.3 \times 10^6\ M^{-1}\ s^{-1}$ at 25 °C (delCardayré and Raines, 1994). This value of k_{cat} corresponds to a 3×10^{11}-fold rate enhancement over the noncatalyzed reaction (Thompson *et al.*, 1995; Raines, 1998). The active site contains two histidine residues (His12 and His 119) that facilitate acid/base catalysis in the proposed mechanism (Figure 1.2) (Findlay *et al.*, 1961) and stabilize the transition state (Figure 1.3). Alanine substitution at position 12 slows the enzyme considerably, decreasing the affinity of the enzyme for the transition state ~10^4-fold (Thompson and Raines, 1994).

Ribonuclease A is a remarkably stable enzyme (T_m = 63 °C) (Leland *et al.*, 1998) as evidenced by Kunitz's early isolation procedure that demanded integrity under harsh conditions: 0.25 N sulfuric acid at 5 °C, and then, pH 3.0 at 95–100 °C (Kunitz and McDonald, 1953). Four native disulfide bonds are key to RNase A stability, as removal of any cysteine decreases the thermal stability (Klink *et al.*, 2000). Additionally, previous work in our lab demonstrated that the introduction of a non-native disulfide bond (A4C/V118C) increased the thermal stability, and decreased the proteolytic susceptibility of an RNase A variant (Klink and Raines, 2000).

RNase A has served as a model protein system for groundbreaking research. In an effort to understand the principles that guide protein folding, Anfinsen and coworkers developed conditions (Anfinsen *et al.*, 1961) to refold RNase A after complete reduction of its four disulfide bonds and its complete denaturation (Sela *et al.*, 1957b). They discovered that although 105 possible pairings of the eight sulfhydryl groups of RNase A were possible, the protein refolded exclusively into the active conformation, suggesting that the amino acid sequence of a protein is sufficient to define its folded, active structure. This and other data led to the "thermodynamic hypothesis", which postulates that "the three-dimensional structure of a native protein in its normal physiological milieu...is the one in which the Gibbs free energy of the whole system is the lowest; that is that the native conformation is determined by the totality of interatomic interactions, and hence the amino acid sequence, in a given environment" (Anfinsen, 1973).

Around the same time, Fred Richards received a sample of ribonuclease A from Armour via Chris Anfinsen (Richards, 1997). He used the enzyme as a substrate, finding that the protease subtilisin preferentially cleaves the peptide backbone of RNase A between residues 20 and 21 (Richards, 1958). The resulting complex, RNase S (wherein "S" refers to subtilisin), is composed of two fragments: S-peptide (residues 1–20) and S-protein (residues 21–124). Separation of the two components abolishes catalytic activity, while recombination *in trans* reconstitutes catalytic activity (Richards and Vithayathil, 1959; Richards, 1992; Richards, 1997).

This protein-fragment complementation system was useful in determining structure-function relationships prior to the advent of recombinant DNA technology. Chemists synthesized S-peptide analogues, including those with nonnatural amino acids, on solid

support and then studied their complexes with S-protein (Hirschmann *et al.*, 1969; Richards *et al.*, 1970; Gutte and Merrifield, 1971; Richards and Wyckoff, 1971). This early research yielded important insights into the principles of protein structure and function. Remarkably, the initial characterization of RNase S, and the genesis of the thermodynamic hypothesis occurred before the crystal structure of either RNase A or RNase S had been solved. Soon, however, both RNase A (Kartha *et al.*, 1967) and RNase S (Wyckoff *et al.*, 1967a; Wyckoff *et al.*, 1967b) simultaneously succumbed to X-ray crystallography (Figure 1.4). Thus both have legitimate claim (Richards, 1997) as the third protein structure to be solved, after myoglobin (Kendrew and Parrish, 1956) and lysozyme (Blake *et al.*, 1965).

RNase S has continued to be a choice system for protein engineering because of several important features of the complex. The interaction between the two fragments is generally stable, and can be tuned by pH (Schreier and Baldwin, 1976), ionic strength (Schreier and Baldwin, 1977), and temperature (Hearn *et al.*, 1971). S-peptide is easily synthesized on solid support (enabling facile incorporation of nonnatural amino acids), and both fragments are soluble at physiological pH. Additionally, the topology of RNase S is such that appendages on the *N*- or *C*-termini of S-peptide do not compromise complex formation. This feature has led to the widespread adoption of the first 15 amino acid of S-peptide (which are sufficient for complex formation with S-protein) as a fusion protein tag (S-Tag®, Novagen Inc., Madison, WI) that facilitates purification (Raines *et al.*, 2000) and sensitive detection (Kim and Raines, 1993; Kim and Raines, 1994b; Raines *et al.*, 2000).

RNase S components have been commandeered further for signal amplification. For instance, attachment of S-peptide or S-protein to a solid support via a polycytidylic acid "leash" can result in $>10^4$-fold activation upon addition of the fragment complementation partner (Cecchini *et al.*, 1986; Ehrat *et al.*, 1986), a useful feature for biosensors.

Additionally, Schultz and coworkers have created a sequence-specific ribonuclease by appending an oligonucleotide to the *N*-terminal cysteine of K1C S-peptide. Treatment of a 62-mer RNA molecule with the oligonucleotide–RNase S complex resulted in cleavage at a single location (Zuckermann and Schultz, 1988).

Although the RNase S protein-fragment complementation system has been the object or historic work in protein chemistry, two limitations compromise its utility. First, the traditional preparation of S-protein by proteolytic digestion with subtilisin yields a heterogeneous mixture of products (Doscher and Hirs, 1967). Secondly, the non-covalent nature of the S-peptide/S-protein interaction leads to the loss of catalytic activity at low concentrations. In CHAPTER 3, we report on the use of site-directed mutagenesis to overcome both limitations by the insertion of an enterokinase cleavage sequence and the installation of a nonperturbative disulfide bond between S-peptide and S-protein.

1.4 Ribonucleases as chemotherapeutics

RNA polymers play an indispensible role in biological systems. RNA not only serves as an essential conduit between DNA and protein, but also functions in several enzymatic systems. Ribonucleases catalyze the depolymerization of RNA, and thus play an important role in RNA turnover. In eukaryotic cells, intracellular ribonucleases such as XRN1 and the exosome are primarily responsible for the degradation of RNA polymers

(Parker and Song, 2004). Much less is known about biological influence of members of the RNase A superfamily which comprise a distinct group of secreted proteins.

Members of the RNase A superfamily are characterized by the ability to degrade RNA, an *N*-terminal signal sequence for secretion, the presence of conserved disulfide bonds, and a kidney-shaped three-dimensional structure (Beintema, 1987; Beintema *et al.*, 1988a; Beintema *et al.*, 1988b; Beintema *et al.*, 1997; Dyer and Rosenberg, 2006). While RNase A, the prototypical family member, had been a favorite study object for decades, technological advances in the 1970's led to a decline in ribonuclease research (Benner and Alleman, 1989). The discovery of other RNase A superfamily members with interesting biological properties has, however, led to a resurgence in ribonuclease research.

A comparative genomics analysis suggests that the RNase A superfamily first evolved as a host-defense mechanism in vertebrates (Cho *et al.*, 2005). Since then, the functions of RNase A superfamily members have rapidly expanded (Cho *et al.*, 2005; Dyer and Rosenberg, 2006) to include a wide range of biological functions including angiogenesis (Riordan, 1997), tumor cell toxicity (Youle and D'Alessio, 1997), immunosuppression, and embryotoxicity (D'Alessio *et al.*, 1997).

Notably, in the early 1970's, embryo extracts from the Northern Leopard frog (*Rana pipiens*) were found to possess antitumoral activity (Shogen and Yoan, 1973). Almost twenty years later, the antitumoral activity was attributed to a basic protein with a striking similarity to RNase A, onconase (Ardelt *et al.*, 1991). Onconase is both cytostatic and cytotoxic towards many tumor cell lines (Darzynkiewicz *et al.*, 1988; Rybak *et al.*, 1996; Juan *et al.*, 1998; Halicka *et al.*, 2000; Leland *et al.*, 2000; Lee and Raines, 2003;

Rodriguez *et al.*, 2007) and, in mouse models, onconase treatment antagonizes xenograft tumor growth (Mikulski *et al.*, 1990a; Rybak *et al.*, 1996; Lee and Raines, 2003; Lee *et al.*, 2007).

In Phase I clinical trials, onconase was well tolerated, although the dose was limited by reversible renal toxicity (Mikulski *et al.*, 1993; Rodriguez *et al.*, 2007). In Phase II, onconase treatment was effective against malignant mesothelioma, pancreatic, breast, and non-small cell lung cancers (Mikulski *et al.*, 1995; Mikulski *et al.*, 2002; Costanzi *et al.*, 2005). Onconase is now in various stages of clinical trials and has been granted orphan-drug and fast-track status as a second-line therapy for patients with malignant mesothelioma. Encouragingly, onconase has shown synergy is combination with several other drugs (tamoxifen (Mikulski *et al.*, 1990b; Lee *et al.*, 2003), trifluoperazine (Mikulski *et al.*, 1990b), vincristine (Rybak *et al.*, 1996), lovastatin (Mikulski *et al.*, 1992), rosiglitazone (Ramos-Nino and Littenberg, 2008)) and proteasome inhibitors (*N*-acetyl-leucinyl-leucinyl-norleucinal and the *N*-acetyl-leucinyl-valinyl-phenylalaninal) (Mikulski *et al.*, 1998). Very recently, onconase has also shown favorable results against the dengue and SARS viruses (TAMIR, 2010).

The proposed mechanism of ribonuclease-mediated cytotoxicity is shown in Figure 1.5 (Lee and Raines, 2008). Ribonucleases bind to the cell surface and are internalized by endocytosis. Then, by a mechanism that is not well understood, ribonucleases translocate across the lipid bilayer to access the cytosol. Cytotoxic ribonucleases are then able to evade the cytosolic ribonuclease inhibitor protein and degrade intracellular RNA, leading to cell death.

The putative mechanism suggests several essential attributes of ribonucleases that elicit cytotoxic effects. First, ribonucleases must bind to the cell surface and be internalized efficiently. Second, ribonuclease must retain its three-dimensional structure (that is, have sufficient conformational stability). And most prominently, a cytotoxic ribonuclease must be able to degrade intracellular RNA in the presence of the ubiquitous ribonuclease inhibitor protein (RI) (Lee and Raines, 2008).

RI is a ubiquitously expressed ~50 kDa horseshoe-shape protein that binds to and inactivates pancreatic-type ribonucleases with 1:1 stoichiometry (Dickson *et al.*, 2005). RI has been found in all cell types studied to date, and its intracellular concentration is estimated to be a nearly invariant 4 μM (Haigis *et al.*, 2003). A broad spectrum of RNase A superfamily members, bind to RI with astounding affinity ($K_d \sim 10^{-15}$ M). Thus, RI is thought to act as an intracellular sentry to inactivate adventitiously internalized ribonucleases (Dickson *et al.*, 2005).

The most distinguishing characteristic of onconase relative to non-cytotoxic ribonucleases is its ability to retain catalytic activity in the presence of RI (Wu *et al.*, 1993; Dickson *et al.*, 2005). Inspired by onconase and bovine seminal ribonuclease (which is a dimeric ribonuclease with a quaternary structure that also evades RI (D'Alessio *et al.*, 1997)), mammalian pancreatic ribonucleases have been endowed with cytotoxic properties by disrupting their interaction with RI (Rutkoski and Raines, 2008).

Evasive mammalian ribonuclease variants, and human ribonuclease variants in particular, may possess advantageous chemotherapeutic properties. First, because enzymes with a low degree of sequence similarity tend to elicit an immune response (De Groot and Scott, 2007), mammalian ribonucleases (with greater sequence identity to the

human ribonucleases) may be less immunogenic. Still, onconase seems to be well-tolerated in a clinical setting (Pavlakis and Vogelzang, 2006). Second, onconase administration is limited by renal toxicity (Mikulski *et al.*, 1993; Pavlakis and Vogelzang, 2006). The renal retention of mammalian ribonucleases, in contrast, is 50- to 100-fold lower than that of onconase (Vasandani *et al.*, 1996). Furthermore, the catalytic efficiency of human RNase 1 is several orders of magnitude greater than that of onconase, suggesting a greater cytotoxic potential (Boix *et al.*, 1996).

Recently an RI-evasive human RNase 1 variant, QBI-139, has entered into Phase I clinical trials. Onconase and human RNase 1, of course, share the general features of the RNase A superfamily (Beintema, 1987): the ability to degrade RNA, a kidney-shaped structure with multiple disulfide bonds, and conserved catalytic residues. Additionally, both are believed to elicit cytotoxic effects through the same general mechanism (Figure 1.5). Despite these similarities, however, important differences remain.

Onconase is smaller (11.8 kDa) (Lee and Raines, 2008) and has higher thermal stability (87 °C) (Notomista *et al.*, 2000) than does human RNase 1 (~14.6 kDa, T_m = 56 °C) (Leland *et al.*, 2001), making it highly resistant to proteolysis (Notomista, 2000). This increased stability may be advantageous, enabling onconase to maintain conformation integrity during endocytosis. Human RNase 1 and onconase share only 19.4% sequence identity (33.3 % sequence similarity) (Rutkoski and Raines, 2008). Onconase also has two additional active-site residues, Lys9, and an *N*-terminal pyroglutamate that is formed by the co-translational cyclization of glutamine in the endoplasmic reticulum (Welker *et al.*, 2007).

Furthermore, the ribonucleolytic activity of onconase with common substrates is ~5 orders of magnitude lower than that of mammalian homologues (Boix *et al.*, 1996). Also, *in vitro*, onconase shows a unique preference for cleavage on the 5′ side of a guanine nucleobase (Lee *et al.*, 2008; Lee and Raines, 2008). tRNA is preferentially degraded *in cellulo* (Saxena *et al.*, 2001) (perhaps cutting between a G –G bond in the variable loop or D-arm) (Suhasini and Sirdeshmukh, 2006). Recent data supports the notion that the tRNA cleavage by onconase may be responsible for its cytotoxic effects (Mei *et al.*, 2010). Others, however, have suggested that the cytotoxic effects of onconase may be due to degradation of small RNA molecules (Zhao *et al.*, 2008).

Finally, important details differentiate the cellular entry of onconase and mammalian ribonucleases. Onconase binds to broad array of cell-surface glycans, whereas RNase A, a bovine homologue, binds only with low affinity (Chao *et al.*, 2010). Further, the internalization of mammalian ribonucleases, but not onconase, correlates with cell anionicity (Chao *et al.*, 2010), suggesting that steps downstream from internalization (*e.g.*, membrane translocation, substrate cleavage) must account for the high cytotoxicity of onconase. Moreover, it is unclear what role the increased cationicity of onconase (calculated pI > 9.5) (Ardelt *et al.*, 1991) relative to human RNase 1 (Z = +6) (Johnson *et al.*, 2007a) may play, although increased cationicity correlates with increased internalization efficiency for human RNase 1 variants (Johnson *et al.*, 2007a).

The extent to which these dissimilarities elicit different cellular responses is not well understood. In CHAPTER 4, we use microarray technology to investigate the transcriptional response of K-562 cells to clinically relevant ribonucleases.

Figure 1.1 A haloalkane dehalogenase variant that is incapable of the second hydrolysis step forms a covalent adduct with chloroalkanes (Los and Wood, 2007; Los *et al.*, 2008).

Figure 1.1

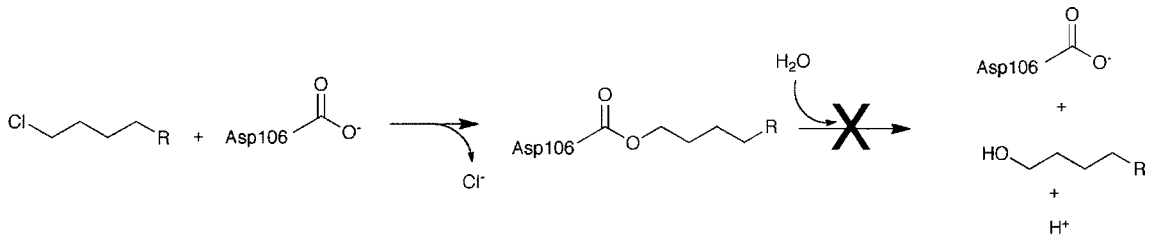

Figure 1.2 Proposed mechanism of RNase A (Findlay *et al.*, 1961).

Figure 1.2

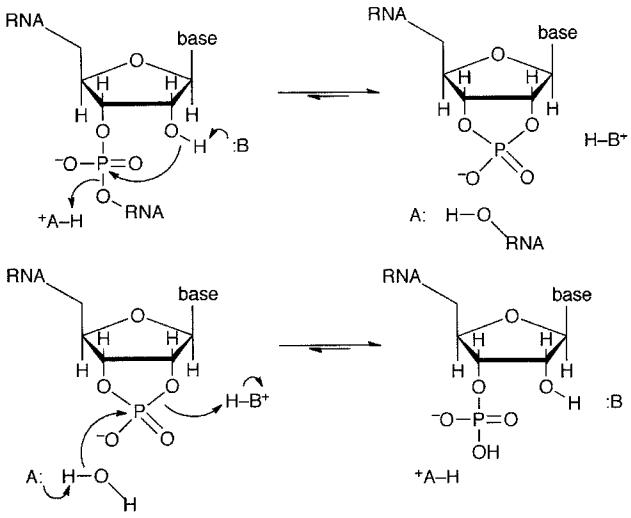

Figure 1.3 Putative transition state of the transphosphorylation step of UpA cleavage by RNase A (Raines, 1998).

Figure 1.3

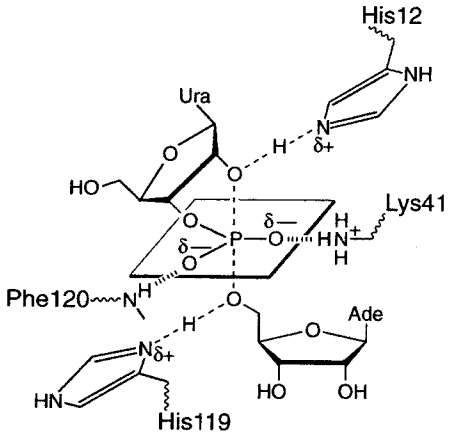
His12
NH
Ura
N
δ+
H
O
HO
O
Lys41
δ—
H
P
O
HN
δ—
O
H
Phe120
N
H
O
Ade
O
H
N
δ+
HO
OH
HN
His119

Figure 1.4 A detail of Irwin Geis' painting of ribonuclease S. A dinucleotide substrate is found in the active site. The painting was commissioned as a gift in honor of Fredric M. Richards by his students at Yale University.

Figure 1.4

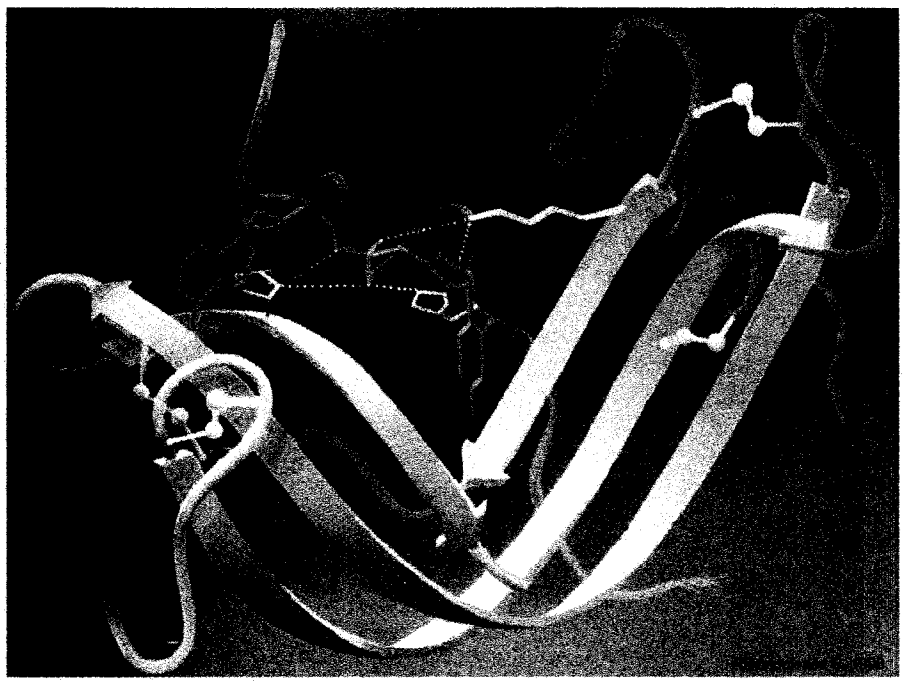

Figure 1.5 Putative routing of cytotoxic ribonucleases: cell surface binding, internalization, translocation, RI evasion, and degradation of cytosolic RNA.

Figure 1.5

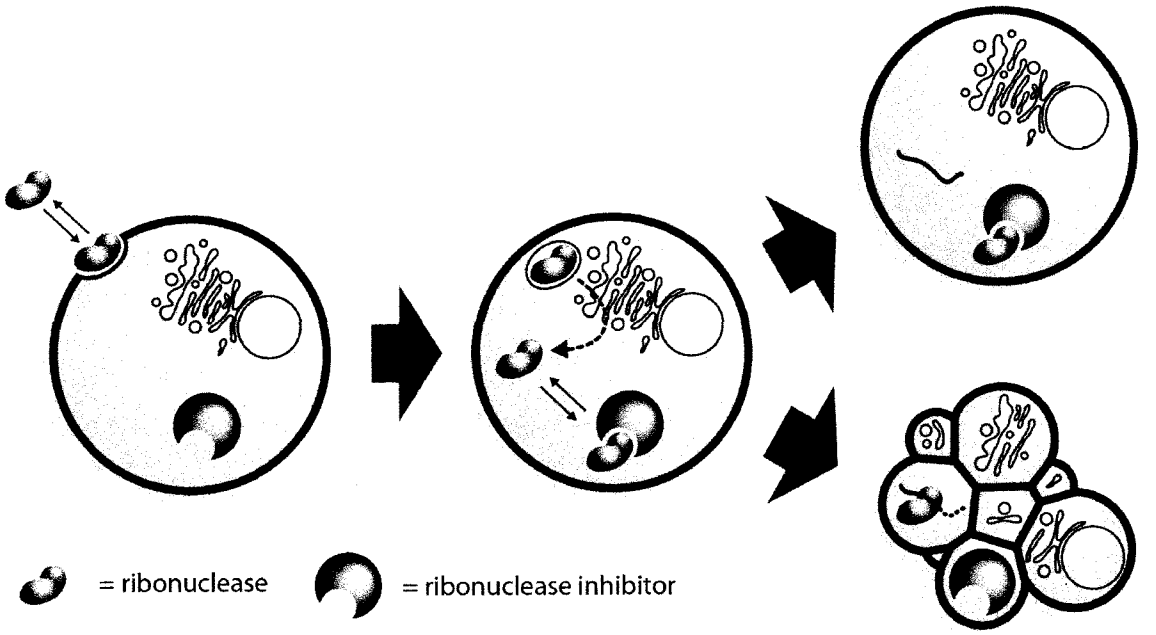

CHAPTER 2

Fluorogenic affinity label for the facile, rapid imaging of proteins in live cells

This chapter was published, in part, as:

Watkins, R.W., Lavis, L.D., Kung, V.M., Los, G.V., Raines, R.T. (2009) Fluorogenic affinity label for the facile, rapid, imaging of proteins in live cells. *Org. Biomol. Chem.* **7**, 3969-3975.

2.1 Abstract

Haloalkane dehalogenase (HD) catalyzes the hydrolysis of haloalkanes via a covalent enzyme–substrate intermediate. Fusing a target protein to an HD variant that cannot hydrolyze the intermediate enables labeling of the target protein with a haloalkane *in cellulo*. The utility of extant probes is hampered, however, by background fluorescence as well as limited membrane permeability. Here, we report on the synthesis and use of a fluorogenic affinity label that, after unmasking by an intracellular esterase, labels an HD variant *in cellulo*. Labeling is rapid and specific, as expected from the reliance upon enzymic catalysts and the high membrane permeance of the probe both before and after unmasking. Most notably, even high concentrations of the fluorogenic affinity label cause minimal background fluorescence without a need to wash the cells. We envision that such fluorogenic affinity labels, which enlist catalysis by two cellular enzymes, will find utility in pulse–chase experiments, high-content screening, and numerous other protocols.

2.2 Introduction

The labeling of proteins with genetically encoded autofluorescent proteins has revolutionized cell imaging (Tsien, 2009). These "tags" can reveal subcellular localization, dynamics, and chemical environment (Chalfie and Kain, 2006). Nonetheless, the utility of autofluorescent proteins has notable limitations, including the restriction of "one clone–one color" and an inability to label temporally disparate pools of protein by using a single genetic construct, thereby precluding pulse–chase as well as other types of experiments.

A recent development has overcome some limitations of autofluorescent proteins. Specifically, genetically encoded enzymic tags now enable the use of small-molecule fluorophores to label proteins *in cellulo* (Lavis and Raines, 2008; Los *et al.*, 2008; Johnsson, 2009). A key advantage of these systems is their modularity. With a single genetic construct, a wide variety of substrate analogs, including fluorophores with disparate spectral properties (Lavis and Raines, 2008), can be attached to a fusion protein of interest (*i.e.*, one clone–many colors) at any time. In addition, this approach avails the high reactivity that has evolved within enzymic active sites. Second-order rate constants for enzyme-mediated labeling have been reported to be as high as $2.7 \times 10^6\ M^{-1}s^{-1}$ (Los *et al.*, 2008), which exceeds by over a million-fold any rate constant reported for a chemoselective labeling reaction involving only small molecules (such as variations of the Huisgen 1,3-dipolar azide–alkyne cycloaddition or Staudinger ligation) (Soellner *et al.*, 2006; Ning *et al.*, 2008).

Haloalkane dehalogenase (HD; EC 3.8.1.5) is perhaps the most often-used enzymic fusion tag. This enzyme catalyzes the hydrolysis of haloalkanes via a covalent enzyme–substrate intermediate that undergoes hydrolysis. An HD variant that cannot perform the second, hydrolysis step (HaloTag®) reacts rapidly and specifically to form a covalent adduct with a wide variety of chloroalkanes, including assorted fluorophores of varied spectral and physiochemical properties (Los and Wood, 2007; Los *et al.*, 2008).

Still, problems remain with HD and other enzymic fusion tags. Background fluorescence from excess probe and the inefficient passage of small-molecule probes through cellular membranes are especially problematic, necessitating long incubation times or vigorous washing steps. We reasoned that a latent fluorophore based on the

venerable trimethyl lock system (Borchardt and Cohen, 1972; Milstein and Cohen, 1972) could both diminish background fluorescence and enhance cellular delivery. Accordingly, we designed and synthesized probe **1** (Figure 2.1) as an affinity label for HD and tested its ability to label HD in living cells. The results are indicative of an advantageous means to label proteins *in cellulo*.

2.3 Results and discussion

2.3.1 Design and synthesis of probe 1

The design of probe **1** was based on previous work in which the trimethyl lock system was used to mask the intrinsic fluorescence or absorbance of a small molecule (Chandran *et al.*, 2005; Huang and Lin, 2006; Lavis *et al.*, 2006a; Lavis *et al.*, 2006b; Johnson *et al.*, 2007a; Levine *et al.*, 2008; Mangold *et al.*, 2008; Yatzeck *et al.*, 2008; Turcotte *et al.*, 2009). The trimethyl lock moiety is stable to spontaneous hydrolysis, but susceptible to intracellular esterase-catalyzed hydrolysis. The use of a urea moiety rather than a second trimethyl lock allows for single-hit kinetics and the facile addition of reactive groups for bioconjugation (Lavis *et al.*, 2006a). The trimethyl lock–urea system is modular, accommodating a variety of dyes and appendages for bioconjugation.

We synthesized probe **1** by condensing two fragments: a fluorogenic substrate for a cellular esterase and a chloroalkane affinity label for HD (Scheme 2.1). Briefly, known *t*-Boc–rhodamine **4** was subjected to reaction with an *in situ*-generated isocyanate from protected succinate **5** (Winkler *et al.*, 2004) to generate *t*-Boc–rhodamine–urea **6**. Deprotection with trifluoroacetic acid furnished the urea–rhodamine **7** that underwent

carbodiimide-mediated coupling with trimethyl lock acid **8** (Amsberry and Borchardt, 1990) to give benzyl-protected **9**. Removal of the benzyl group by catalytic hydrogenation at –5 °C (Zaikova *et al.*, 2001) afforded acid **10**. Activation of the acid to the succimidyl ester, followed by reaction with alkyl chloride **11** gave the desired probe **1**.

2.3.2 Cell imaging with probe 1

We compared the utility of probe **1** for live-cell imaging with that of known probes **2** (diAcFAM) and **3** (R110Direct™). In these experiments, we used a cell line, U2OS, that had been stably transfected to produce a nucleus-directed HD variant (HaloTag®–NLS_3). The nuclear envelope is covered with pores that allow small molecules such as probes **1**–**3** to enter the nucleus by passive diffusion from the cytosol (Monnè, 1935).

We found that images of U2OS cells exposed to probes **1**–**3** differed significantly. Incubation of cells with probes **2** and **3** resulted in non-specific fluorescence after 15 min (Figure 2.1A). This unsolicited fluorescence was intracellular for **2** and extracellular for **3**. In contrast, probe **1** showed remarkable specificity with virtually no background fluorescence. Additionally, imaging with **1** was strikingly rapid, as images had developed nearly fully after only 10 min (Figure 2.1B). Labeling with a ten-fold higher concentration of **1** retained specificity without a large increase in background fluorescence (Figure 2.1C).

We suspected that the variation in labeling between the fluorogenic affinity labels **1** and **2** is due to differing abilities of the masked and unmasked probes to cross the cell membrane. Although masked **1** and **2** have a net charge of $Z = 0$, unmasked **1** has $Z = 0$

whereas unmasked **2** has $Z = -2$. Cell images suggest that unmasked **2** that has not reacted with the HD variant becomes trapped in the cell, leading to intracellular background fluorescence (Figure 2.1A*ii* and *v*). Conversely, unmasked **1** that has not reacted with the HD variant can exude from the cell, leading to low background fluorescence.

The low background fluorescence observed with probe **1** could be attributed solely to the latency of its fluorescence. To address this issue, we treated probes **1** and **2** with porcine liver esterase prior to the no-wash labeling procedure. As anticipated from its net charge of $Z = -2$, unmasked **2** was largely membrane impermeant (Figure 2.1D*ii*). Remarkably, unmasked **1** (Figure 2.1D*i*) displayed much less intracellular and extracellular background fluorescence than did **3** (Figure 2.1D*iii*). These data demonstrate that the fluorescence-masking trimethyl lock moiety is not the singular determinant for preventing extracellular background fluorescence. Rather, the intrinsic cell-permeability of probe **1**, in its masked and unmasked state, plays an important role.

2.3.3 Probe lipophilicity

To seek an explanation for the differences in probe internalization, we first calculated the value of log*D* for the predominant form of relevant labels at pH 7.4 (Table 2.1). Because increased lipophilicity generally correlates with increased membrane permeability, probes with higher log*D* values are expected to permeate the membrane more rapidly. The relatively low calculated log*D* value of unmasked **2** corresponds with its slower rate of internalization. There is, however, only a small difference between the

calculated values of unmasked **1** and **3**, even though cell-imaging experiments demonstrate that unmasked **1** is much more membrane permeant (Figure 2.1D).

The inconsistency in the anticipated and demonstrated membrane permeability led us to hypothesize that the increased rate of internalization of unmasked **1** relative to **3** is due to perturbation of the lactone–quinoid equilibrium of the two rhodamine-based dyes (Lavis *et al.*, 2006a) (Figure 2.3). We reasoned that electron-withdrawal by the urea moiety shifts the equilibrium somewhat from the relatively membrane-impermeant quinoid (which is zwitterionic and hence polar) to the lactone.

To investigate the propensity of rhodamine–urea dyes to form the lactone, we determined the effect of solvent dielectric constant (ε) on the lactone–quinoid equilibrium of unmasked **1** and related compounds **12** (rhodamine 110) and **13** (a rhodamine–urea) (Lavis *et al.*, 2006a). The ultraviolet–visible spectrum of the quinoid is characterized by a relative absorbance maximum at ~500 nm, which is absent in the spectrum of the lactone (Ioffe and Otten, 1965). The value of ε was varied by altering dioxane/water ratios (Kuila and Lahiri, 2004). We found that formation of the less polar lactones of unmasked **1** and **13**, which contain a urea moiety, is favorable in solutions of higher polarity than with compound **12** (Figure 2.4). We conclude that the increased rate of internalization of rhodamine–urea dyes is likely due to their increased propensity for lactone formation. This feature ameliorates the difficulty of cell-membrane penetration and lowers background fluorescence.

2.3.4 Recapitulation

Together, the data indicate that probe **3**, which is always fluorescent, is not especially membrane-permeant and produces much extracellular, background fluorescence with our rapid-imaging protocol (Figure 2.1A, panels *iii* and *vi*). Although the acetyl groups of probe **2** mask its fluorescence, these groups are vulnerable to hydrolysis in cell-free medium and even PBS (Lavis *et al.*, 2006a). At short time scales (*i.e.*, minutes), the resultant unmasking is not a severe problem. The intracellular background is due to the anionic unmasked fluor that has not reacted with the HD protein but cannot exit the cell because of its membrane impermeance. Only probe **1** has the attributes necessary.

2.4 Conclusions

We have demonstrated that probe **1** is a useful cell-permeant affinity label for the facile, rapid labeling of target proteins in live cells. The omission of wash steps is particularly advantageous for the labeling of proteins in non-adherent cells, which are more tedious to separate from excess probe than are adherent cells. In addition, as probe **1** exhibits low background fluorescence, little effort is needed to determine a useful concentration. This attribute could be useful for the labeling of target proteins within a population of transiently transfected cells. The rapidity of cellular labeling with probe **1** enables interrogations with high temporal resolution. This attribute is particularly beneficial for pulse–chase experiments, which require differential labeling of temporally disparate pools of protein. Finally, we suspect that probe **1** will be useful in high-content screens, wherein wash steps, optimization of label concentration, and probe instability are especially problematic and costly. Accordingly, we envision that probe **1** and analogous

fluorogenic affinity labels will be a useful addition to the armamentarium for the labeling of proteins *in cellulo*.

2.5 Experimental

2.5.1 Synthesis of ***1***

General. Amine **11** was a generous gift from the Promega Corporation (Madison, WI). Dimethylformamide (DMF), tetrahydrofuran (THF), and dichloromethane (CH_2Cl_2) were drawn from a Baker CYCLE-TAINER solvent delivery system. All other reagents were obtained from Sigma (Saint Louis, MO) or Fisher Scientific (Hanover Park, IL) and used without further purification.

Thin-layer chromatography was performed with aluminum-backed plates coated with silica gel containing F_{254} phosphor and visualized by UV illumination or staining with I_2, ceric ammonium molybdate, or phosphomolybdic acid. Flash chromatography was performed by using open columns loaded with silica gel-60 (230–400 mesh), or on a FlashMaster Solo system (Argonaut, Redwood City, CA) with Isolute Flash Si II columns (International Sorbent Technology, Hengoed, Mid Glamorgan, UK). The term "concentrated under reduced pressure" refers to the removal of solvents and other volatile materials using a rotary evaporator at water-aspirator pressure (<20 mm Hg) while maintaining the water-bath temperature below 40 °C. The term "high vacuum" refers to vacuum achieved by a mechanical belt-drive oil pump.

NMR spectra were obtained with a Bruker DMX-400 Avance spectrometer at the National Magnetic Resonance Facility at Madison (NMRFAM). Mass spectrometry was

performed with a Micromass LCT (electrospray ionization, ESI) mass spectrometer in the Mass Spectrometry Facility in the Department of Chemistry.

Synthesis of succinic acid monobenzyl ester (**5**). Compound **5** was synthesized according to a published procedure (Winkler *et al.*, 2004). The white crystalline material afforded in the published procedure was dissolved in a minimal amount of 1:1 hexanes/EtOAc and cooled to 4 °C. Crystallization was initiated by the dropwise addition of hexane (~20 drops). The mixture was stored overnight at –20 °C. The crystals were isolated by filtration, washed with cold hexane (4 °C), and dried in the air. Residual solvent was removed under high vacuum to yield compound **5** as a white crystalline solid (3.44 g, 83%). ^{1}H NMR (400 MHz, DMSO-d_6) δ (ppm): 12.25 (s, 1H), 7.36 (m, 5H), 5.10 (s, 2H), 2.58 (m, 2H), 2.50 (m, 2H). ^{13}C NMR (400 MHz, DMSO-d_6) δ (ppm): 173.47, 172.10, 136.25, 128.45, 128.00, 127.84, 65.53, 28.78, 28.72. HRMS (ESI): $[M+Na]^+$ calculated, 231.0628; found, 231.0635.

Synthesis of t-Boc–rhodamine–urea ***6***. Succinic acid monobenzyl ester (**5**; 193 mg, 0.929 mmol) was dissolved in anhydrous THF (2.0 mL) under Ar(g). Hünig's base (DIEA; 202 μL, 1.16 mmol) was then added, followed by the dropwise addition of diphenyl phosphoryl azide (DPPA; 256 mg, 0.929 mmol). The solution was stirred for 6 h and subsequently heated at reflux for an additional 2 h. Then, known *t*-Boc–rhodamine **4** (100 mg, 0.232 mmol) was added, and the reaction mixture was stirred at reflux for 18 h. The reaction mixture was then partitioned between 5% v/v HCl(aq) and CH_2Cl_2. The organic extract was washed consecutively with 5% v/v HCl, water (3×), 5% w/v $NaHCO_3$(aq) (2×), water (3×), and saturated brine, and dried over $MgSO_4$(s). The solution was concentrated under reduced pressure, and the residue was purified by

column chromatography (silica gel; first column: 5:3:2 hexanes/EtOAc/CH_2Cl_2→4:4:2 hexanes/EtOAc/CH_2Cl_2, second column: 0→2% v/v MeOH in CH_2Cl_2 containing AcOH (1% v/v), third column: 5:3:2 hexanes/EtOAc/CH_2Cl_2). Compound **6** was obtained as a pale yellow solid (137.2 mg, 93%). ^{1}H NMR (400 MHz, $CDCl_3$) δ (ppm): 7.99 (d, J = 7.0 Hz, 1H), 7.65–7.56 (m, 3H), 7.37–7.29 (m, 6H), 7.10 (s, 1H), 7.06 (m, 3H), 6.99 (d, J = 8.4 Hz, 1H), 6.66 (d, J = 8.6 Hz, 1H), 6.55 (d, J = 8.7 Hz, 1H), 6.00 (t, J = 5.6 Hz, 1H), 5.11 (s, 2H), 3.53 (dd, J = 11.5, 5.7 Hz, 2H), 2.62 (t, J = 6.1 Hz, 2H), 1.52 (s, 9H). ^{13}C NMR (400 MHz, $CDCl_3$) δ (ppm): 172.42, 170.12, 155.20, 152.59, 151.98, 151.82, 142.15, 141.21, 135.67, 135.25, 129.82, 128.57, 128.28, 128.18, 126.32, 125.29, 124.34, 115.40, 114.41, 112.91, 112.17, 106.34, 106.15, 81.17, 66.47, 35.71, 34.76, 28.33. HRMS (ESI): $[M+H]^+$ calculated, 636.2341; found, 636.2341.

Synthesis of rhodamine–urea 7. *t*-Boc–rhodamine–urea **6** (54.0 mg, 0.0848 mmol) was dissolved in CH_2Cl_2 (2.0 mL). Trifluoroacetic acid (TFA, 400 μL) was added, and the reaction mixture was stirred at 0 °C for 2 h. The reaction mixture was then allowed to warm to ambient temperature and stirred for an additional 3 h. The solution was concentrated under reduced pressure, and residual TFA was removed by azeotropic distillation with toluene. The residue was then dissolved in a minimal amount of acetone and purified by column chromatography (silica gel, 5→10% v/v MeOH:CH_2Cl_2) to afford compound **7** as an orange crystalline solid (40 mg, 88%). ^{1}H NMR (400 MHz, acetone-d_6) δ (ppm): 8.34 (s, 1H), 7.97 (d, J = 7.6 Hz, 1H), 7.81–7.76 (m, 2H), 7.70 (t, J = 7.1 Hz, 1H), 7.39–7.25 (m, 6H), 6.92 (dd, J = 8.6, 2.2 Hz, 1H), 6.61 (d, J = 8.6 Hz, 1H), 6.58 (d, J = 2.1 Hz, 1H), 6.47 (d, J = 8.5 Hz, 1H), 6.42 (dd, J = 8.5, 2.1 Hz, 1H),

6.09 (br, 1H), 5.14 (m, 2H), 3.50 (q, J = 6.3 Hz, 2H), 2.63 (t, J = 6.5 Hz, 2H), 2.09 (s, 2H). HRMS (ESI): $[M+H]^+$ calculated, 536.1822; found, 536.1816.

Synthesis of trimethyl lock–rhodamine–urea **9**. Compound **7** (39.0 mg, 0.0728 mmol) was dissolved in 2.0 mL DMF and 2.0 mL pyridine. Trimethyl lock acid **8** (Amsberry and Borchardt, 1990) (38.5 mg, 0.146 mmol) and 1-ethyl-3-(3-dimethylaminopropyl)carbodiimide (EDC; 28 mg, 0.146 mmol) were then added, and the reaction mixture was stirred overnight at ambient temperature. The solution was concentrated under reduced pressure, and the residue was dissolved in CH_2Cl_2 (200 mL). The resulting solution was washed consecutively with 5% v/v HCl(aq), water, saturated $NaHCO_3$(aq), and saturated brine. The organic fraction was dried over Na_2SO_4(s). The residue was purified by column chromatography (silica gel, 4:6→5:5 hexanes/EtOAc) to give compound **9** as an orange solid (46 mg, 81%). ^{1}H NMR (400 MHz, $CDCl_3$) δ (ppm): 7.98 (d, J = 7.3 Hz, 1H), 7.66–7.56 (m, 3H), 7.38 (s, 1H), 7.32 (s, 5H), 7.20 (s, 1H), 7.06–7.02 (m, 3H), 6.80 (s, 1H), 6.67–6.61 (m, 2H), 6.57–6.53 (m, 2H), 5.74 (t, J = 5.7 Hz, 1H), 5.12 (s, 2H), 3.57–3.50 (m, 2H), 2.63–2.61 (m, 4H), 2.43 (s, 3H), 2.37 (s, 3H), 2.21 (s, 3H), 1.69–1.67 (m, 6H). ^{13}C NMR (400 MHz, $CDCl_3$) δ (ppm): 172.40, 171.96, 170.39, 170.24, 155.18, 153.15, 151.48, 149.97, 141.74, 139.91, 138.85, 137.18, 135.70, 135.31, 133.13, 132.96, 129.75, 128.55, 128.25, 128.13, 126.18, 124.90, 124.10, 123.42, 115.32, 114.93, 113.70, 111.65, 107.66, 106.22, 83.74, 66.38, 50.81, 40.25, 35.60, 34.77, 32.02, 25.53, 21.93, 20.16. HRMS (ESI): $[M+H]^+$ calculated, 782.3073; found, 782.3062.

Synthesis of trimethyl lock–rhodamine–urea ***10***. Ethanol (10 mL) was added to compound **9** (35 mg, 0.045 mmol) and Pd/C (10% w/w, 14 mg) at −5 °C. The resulting mixture was stirred under an H_2(g) atmosphere for 30 min. The reaction mixture was

filtered through celite and washed consecutively with CH_2Cl_2 and EtOH. The washings were combined and concentrated under reduced pressure. The residue was then adsorbed onto celite and purified by column chromatography (silica gel, 0→10% v/v MeOH in CH_2Cl_2 containing 1% v/v AcOH) to afford compound **10** as a pale-yellow solid (26 mg, 84%). ^{1}H NMR (400 MHz, $CDCl_3$) δ (ppm): 8.00–7.90 (m, 2H), 7.84 (s, 1H), 7.59–7.49 (m, 2H), 7.34 (s, 1H), 7.22 (s, 1H), 6.95 (d, J = 7.3 Hz, 1H), 6.81 (d, J = 7.2 Hz, 1H), 6.74 (s, 1H), 6.64–6.55 (m, 2H), 6.53–6.42 (m, 2H), 6.10 (b, 1H), 3.39 (s, 2H), 2.62 (s, 2H), 2.46 (s, 2H), 2.39 (s, 3H), 2.32 (s, 3H), 2.16 (s, 3H), 1.63 (s, 6H). ^{13}C NMR (400 MHz, $CDCl_3$) δ (ppm): 176.38, 171.97, 170.60, 170.04, 155.88, 152.83, 151.52, 151.48, 149.89, 141.58, 139.74, 138.76, 137.08, 135.31, 133.03, 132.93, 129.77, 128.00, 126.17, 124.87, 124.03, 123.35, 115.45, 114.93, 113.94, 111.88, 107.83, 106.40, 83.66, 50.65, 40.17, 35.53, 34.76, 32.00, 25.48, 21.88, 20.12. HRMS (ESI): $[M+Na]^+$ calculated, 714.2422; found, 714.2396.

*Synthesis of probe **1**.* Compound **10** (26 mg, 0.038 mmol) was dissolved in DMF (1.0 mL) and pyridine (1.0 mL each). EDC (22 mg, 0.113 mmol) was added, and the resulting mixture was stirred for 1 h. *N*-Hydroxysuccinimide (NHS; 13 mg, 0.113 mmol) was then added, and the reaction mixture was stirred for 36 h under Ar(g). The solution was concentrated under reduced pressure, and the residue was partitioned between 10% w/v citric acid(aq) and CH_2Cl_2. The layers were separated, and the aqueous layer was extracted with CH_2Cl_2. The organic extracts were combined, washed consecutively with water and saturated brine, and dried over Na_2SO_4(s) to give the crude succinimide intermediate as a pale-yellow solid (35 mg). This intermediate (35 mg) was then dissolved in 2.0 mL of 9:1 DMF/DIEA. Amine **11** (10 mg, 0.044) was added, and the

reaction mixture was stirred under Ar(g) for 72 h. The solution was concentrated under reduced pressure, and the residue was partitioned between EtOAc and 6% v/v HCl(aq). The layers were separated, and the aqueous phase was extracted with EtOAc. The organic extracts were combined, washed consecutively with water and saturated brine, and dried over Na_2SO_4(s). Probe **1** was isolated by column chromatography (silica gel; first column: 5:3:2 hexanes/EtOAc/CH_2Cl_2, second column: 2% v/v MeOH in CH_2Cl_2) as an off-white solid (12.5 mg, 32%). ^{1}H NMR (400 MHz, $CDCl_3$) δ (ppm): 7.98 (d, J = 6.5 Hz, 1H), 7.87 (s, 1H), 7.60 (dt, J = 4.3, 1.4 Hz, 2H), 7.46 (s, 1H), 7.39 (dd, J = 10.3, 2.2 Hz, 2H), 7.09 (d, J = 7.3 Hz, 1H), 6.97 (dd, J = 8.6, 2.2 Hz, 1H), 6.79 (s, 1H), 6.62–6.52 (m, 4H), 6.17 (br, 1H), 5.80 (br, 1H), 3.62 (s, 4H), 3.53–3.45 (m, 10H), 2.56 (m, 2H), 2.42 (m, 5H), 2.38 (s, 3H), 2.23 (s, 3H), 1.75–1.64 (m, 8H), 1.63–1.54 (m, 2H), 1.46–1.26 (m, 4H). HRMS (ESI): $[M+Na]^+$ calculated, 919.3656; found, 919.3617.

2.5.2 Cell imaging

General. Probe **2** and U2OS cells were generous gifts from Promega. Probe **3** was from Promega. Rhodamine 110 was from Sigma–Aldrich. Cell-culture medium was from Invitrogen or Hyclone (Fisher Scientific). Dulbecco's phosphate-buffered saline (PBS) and fetal bovine serum were from Invitrogen. Porcine liver esterase, MW ~163 kDa, as a suspension in 3.2 M $(NH_4)_2SO_4$ was from Sigma Chemical (product number E2884). For labeling experiments, fluorogenic and fluorescent probes were stored as stock concentrations in DMSO and diluted such that DMSO concentration did not exceed 1%. Absorbance measurements were recorded at ambient temperature (23 ± 2 °C) in 1-cm path-length cuvettes on a Cary model 50 spectrometer from Varian.

Cell Preparation. U2OS cells (ATCC HTB-96TM) were plated on glass-bottom culture dishes (35 × 10 mm; Electron Microscopy Sciences) and grown to 60–90% confluence at 37 °C in McCoy's 5A modified media containing FBS (10% v/v). Prior to the addition of probes, the medium was replaced with phenol red-free McCoy's 5A medium (800 μL) that had been incubated at 37 °C. Probes were dissolved at a 5× working concentration in phenol red-free medium (200 μL) that had been incubated at 37 °C. For the experiments with unmasked probes (Figure 2.1D), porcine liver esterase (10 μL, 1.66 U/μL) was then added, and the resulting medium was incubated at room temperature for 3½ h. The probe-containing medium was added to the cell-containing medium, and the resulting medium was incubated at 37 °C. Cells were visualized by confocal microscopy after 10, 15, or 30 min.

Microscopy. Images of cells were obtained with a Nikon Eclipse TE2000-U confocal microscope equipped with a Zeiss AxioCam digital camera. Excitation at 488 nm was provided by an argon-ion laser, and emission light was passed through a filter centered at 515 nm and having a 40-nm band-pass. Brightfield images indicated that the cells were alive and appeared to have normal physiology, both before and after imaging.

2.5.3 Ultraviolet–visible spectroscopy

For each measurement, a probe was initially added to 20 μL PBS. To unmask the fluorescence of **1**, porcine liver esterase (3.0 μL, 1.66 U/μL) was added, and the solution was left at ambient temperature for 4 h. Then, varying ratios of water and dioxane were added to a final volume of 200 μL, and absorbance was measured from 400–600 nm.

*2.5.4 Calculation of log*D

The parameter log*D* refers to the ratio of concentration of all probe microspecies (including both ionized and neutral forms) in octanol to that in water, according to eq 1 (van de Waterbeemd, 2009):

$$\log D = \log\left(\frac{\sum[\text{microspecies}]_{\text{octanol}}}{\sum[\text{microspecies}]_{\text{water}}}\right) \quad (1)$$

Values of log*D* were calculated with ACD/PhysChem Suite, version 12 (ACD, 2009). Parameters of fluorescein (pK_a 6.32 (Goldberg and Baldwin, 1998); log*D* –0.99 (Cheruvu and Kompella, 2006)) and rhodamine 110 (log*D* 0.8) (Lampidis *et al.*, 1989) were entered into the software training database.

2.5.5 NMR spectra

400 MHz ^{1}H NMR spectrum of compound **5** in DMSO-d_6.

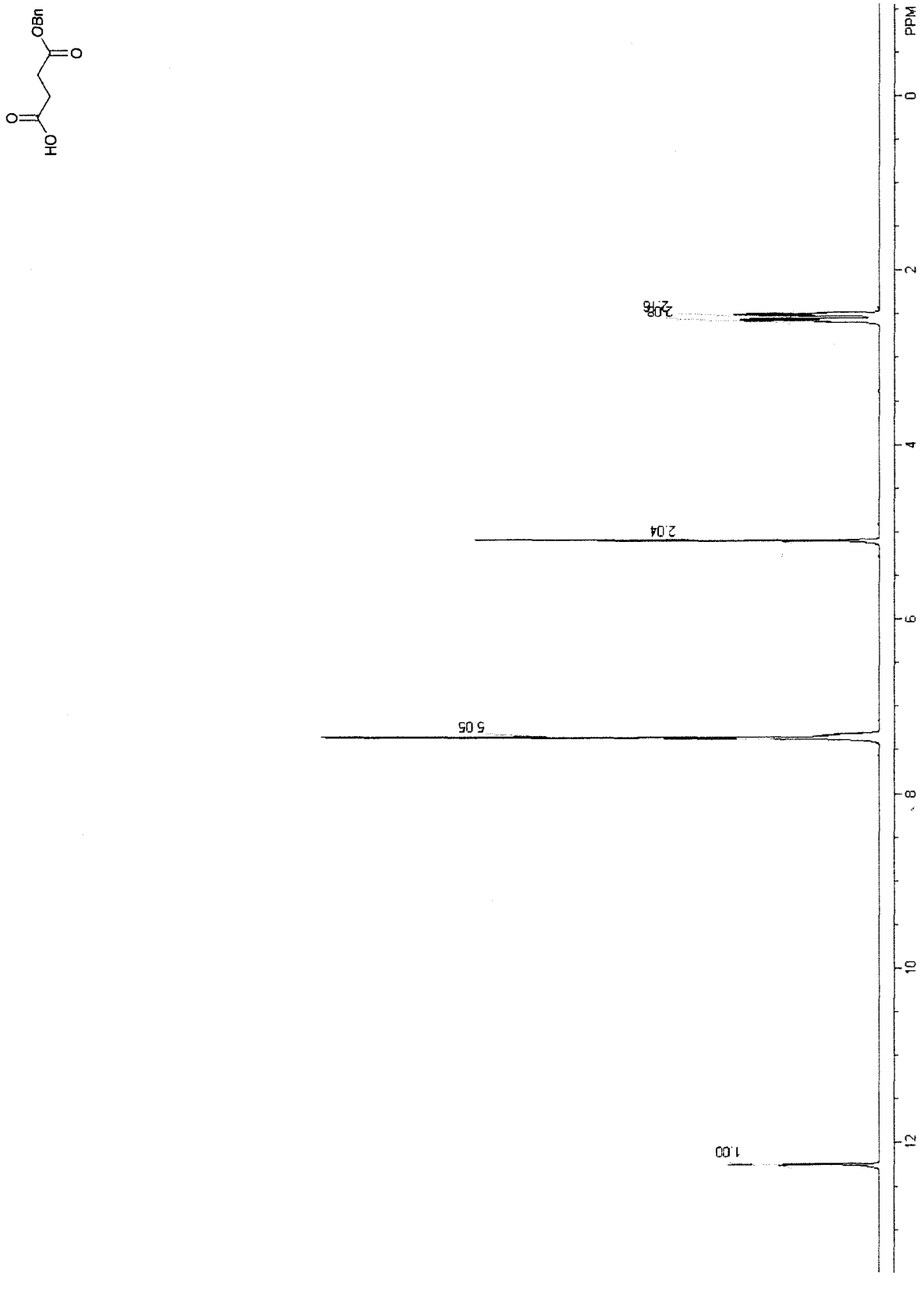

400 MHz ^{13}C NMR spectrum of compound **5** in DMSO-d_6.

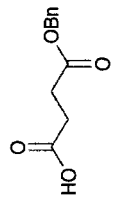

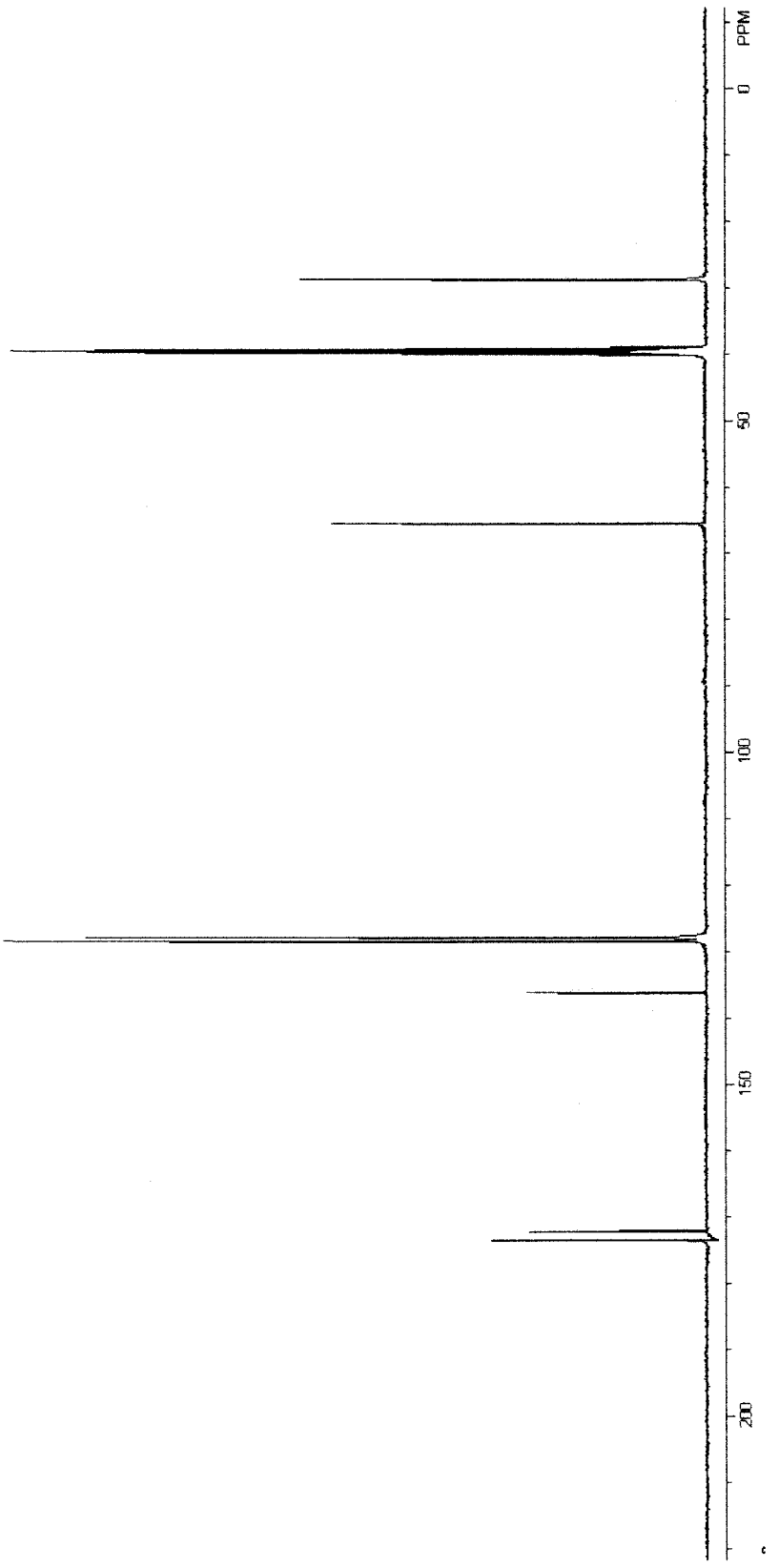

400 MHz ^{1}H NMR spectrum of compound **6** in $CDCl_3$.

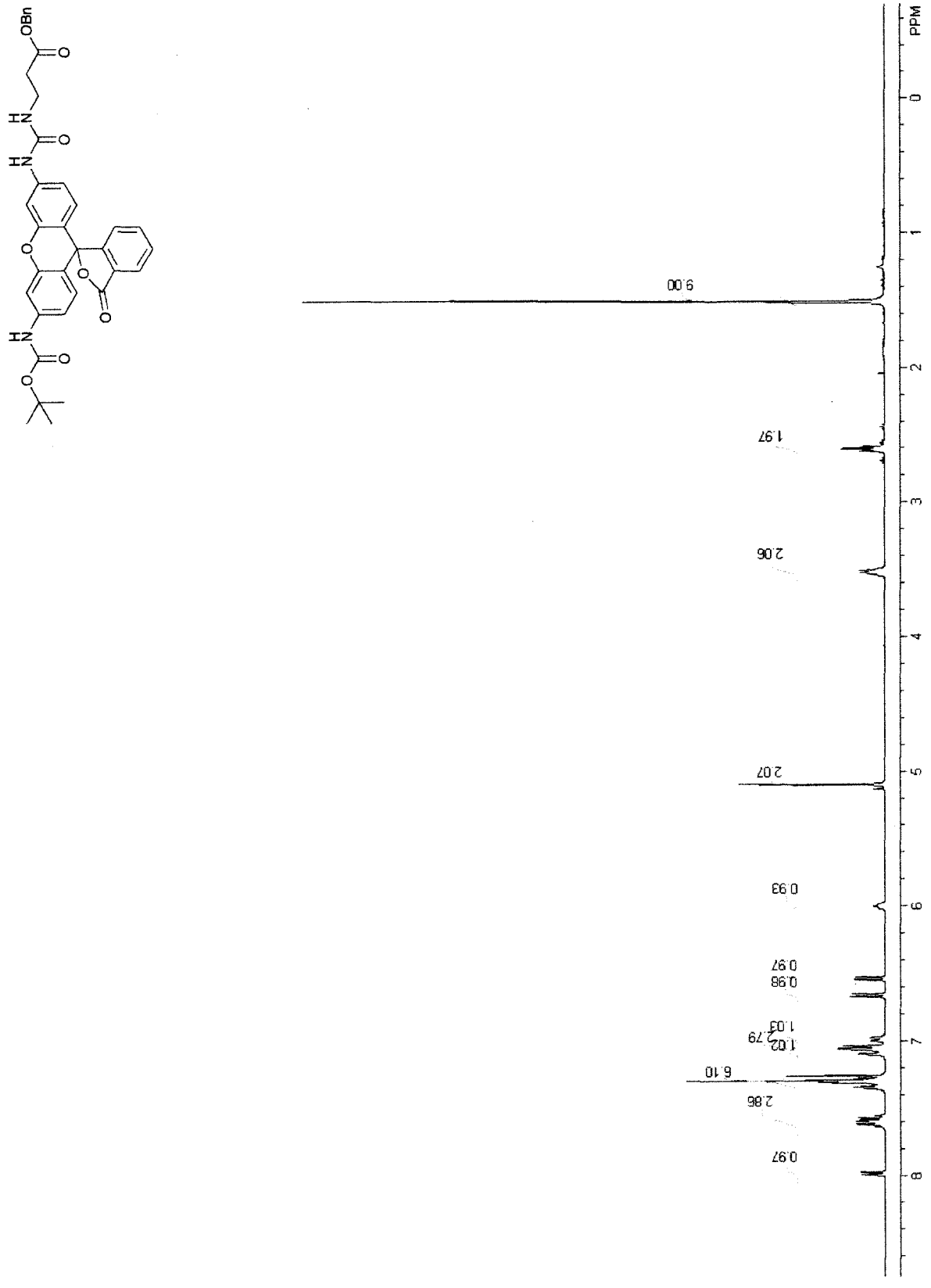

400 MHz ^{13}C NMR spectrum of compound **6** in $CDCl_3$.

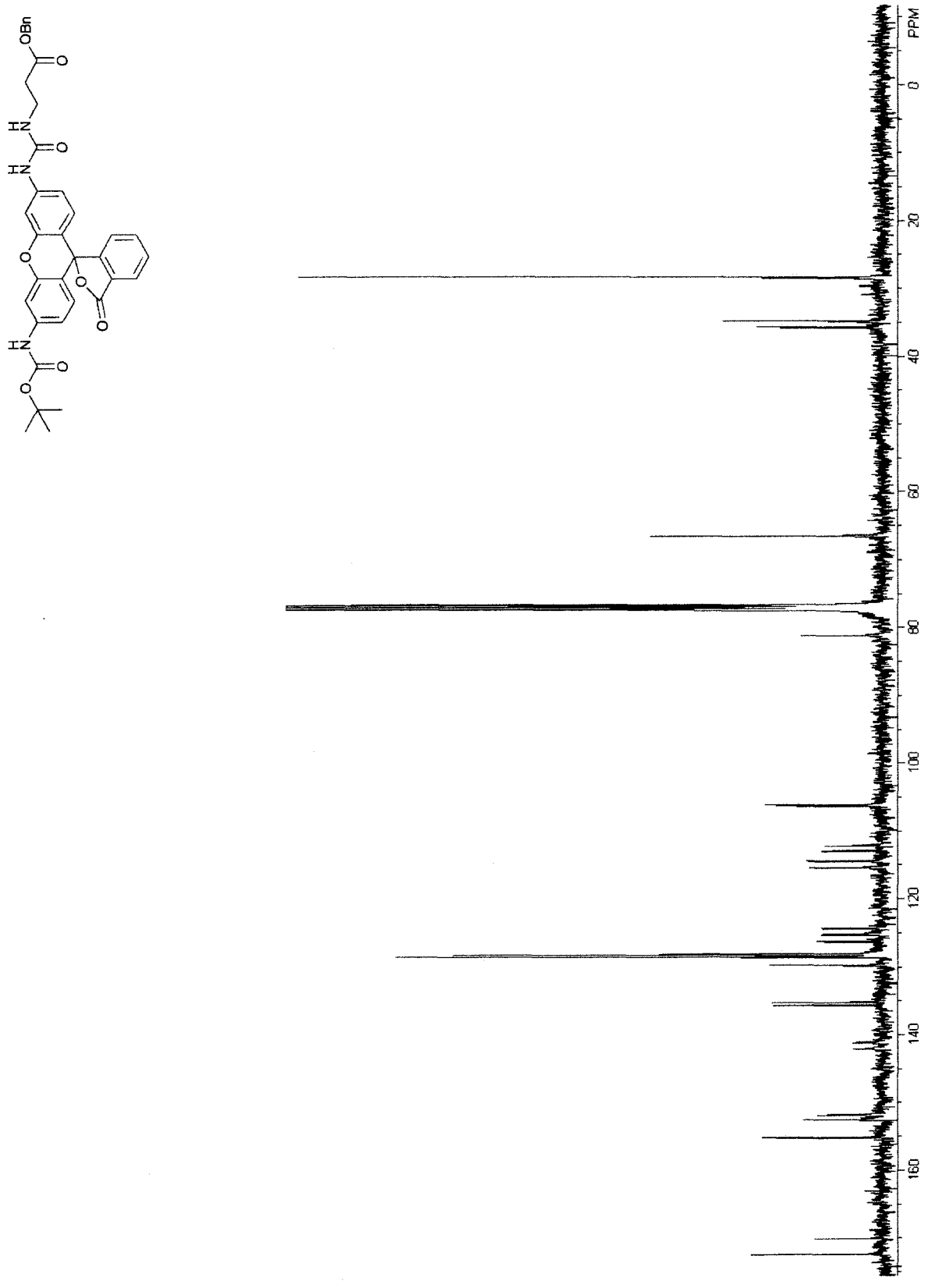

400 MHz ^{1}H NMR spectrum of compound **7** in acetone-d_6.

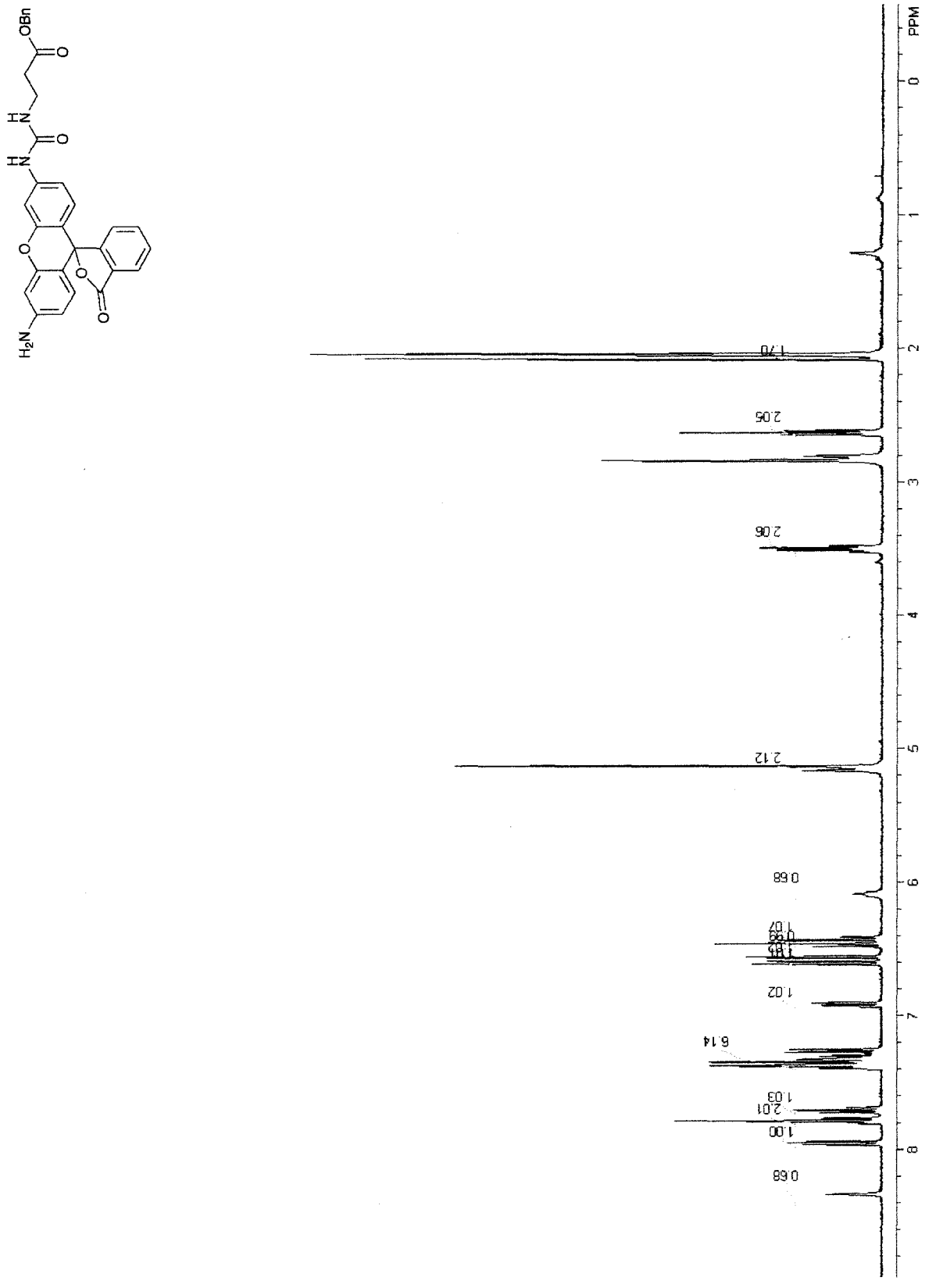

400 MHz ^{1}H NMR spectrum of compound **9** in $CDCl_3$.

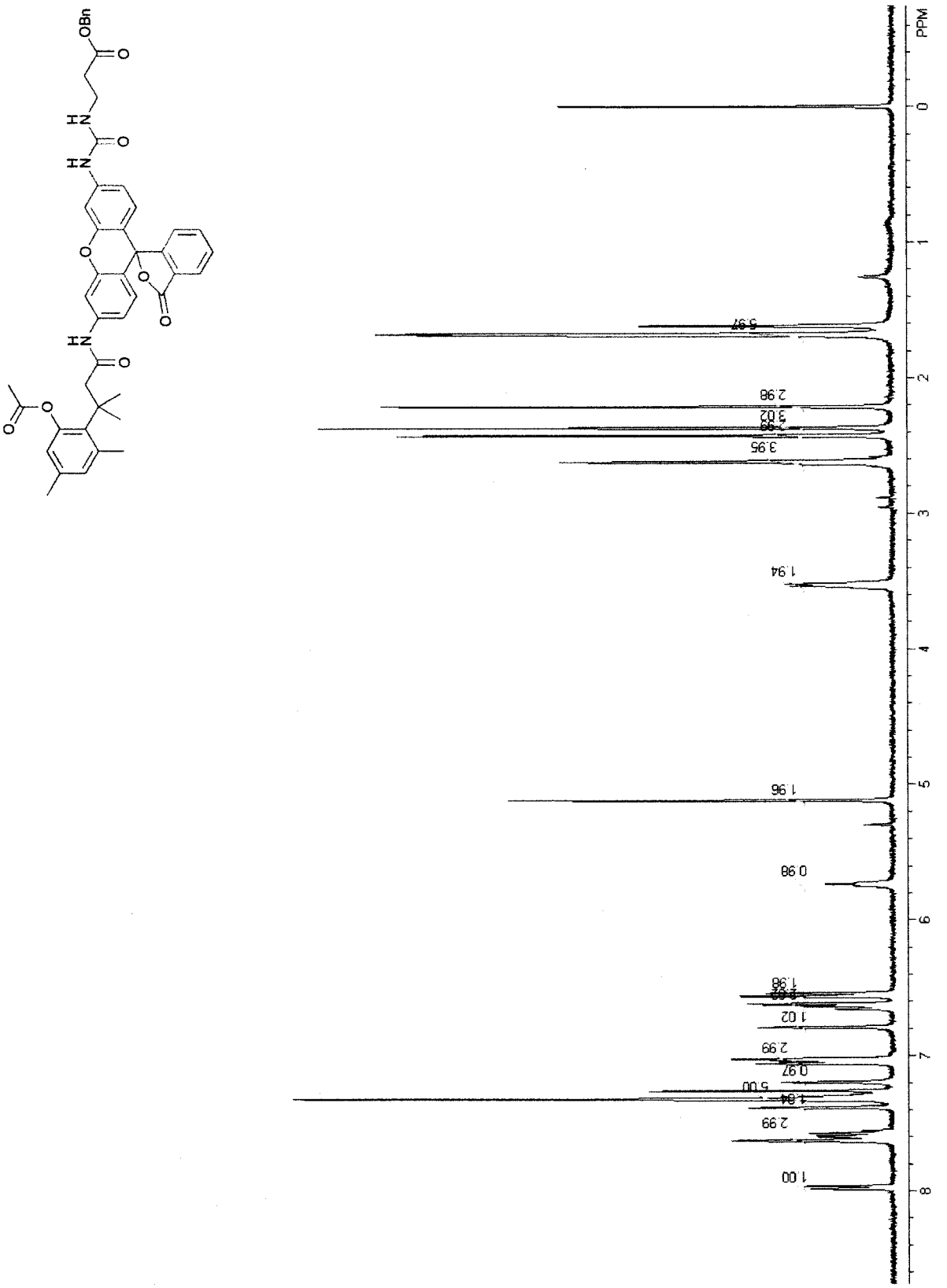

400 MHz ^{13}C NMR spectrum of compound **9** in $CDCl_3$.

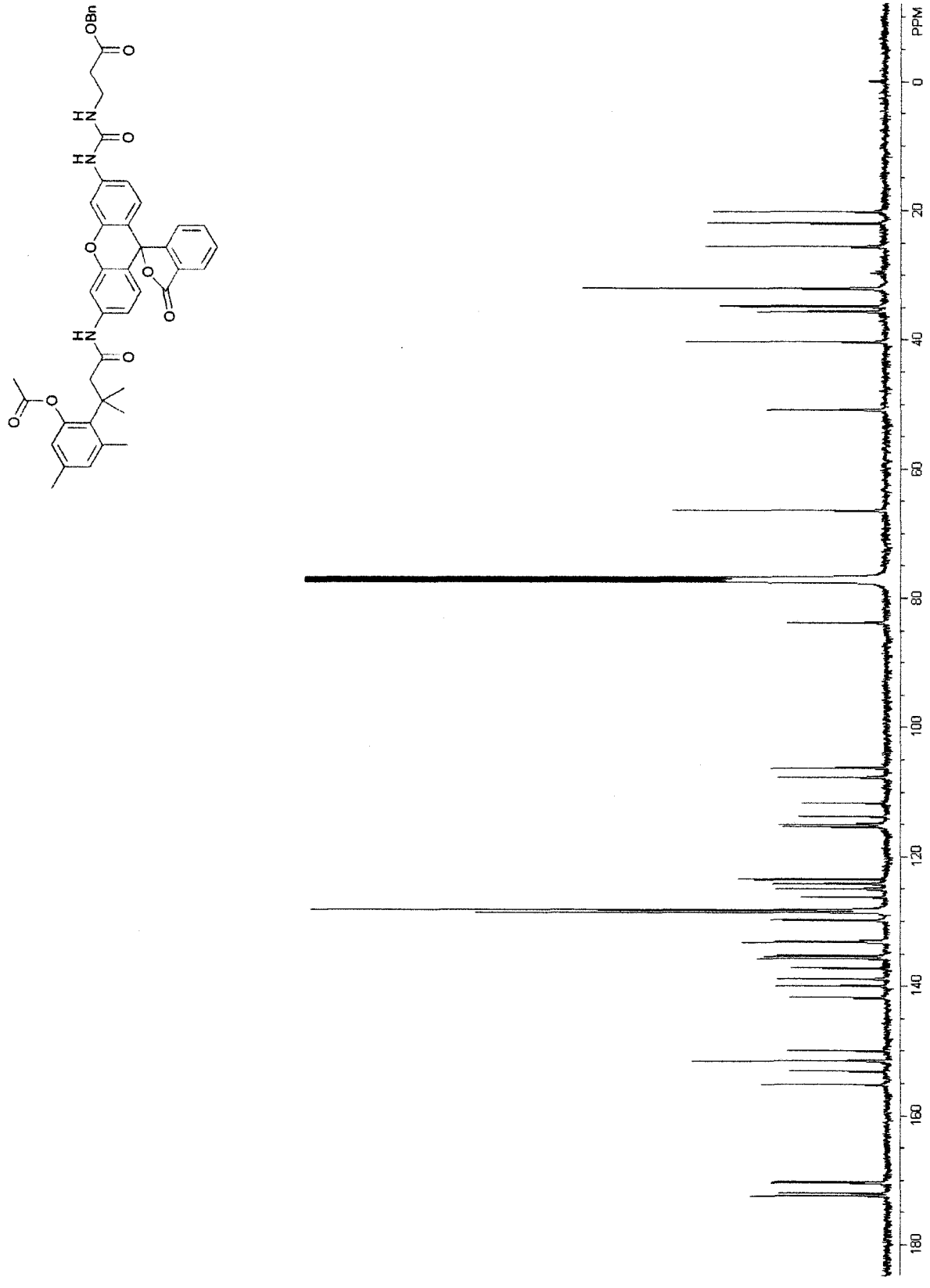

400 MHz ^{1}H NMR spectrum of compound **10** in $CDCl_3$.

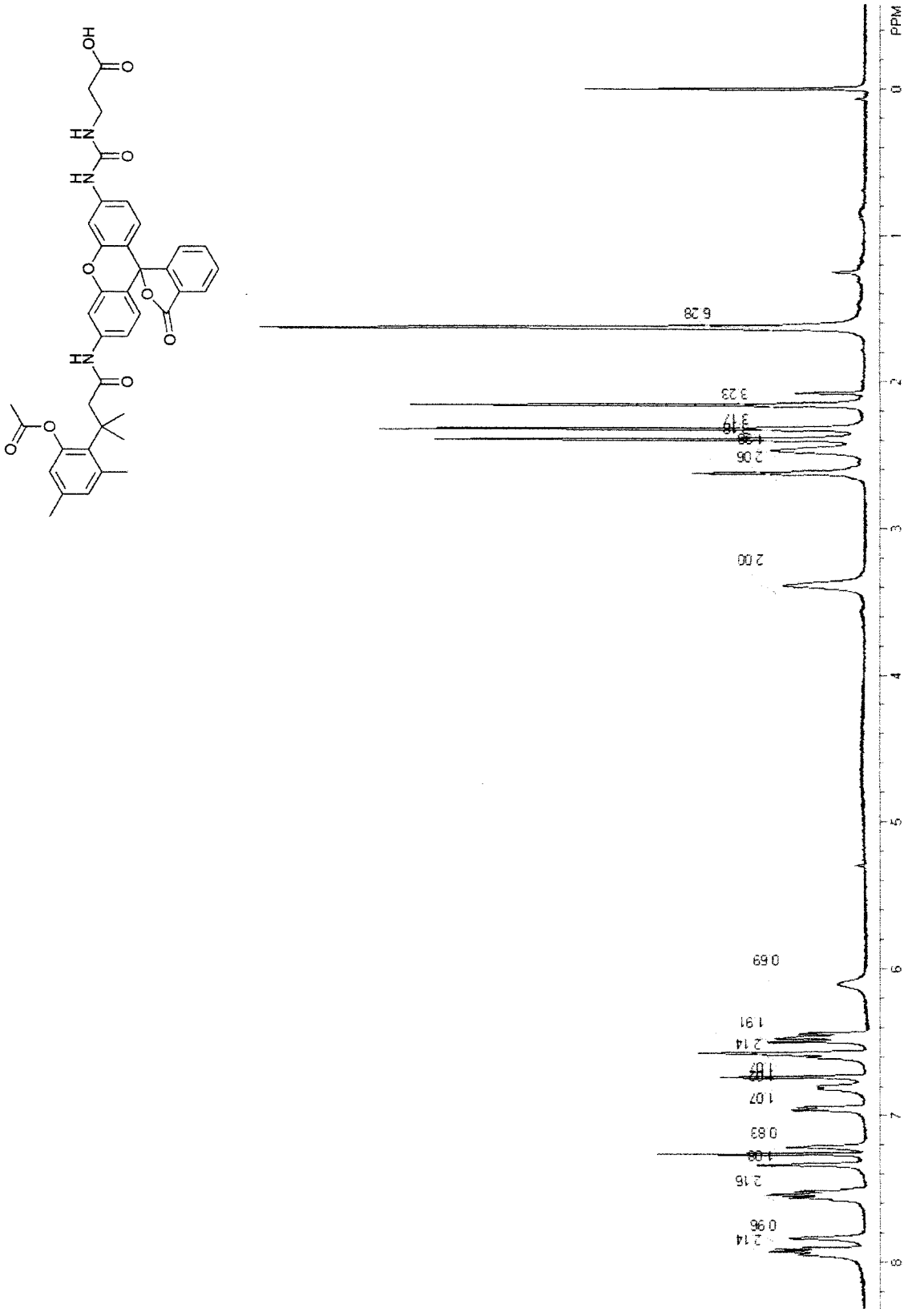

400 MHz ^{13}C NMR spectrum of compound **10** in $CDCl_3$.

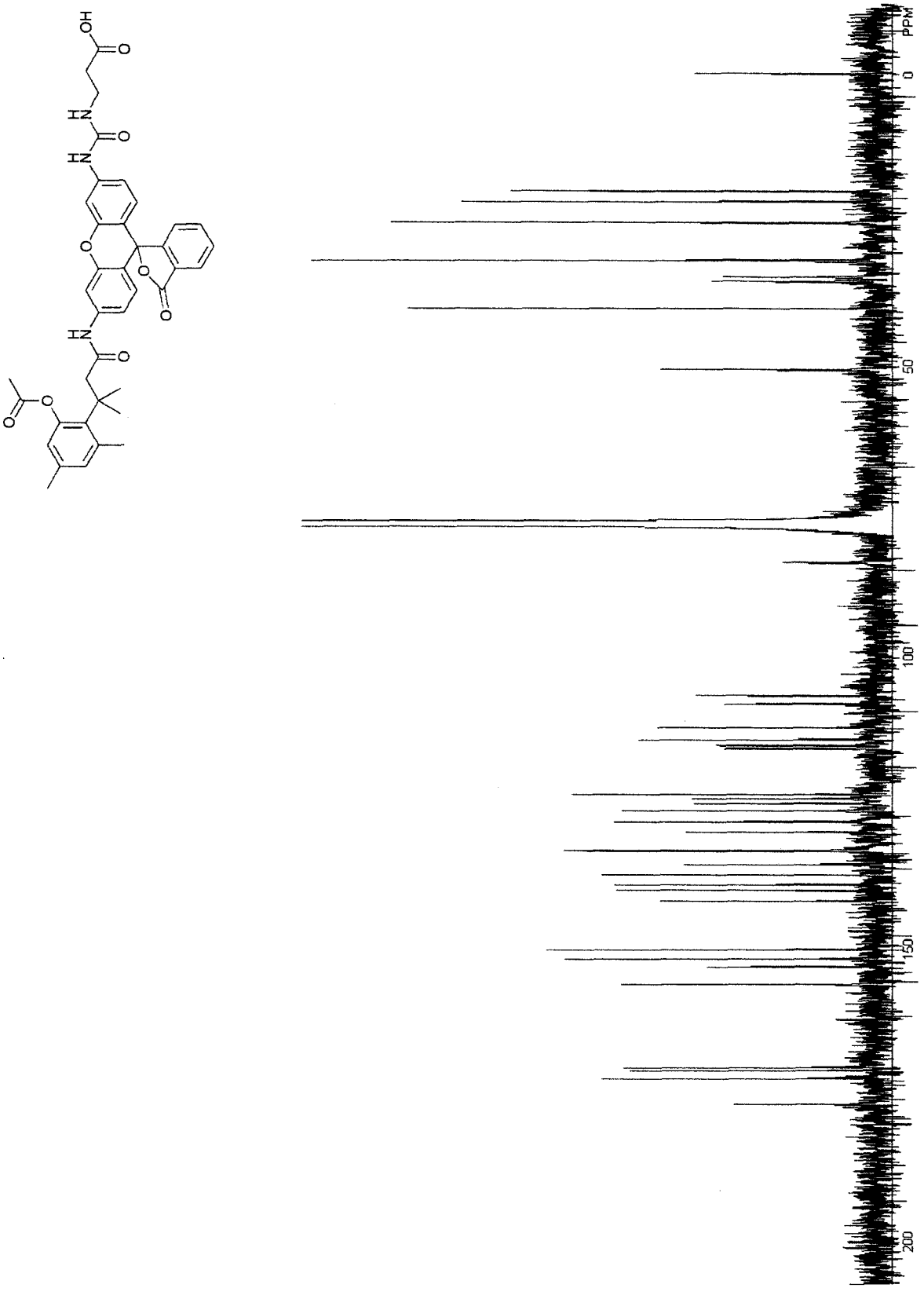

400 MHz ^{1}H NMR spectrum of compound **1** in $CDCl_3$.

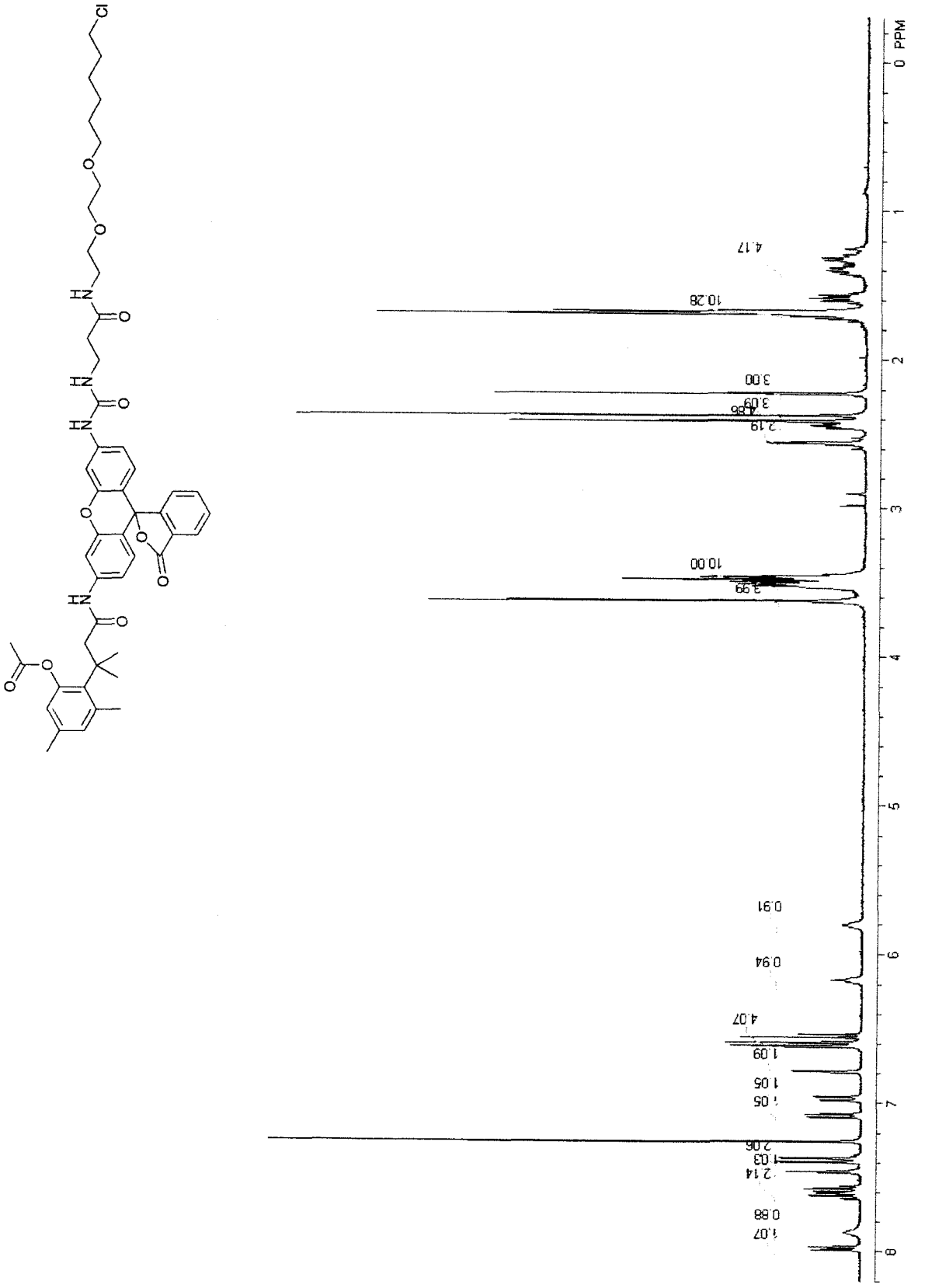

Acknowledgements We are grateful to the Promega Corporation for gifts of compounds **2** and **11**, and U2OS cells. This work was supported by grant CA073808 (NIH). R.W.W. was supported by an NSF Graduate Research Fellowship and by Chemistry–Biology Interface Training Grant GM008505 (NIH). L.D.L was supported by an ACS Division of Organic Chemistry Fellowship sponsored by the Genentech Foundation and by Biotechnology Training Grant GM008349 (NIH). V.M.K. was supported by a Barry M. Goldwater Scholarship and a Hilldale Undergraduate/Faculty Research Fellowship. NMRFAM was supported by grant P41RR02301 (NIH).

Table 2.1 Calculated values of log*D* for masked and unmasked probes at pH 7.4.

Probe	log*D*
1	4.82
2	3.93
3	2.37
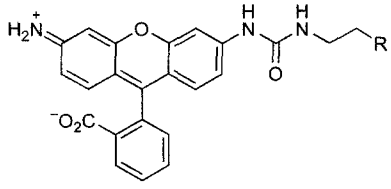	2.63
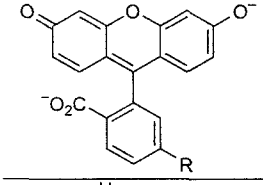	0.12

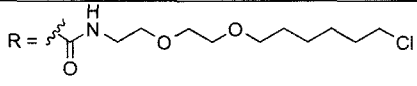

Scheme 2.1 Synthesis of probe **1**.

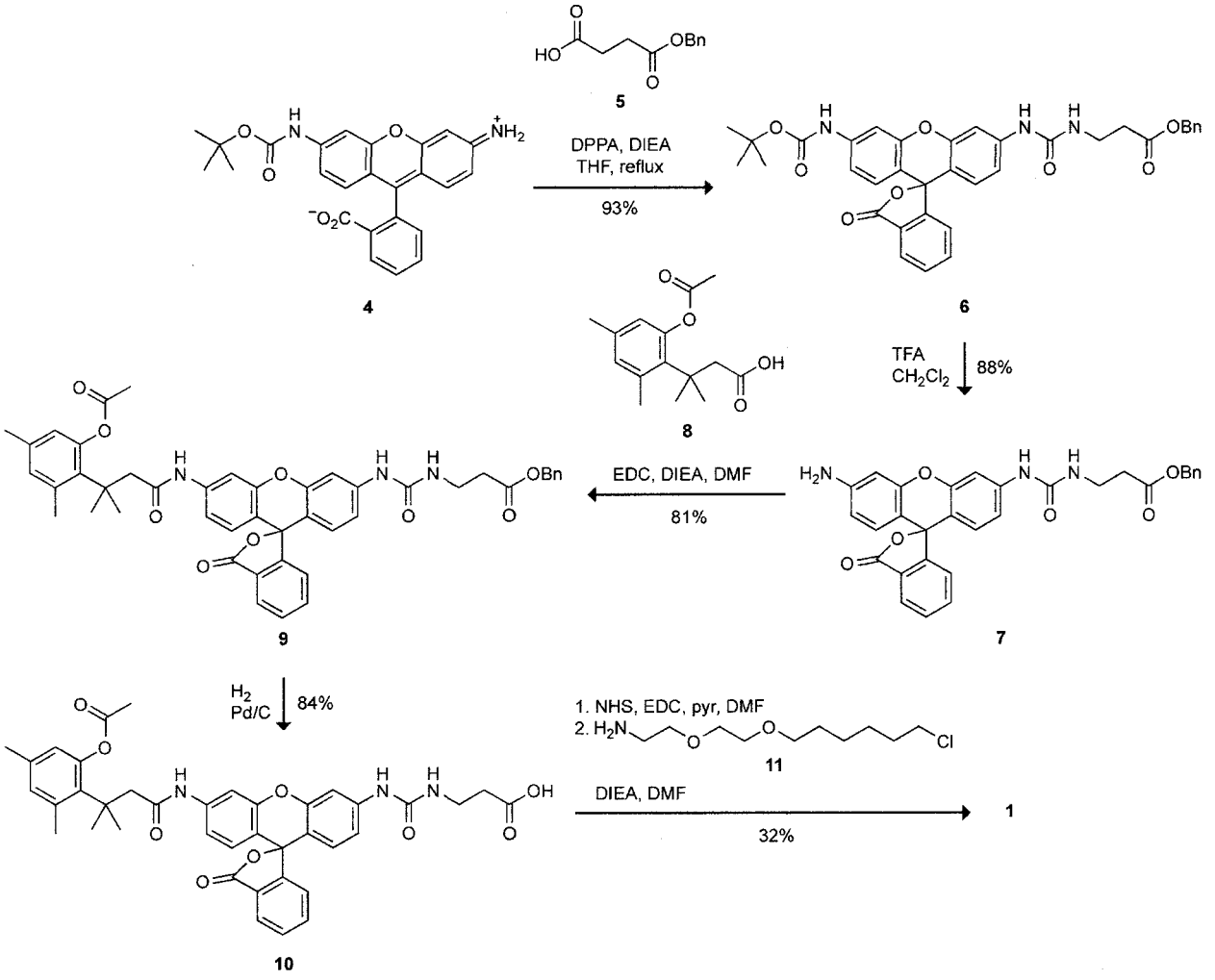

Figure 2.1 Fluorogenic (**1** and **2**) and fluorescent (**3**) labels for haloalkane dehalogenase.

Figure 2.1

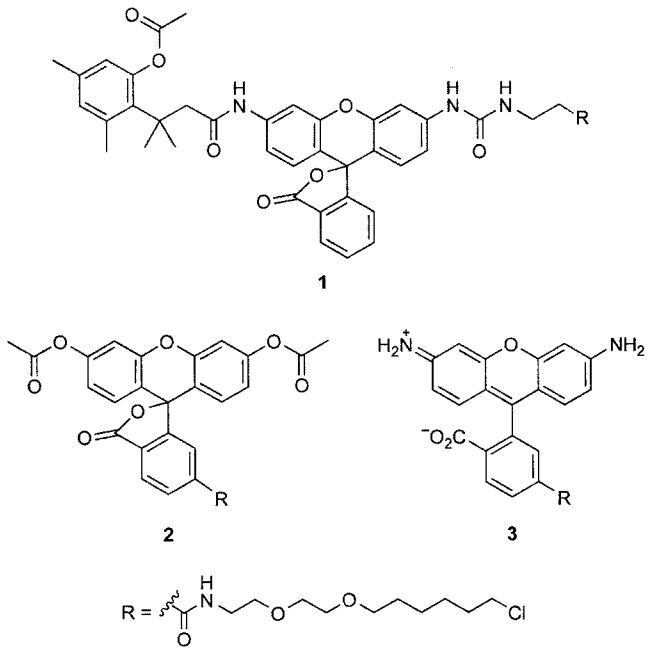

Figure 2.2 Labeling of an HD variant (HaloTag®–NLS_3) in live, unwashed U2OS cells at 37 °C as visualized by confocal microscopy. Scale bars = 200 μm. (A) Effect of probe type. Probe (1.0 μM) was incubated with cells for 15 min; (*i*) **1**, (*ii*) **2**, (*iii*) **3**, (*iv*, *v*, and *vi*) overlay with brightfield images. (B) Effect of incubation time. Probe **1** (1.0 μM) was incubated with cells for (*i*) 10 min, (*ii*) 15 min, and (*iii*) 30 min. (C) Effect of probe concentration. Probe **1** was incubated with cells for 15 min at (*i*) 1 mM, (*ii*) 10 mM, (*iii* and *iv*) overlay with brightfield images. (D) Effect of probe unmasking. Probe (1.0 μM) was incubated with cells for 15 min; (*i*) unmasked **1**, (*ii*) unmasked **2**, and (*iii*) **3**.

Figure 2.2

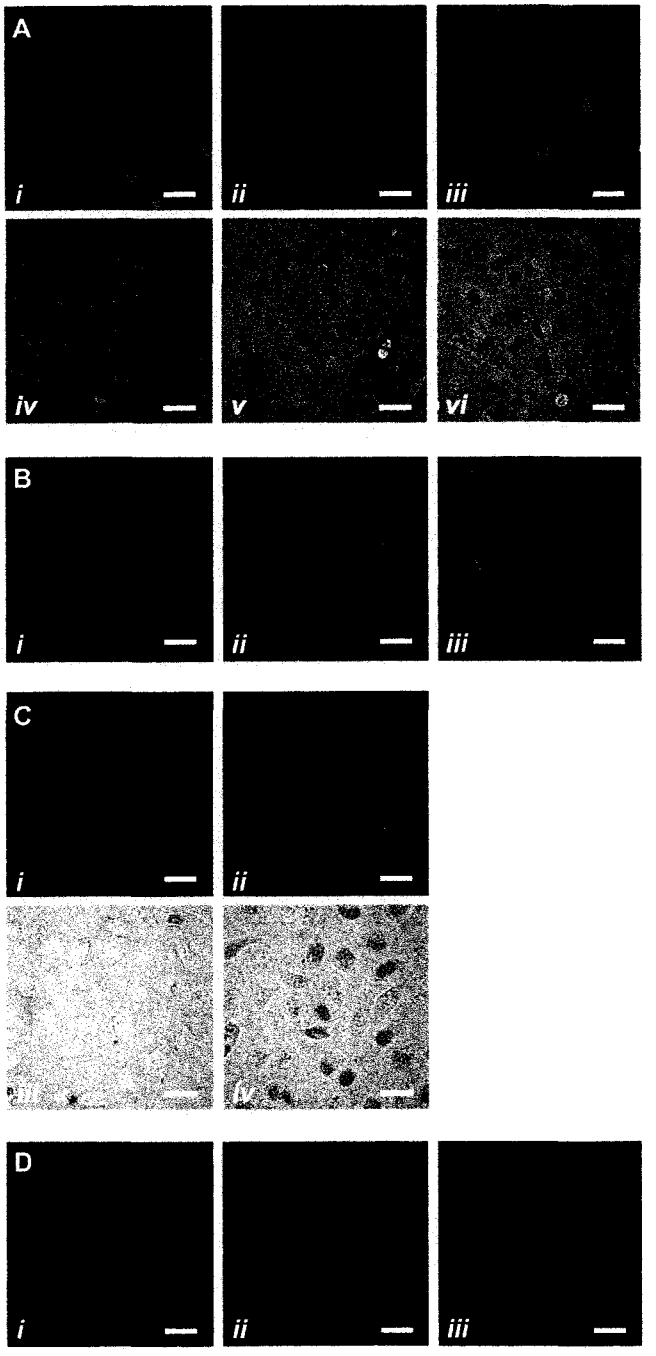

Figure 2.3 Lactone–quinoid equilibrium of **1**, **12**, and **13**.

Figure 2.3

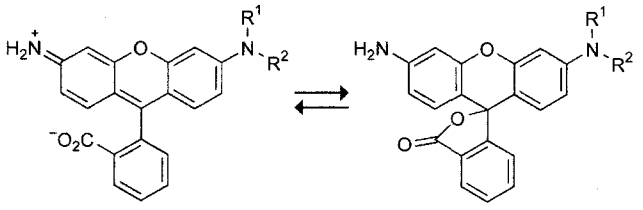

unmasked **1** $R^1 = H, R^2 = X$
12 $R^1 = R^2 = H$
13 $R^1 = H, R^2 = C(O)N(CH_3)_2$

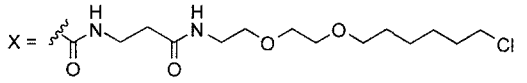

Figure 2.4 Effect of dielectric constant on the lactone–quinoid equilibrium of unmasked **12**, **13**, and unmasked **1**. Absorption spectra of (A) **12** (50 μM), (B) **13** (12.5 μM), and (C) unmasked **1** (12.5 μM) in mixtures of dioxane and water. (D) Absorption at λ_{max} in the spectra in panels A–C. Values of ε are from the literature (Kuila and Lahiri, 2004).

Figure 2.4

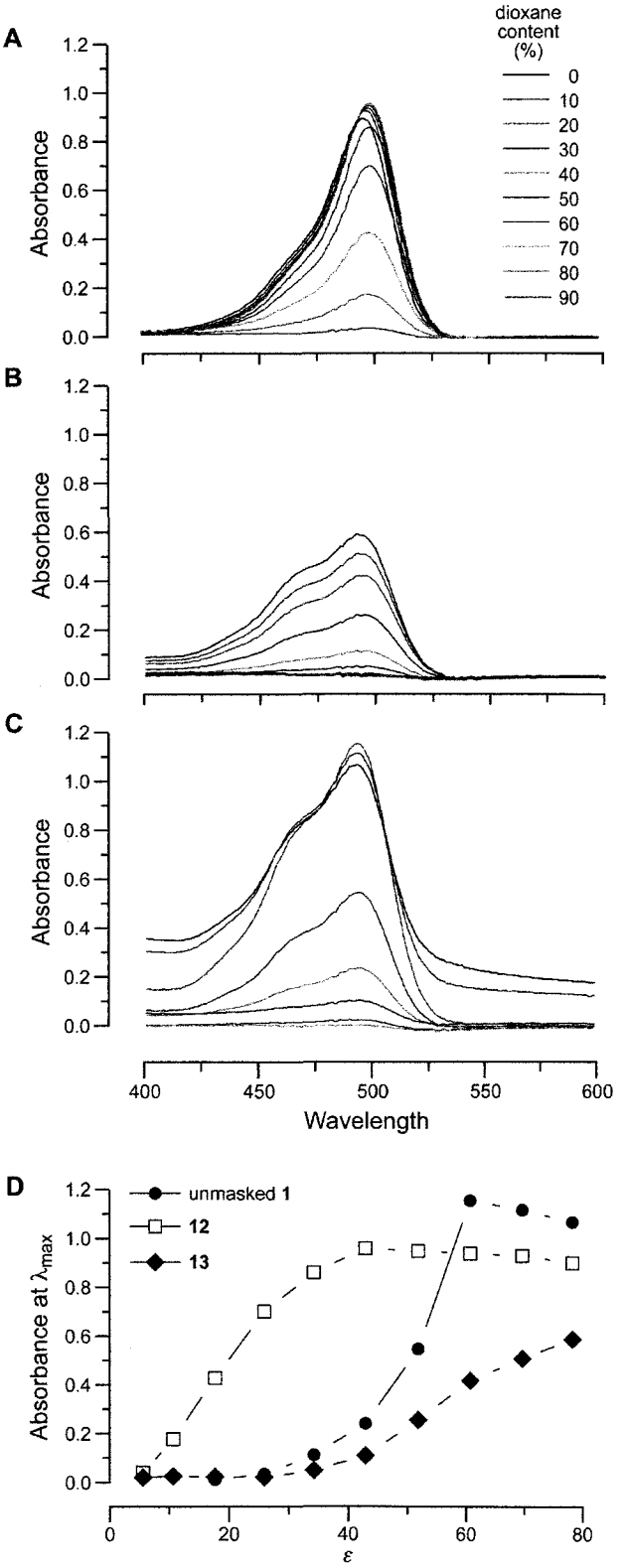
A
B
C
D
dioxane content (%)
0
10
20
30
40
50
60
70
80
90
Absorbance
Wavelength
400
450
500
550
600
unmasked 1
12
13
Absorbance at λ_{max}
ε
0
20
40
60
80

CHAPTER 3

Ribonuclease S redux

This chapter was prepared for submission to Chemical Communications as:

Watkins, R.W., Arnold, U., Raines, R.T. (2010) Ribonuclease S redux.

3.1 Abstract

The S-peptide and S-protein components of bovine pancreatic ribonuclease form a noncovalent complex with ribonucleolytic activity. Although this original of protein-fragment complementation systems has been the object of historic work in protein chemistry, two limitations compromise its utility. First, the traditional preparation of S-protein by proteolytic digestion with subtilisin yields a heterogeneous mixture of products. Secondly, the noncovalent nature of the S-peptide–S-protein interaction leads to the loss of catalytic activity at low concentrations. Here, we report on the use of site-directed mutagenesis to overcome both limitations. First, we install a site for enterokinase, which has much greater substrate specificity than does subtilisin and hence enables facile S-protein isolations. Secondly, we install a nonperturbative disulfide bond between the two components. The resulting complex is easy to prepare and retains its catalytic activity at low concentrations, enabling new uses for this venerable system.

3.2 Introduction

In the late 1950's, Fred Richards discovered protein-fragment complementation—the restoration of protein function by the noncovalent interaction of component polypeptides. Working in the renowned Carlsberg Laboratory in Copenhagen, he found that the protease subtilisin catalyzes the cleavage of bovine pancreatic ribonuclease (RNase A; EC 3.1.27.5) (Raines, 1998; Marshall *et al.*, 2008; Marshall and Feng, D.J. Kuster) between residues 20 and 21 (Richards, 1958). The resulting complex, RNase S (wherein "S" refers to subtilisin), is composed of two fragments: S-peptide (residues 1–20) and S-protein (residues 21–124). Separation of these two components abolished ribonucleolytic

activity, which was restored by their mixing (Richards and Vithayathil, 1959; Richards, 1992; Richards, 1997). This work, which served to launch the field of molecular recognition, was done before the three-dimensional structure of any protein was known. Chris Anfinsen and coworkers later found that the first 15 residues of S-peptide (S15) yield a fully active complex (Potts *et al.*, 1963). In the last fifty years, many other proteins have ceded to fragment complementation, including β-galactosidase, dihydrofolate reductase, β-lactamase, luciferase, ubiquitin, and the green fluorescent protein (Michnick *et al.*, 2007).

The RNase S system has had a singular role in protein chemistry. Prior to the advent of recombinant DNA technology, Bruce Merrifield (Gutte and Merrifield, 1971), Ralph Hirschmann (Hirschmann *et al.*, 1969), and others synthesized S-peptide analogues and studied their complexes with S-protein. A harbinger of current work on proteins containing nonnatural residues, these studies revealed important principles of protein folding (Kato and Anfinsen, 1969), protein–protein interactions (Schreier and Baldwin, 1976; Thomson *et al.*, 1994), and enzymology (Dunn *et al.*, 1974). More recently, the association of S-peptide with S-protein has found widespread use in fusion protein systems (Kim and Raines, 1993; Kim and Raines, 1994a). Vectors for making S-peptide ("S·tag") fusions facilitate the purification and sensitive detection of fusion proteins (Raines *et al.*, 2000). The RNase S complex has also been used as a molecular vehicle for targeted delivery (Gaidamakova *et al.*, 2001; Backer *et al.*, 2002; Backer *et al.*, 2006).

Despite its venerable history, the traditional RNase S system is compromised in its utility. First, the isolation of the individual RNase S components is not trivial. A major problem is that subtilisin (Markland and Smith, 1971) is a non-specific protease that

cleaves RNase A not only between residues 20 and 21, but also at other peptide bonds (Doscher and Hirs, 1967; Richards and Wyckoff, 1971). Hence, digestion is commonly quenched prior to complete cleavage at the S-peptide/S-protein boundary. The result is an inefficient conversion to RNase S (Gaynutdinov *et al.*, 2003), and a tedious isolation from intact RNase A (which contaminates commercial preparations). Moreover, subtilisin is not suitable for selective cleavage at the analogous S-protein/S-peptide boundary of RNase A homologues (Gaynutdinov *et al.*, 2003). Likewise, amino-acid substitutions near residues 20 and 21 of RNase A can hinder digestion by subtilisin (Markert *et al.*, 2001).

A second major problem relates to the stability of the S-protein·S-peptide complex, which has a K_d value in the micromolar–nanomolar range (Schreier and Baldwin, 1976; Connelly *et al.*, 1990). At lower concentrations, the complex is nearly fully dissociated, abolishing catalytic activity. Moreover, RNase S has a lower thermal stability than does RNase A (Ratnaparkhi and Varadarajan, 2001), and is more susceptive to chemical denaturation (Richards and Vithayathil, 1959) and proteolytic degradation (Richards, 1958; Allende and Richards, 1962).

Here, we revisit RNase S. We use modern methods of molecular biology and protein chemistry to facilitate the production and purification of S-protein and to install a covalent bond between the components, thereby generating "RNase–S" (Figure 3.1). These changes overcome the major limitations of the traditional system and provide new opportunities.

3.3 Results and Discussion

The non-specific proteolytic activity of subtilisin complicates the isolation of pure RNase S components. In our hands, digestion of RNase A with subtilisin resulted in a complex mixture of products and a daunting separation (Fig. 3.2). We reasoned that increased specificity for proteolytic cleavage between the S-peptide and S-protein regions of RNase A would simplify the isolation procedure.

Enterokinase is a digestive protease that catalyzes cleavage on the *C*-terminal side of the amino-acid sequence AspAspAspAspLys (Zheng *et al.*, 2009). To avail the higher substrate specificity of enterokinase relative to subtilisin, we inserted an enterokinase cleavage site between residues 20 and 21 of RNase A variants.

Enterokinase digestion of wild-type RNase A with an inserted enterokinase cleavage site (DDDDK RNase A) resulted in essentially complete conversion to the desired RNase S product (Figure 3.2). S-protein and S-peptide (containing the *C*-terminal DDDDK sequence) were separated easily by high-performance liquid chromatography (HPLC) (Figure 3.3) to yield purified components.

Next, we took advantage of previous work in our laboratory, which demonstrated that the introduction of cysteine residues at positions 4 and 118 of RNase A results in the spontaneous formation of a stabilizing disulfide bond (Klink and Raines, 2000; Dickson *et al.*, 2003; Plainkum *et al.*, 2003). Analogous disulfides also stabilize homologous ribonucleases (Futami *et al.*, 2000; Leland *et al.*, 2001; Backer *et al.*, 2006). We reasoned that the introduction of this disulfide bond in the RNase S complex would remove many of the drawbacks and complications of the noncovalent system. Accordingly, we replaced Val118 with a cysteine residue in DDDDK RNase A.

To enhance our system still further, we added another substitution, H12A, to DDDDK/V118C RNase A. His12 is in the active site of RNase A, and its replacement with an alanine residue decreases ribonucleolytic activity by $>10^4$-fold without perturbing the three-dimensional structure (Thompson and Raines, 1994; Park *et al.*, 2001). As residue 12 will be discarded after digestion with enterokinase, the H12A substitution serves as a safeguard, diminishing catalytic activity from any trace contaminant of RNase A in an S-protein sample. Finally, to prevent the adventitious air oxidation of Cys118, we protected the purified V118C S-protein by reaction with 5,5′-dithio-bis(2-nitrobenzoic acid) (DTNB), thereby forming a mixed disulfide.

To effect the semisynthesis of RNase–S, we added deprotected V118C S-protein to the A4C variant of S15, which had been activated as a mixed disulfide with 2-nitro-5-thiobenzoic acid (NTB). After removal of the NTB byproduct, the presence of the disulfide linkage between A4C S15 and V118C S-protein was apparent by both SDS–PAGE (Fig. 4, lane 4) and MALDI–TOF mass spectrometry (*m/z* 13324; expected: 13317). The semisynthesis of RNase–S in the opposite manner (that is, by reacting unactivated A4C S15 with NTB-activated S-protein) was less effective.

We analyzed RNase A and the components of RNase S by non-reducing zymogram electrophoresis, an extremely sensitive technique for detecting ribonucleolytic activity (Bravo *et al.*, 1994). Clear bands on a dark background are indicative of ribonucleolytic activity.

Neither V118C S-protein (Fig 3.5, lane 2) nor V118C S-protein mixed with cysteine-free S-peptide (Fig 3.5, lane 3) displayed detectable activity. In marked contrast, RNase–

S had robust activity (Figure 3.5, lane 4). The activity due to RNase A contamination of commercial RNase S is apparent (Figure 3.5, lane 6).

Finally, we assessed the activities of RNase S and RNase–S as catalysts of RNA cleavage at high and low enzymic concentrations. RNase–S retains nearly all of the ribonucleolytic activity of RNase A across a concentration range of nearly 10^6-fold (Figure 3.6). In contrast, RNase S loses detectable activity over that range.

3.4 Conclusions

Despite many advances since the 1950's, the isolation of RNase S components has remained an arduous challenge. In their initial isolation of S-protein and S-peptide, Richards and Vithayathil digested a whopping 730 mg of RNase A with subtilisin (Richards and Vithayathil, 1959). S-protein was separated from S-peptide by acid precipitation. In our hands, however, a subtilisin-digest of RNase A results in a complex mixture of products (Figure 3.2). S-protein can be isolated from such mixtures by using S-peptide–affinity chromatography (Gaynutdinov *et al.*, 2003). This method requires an expensive custom-made column, and still suffers from the inefficient conversion of RNase A to RNase S. Furthermore, subtilisin is an ineffective means to generate RNase S from some RNase A variants (Markert *et al.*, 2001) and homologues (Gaynutdinov *et al.*, 2003). An alternative strategy could be the recombinant expression of S-protein. But because S-protein does not fold properly in the absence of S-peptide (Kato and Anfinsen, 1969), synthetic S-peptide must be added during the folding process which is wasteful and inefficient (Backer *et al.*, 2002).

Our strategy takes advantage of the superior selectivity and general applicability of the protease enterokinase. Insertion of an enterokinase cleavage site into RNase variants enables complete cleavage of S-peptide from S-protein without unwanted side-products. This facilitates the facile separation of S-peptide and S-protein by HPLC. Historically, changes to the RNase S system have been restricted almost exclusively to S-peptide. This S-protein isolation methodology now makes S-protein variants more accessible, allowing manipulation and greater understanding of both parts of the RNase S system.

The noncovalent interaction of S-protein and S-peptide limits the use and complicates the characterization of RNase S complexes. RNase S is not active at low concentrations because RNase S has modest stability that is dependent on solution conditions (Schreier and Baldwin, 1976; Connelly *et al.*, 1990). Further, the traditional RNase S system has less thermal stability (ΔT_m ~17 °C) (Ratnaparkhi and Varadarajan, 2001), and less resistance to denaturants (Richards and Vithayathil, 1959) and proteases (Richards and Vithayathil, 1959; Allende and Richards, 1962; Nadig *et al.*, 1996).

The covalent attachment of S-peptide to S-protein overcomes this intrinsic liability of the natural system. In particular, we demonstrate here that a nonnative disulfide bond between S-peptide and S-protein (linking residues 4 and 118) endows RNase–S with high enzymatic activity at low concentrations (Figure 3.6). We envision that this improvement will assist in the definition of structure–function relationships. Moreover, the disulfide bond in RNase–S could enable the discovery of higher affinity S-peptide ligands by the application of tethering strategies (Erlanson *et al.*, 2000).

3.5 Experimental

3.5.1 Materials

DTNB, guanidine–HCl, ampicillin (sodium salt), isopropyl β-D-1-thiogalactopyranoside (IPTG), and dithiothreitol (DTT) were from Research Products International (Mount Prospect, IL). Enterokinase was from EMD Chemicals (Gibbstown, New Jersey). 6-carboxyfluorescein–dArU$(dA)_2$–6-tetramethylrhodamine was from Integrated DNA Technology (Coralville, IA). All other reagents, including subtilisin A (type VIII from bacillus licheniformis), RNase S, and RNase A were from Sigma–Aldrich (St. Louis, MO) and were used without further purification. Total yeast RNA was from Boehringer Mannheim (Damstadt, Germany).

3.5.2 Analytical methods

DNA was sequenced with a 3730xl DNA Analyzer (Applied Biosystems, Carlsbad, CA) at the Biotechnology Center of the University of Wisconsin–Madison. Peptides were synthesized with a Symphony (Protein Technologies, Tucson, AZ) automated synthesizer at the Biotechnology Center, and purified by semi-preparative HPLC using an UltiMate 3000 instrument (Dionex, Bannockburn, IL). Analytical HPLC was performed with a system from Waters (Milford, MA) equipped with two 515 pumps, a 717 plus autosampler, a 996 photodiode array detector, and a C-18 column from Varian (Palo Alto, CA). Non-kinetic ultraviolet/visible measurements were recorded with a Cary 50 spectrophotometer (Varian). An AKTA system (Amersham–Pharmacia, Piscataway, NJ) was used for fast protein liquid chromatography (FPLC), and the results were analyzed

with the UNICORN Control System. A Voyager-DE-PRO Biospectrometry Workstation (Applied Biosystems) at the Biophysics Instrumentation Facility of the University of Wisconsin–Madison was used for matrix-assisted laser desorption ionization time of flight (MALDI–TOF) mass spectrometry. A Cary Bio400 spectrophotometer (Varian) and an Infinite M1000 microplate reader (Tecan, Männedorf, Switzerland) were used for kinetic assays.

3.5.3 Site-directed mutagenesis

Plasmids encoding variants of RNase A were generated from plasmid pBXR (delCardayré *et al.*, 1995) by Quikchange site-directed mutagenesis (Stratagene, La Jolla, CA) using these oligonucleotides and their reverse complements from Integrated DNA Technology or the Biotechnology Center: DDDDK insertion between residues 20 and 21, GCACTTCCGCTGCCGATGATGATGATAAAAGCAGCTCCAACTAC;
H12A, CCAAGTTTGAGCGGCAGGCTATGGACTCCAGCACTTCC;
V118C, GCATCAAAGTGACATGGCACATACGGGTTTCC. All mutated genes were verified by DNA sequencing.

3.5.4 Production of ribonucleases

RNase A variants were produced and purified essentially as described elsewhere (Rutkoski *et al.*, 2005). Briefly, transformed BL21(DE3) cells were grown at 37 °C with shaking in Terrific Broth containing ampicillin (400 μg/mL) until OD = 1.8–2.2 at 600 nm. Gene expression was induced by the addition of IPTG (0.5 mM). After 3–4 h, cells were harvested by centrifugation and lysed with a French pressure cell. Inclusion bodies

were recovered after centrifugation and solubilized for 2 h at room temperature with denaturing solution (20 mM Tris–HCl buffer, pH 8.0, containing 7 M guanidine–HCl, 0.10 M DTT, and 10 mM EDTA). Solubilized inclusion bodies were then diluted 10-fold with 20 mM HOAc. The precipitate was removed by centrifugation, and the solution was dialyzed overnight against 20 mM HOAc at 4 °C. After removal of further precipitate, the ribonuclease solution was added dropwise to refolding buffer (0.10 M Tris–HCl buffer, pH 7.8, containing 0.5 M L-arginine–HCl, 1.0 mM reduced glutathione, and 0.2 mM oxidized glutathione). After >3 days at 4 °C, the solution was adjusted to pH 5, and concentrated using an Amicon YM10 membrane (Millipore, Billerica, MA). A 10-mL sample was applied to a G75 gel filtration FPLC column (Amersham–Pharmacia). The major peak after isocratic elution (50 mM sodium acetate buffer, pH 5.0, containing 0.10 M NaCl, 10 mM EDTA, and 0.02% w/v NaN_3) was collected and applied to a Mono S cation-exchange FPLC column (Amersham–Pharmacia). Ribonucleases were eluted with a linear gradient of NaCl (0–0.40 M) in 50 mM NaOAc buffer, pH 5.0, containing EDTA (10 mM). Protein concentrations were determined by absorbance at 278 nm using ε = 0.72 $mg^{-1} \cdot mL \cdot cm^{-1}$ (Sela *et al.*, 1957a). The identity of each variant was verified by MALDI–TOF mass spectrometry.

3.5.5 Protection of H12A/DDDDK/V118C RNase A with DTNB

After cation-exchange chromatography, the fractions that contained H12A/DDDDK/V118C RNase A were combined, and the pH of the resulting solution was increased by adding (to 8% v/v) 1.0 M Tris–HCl buffer, pH 8.3, containing EDTA (10 mM). To this solution was added 50 mM Tris–HCl buffer, pH 8.0, containing DTNB

(5 mM) and EDTA (50 mM) such that the DTNB was in 4-fold molar excess to the protein. After incubation for 10 min, the solution was dialyzed overnight at 4 °C against 20 mM Tris–HCl buffer, pH 7.4, containing NaCl (50 mM).

3.5.6 Synthesis, activation with DTNB, and purification of peptides

S15 (KETAAAKFERQHMDS) and A4C S15 (KETCAAKFERQHMDS) were synthesized on a 50-μmol scale by standard fluorenylmethoxycarbonyl chemistry using HATU activation and an Fmoc-Ser(*t*Bu) Wang resin (EMD Biosciences, La Jolla, CA). Peptides were deprotected and cleaved from the resin with 4 mL of 92.5:5:2.5 trifluoroacetic acid (TFA)/thioanisole/ethanedithiol for 4 h. Peptides were then precipitated with *tert*-butyl methyl ether and dried under vacuum. S15 and A4C S15 were purified by reversed-phase HPLC on a C-18 semipreparative column. TFA (0.1%) was included as an ion-pairing agent in HPLC solvents. Peptides were eluted with a linear gradient of acetonitrile (10–30% v/v). One-quarter volume 0.10 M Tris–HCl buffer, pH 8.0, containing DTNB (5 mM) was added to fractions containing A4C S-peptide. The solvent was then removed under reduced pressure. NTB-activated A4C S-peptide was then purified again under the same HPLC conditions. The mass of purified peptides was confirmed by MALDI–TOF mass spectrometry.

3.5.7 Digestion of RNase A with subtilisin

Subtilisin (5 μg) was added to a solution of RNase A (0.5 mg, 88 μL) in phosphate-buffered saline (PBS) and incubated at 4 °C. Aliquots were removed over 24 h and subjected to SDS–PAGE (15% w/v acrylamide).

3.5.8 Digestion of ribonucleases with enterokinase

$CaCl_2$ (2 mM final concentration) was added to RNase A and its DDDDK and H12A/DDDDK/V118C variants (~5 mL of a 0.85 mg/mL solution) that had been dialyzed against 20 mM Tris–HCl buffer, pH 7.4, containing NaCl (50 mM). Enterokinase (5 μL, 5 U) was added, and the reaction mixture was incubated at room temperature. Aliquots were removed over 24 h and subjected to SDS–PAGE.

3.5.9 Separation of S-peptide and S-protein components

The S-peptide and S-protein fragment from the enterokinase-digestion of the DDDDK and H12A/DDDDK/V118C variants of RNase A were separated by analytical or semi-preparative reverse-phase HPLC with a C-18 column and two-step linear gradient (Step 1: 20–50% B over 3 min. Step 2: 50–100% B over 25 min. A: 50 mM sodium phosphate buffer, pH 2.7. B: 40% A + 60% acetonitrile) (Brems and Baldwin, 1984). Fractions containing S-protein were pooled and dialyzed overnight against PBS at 4 °C. The concentration of S-protein was determined by absorbance at 280 nm using ε = 9055 $M^{-1} \cdot cm^{-1}$ (Gilmanshin *et al.*, 1996). The identity of each peak on the HPLC trace was confirmed by MALDI–TOF mass spectrometry.

3.5.10 Fragment complementation

To V118C S-protein (100 μL of a 1.76 mg/mL solution) was added 1.0 M Tris–HCl buffer, pH 8.0, containing EDTA (10 mM) (8 μL), and DTT (25 mM) (2 μL). After 2 min, the mixture was desalted with a Zeba Spin column, 7K MWCO (Pierce, Rockford,

IL). To the collection tube was added S15 or NTB-activated A4C S15 (4 μL of 20 mg/mL). After ~10 min, the reactions were desalted again with the spin columns. SDS–PAGE and MALDI–TOF mass spectrometry confirmed the covalent linkage between A4C S15 and V118C S-protein (*m*/z 13324; expected: 13317).

3.5.11 Zymogram electrophoresis

The potassium salt of poly(cytidylic acid) (final concentration: 0.5 mg/mL) was included during the casting of a 15% w/v polyacrylamide gel. Laemmli buffer (no reducing agent) was added to each sample (2 ng). After SDS–PAGE, the gel was washed with isopropanol (20% v/v) in 10 mM Tris–HCl buffer, pH 7.0 (2×), 10 mM Tris–HCl buffer, pH 7.0 (2×), and 0.10 M Tris–HCl buffer, pH 7.5 (1×) for 10 min each. The gel was then stained for 10 min with 10 mM Tris–HCl buffer, pH 7.5, containing toluidine blue (0.02% w/v). The stained gel was rinsed several times in water, and soaked in water overnight.

3.5.12 Assays of ribonucleolytic activity

Initial velocities for catalysis of RNA cleavage were determined at high and low concentrations of RNase A, RNase S, and RNase–S in 50 mM NaOAc buffer, pH 6.0, containing NaCl (0.10 M). To avoid the contamination apparent in commercial preparations of RNase S (Figure 5, lane 6), the noncovalent complex assayed here was that of S15 and the deprotected S-protein derived from H12A/DDDDK/V118 RNase A.

A fluorogenic ribonuclease substrate, 6-carboxyfluorescein–dArU$(dA)_2$–6-tetramethylrhodamine (Kelemen *et al.*, 1999), was used for assays at low ribonuclease

concentration. Briefly, a ribonuclease (50 μL of a 50 pM solution) was equilibrated at 37 °C in a 96-well plate. To each sample was added 6-carboxyfluorescein–dArU$(dA)_2$–6-tetramethylrhodamine (50 μL of a 100 nM solution in sample buffer). Reaction progress was monitored at 37 °C by the increase in fluorescence emission at 515 nm upon excitation at 493 nm over 5 min.

A modified Kunitz assay was used at high ribonuclease concentration (Kunitz, 1946). Briefly, to total yeast RNA (100 μL of a 1 mg/mL solution) was added a ribonuclease (100 μL of a 0.29 μM solution). The decrease in absorbance at 300 nm was monitored at 37 °C for 10 min. Data from the first 2 min were used to determine initial velocities (v_o).

Acknowledgements and Dedication. This article is dedicated to the memory of Fred Richards (1925–2009). This work was supported by grants CA073808 and GM044783 (NIH). R.W.W. was supported by an NSF Graduate Research Fellowship and by Chemistry–Biology Interface Training Grant GM008505 (NIH).

Figure 3.1 Notional structure of "RNase–S", the covalent complex of A4C S15 and V118C S-protein. The image is based on the known structure of the noncovalent S15·S-protein complex (Taylor *et al.*, 1981).

Figure 3.1

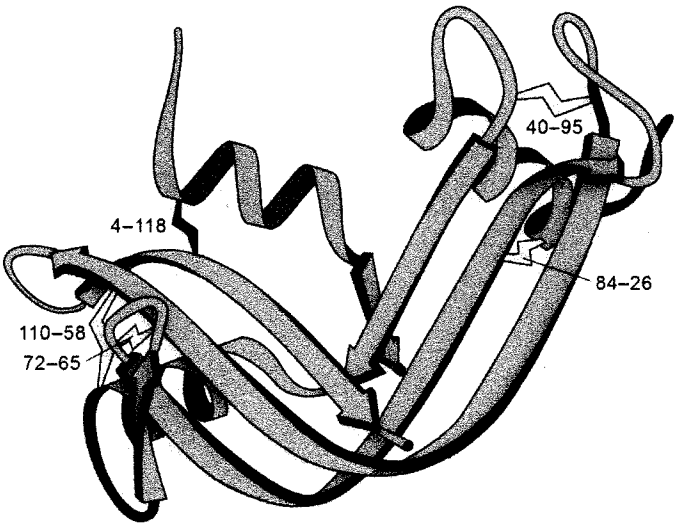

RNase–S

Figure 3.2 Analysis of the proteolytic digestion of ribonucleases with SDS–PAGE. Left, subtilisin-catalyzed cleavage of wild-type RNase A. Right, enterokinase-catalyzed cleavage of DDDDK RNase A and the wild-type enzyme.

Figure 3.2

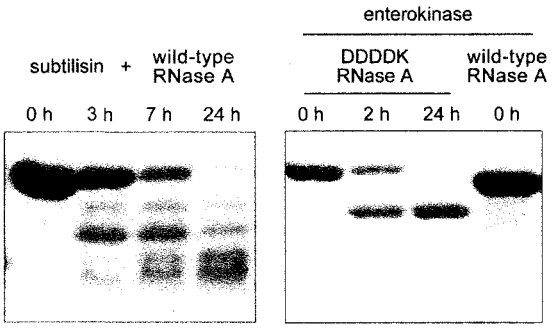
enterokinase
subtilisin + wild-type RNase A
DDDDK RNase A
wild-type RNase A
0 h 3 h 7 h 24 h
0 h 2 h 24 h 0 h

Figure 3.3 Separation of S-peptide and S-protein components from DDDDK RNase A by reversed-phase HPLC.

Figure 3.3

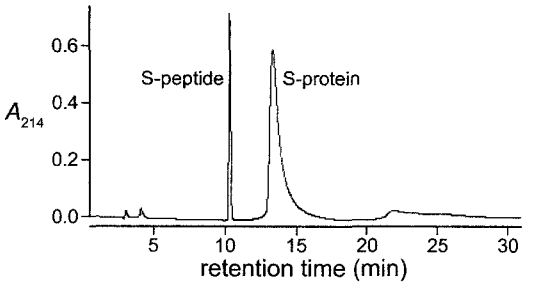
0.6
0.4
0.2
0.0
A_{214}
S-peptide
S-protein
5
10
15
20
25
30
retention time (min)

Figure 3.4 Analysis of RNase–S semisynthesis with SDS–PAGE. Lane 1, RNase A; lane 2, RNase S; lane 3, S-protein derived from H12A/DDDDK/V118C RNase A; lane 4, A4C S-peptide + V118C S-protein of lane 3.

Figure 3.4

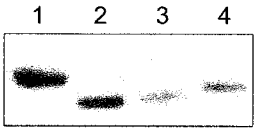

Figure 3.5 Analysis of RNase–S semisynthesis with zymogram electrophoresis. Lane 1, RNase A; lane 2, S-protein derived from H12A/DDDDK/V118C RNase A; lane 3, S15 + V118C S-protein of lane 2; lane 4, A4C S15 + V118C S-protein of lane 2; lane 5, RNase A; lane 6, commercial RNase S.

Figure 3.5

Figure 3.6 Initial velocities of RNA cleavage at high (0.15 μM) and low (25 pM) ribonuclease concentrations, relative to RNase A. "RNase S" refers to the noncovalent complex of S15 and the S-protein derived from H12A/DDDDK/V118 RNase A.

Figure 3.6

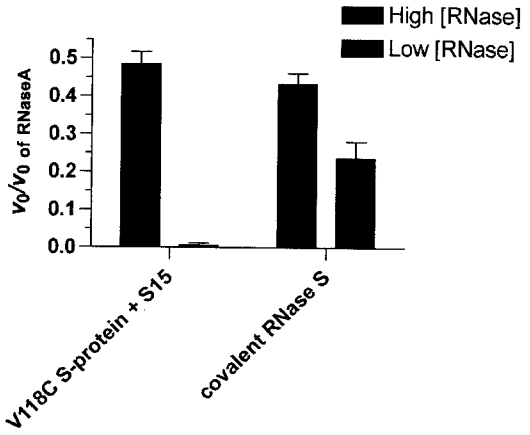
High [RNase]
Low [RNase]
V_0/V_0 of RNaseA
0.5
0.4
0.3
0.2
0.1
0.0
V118C S-protein + S15
covalent RNase S

CHAPTER 4

Gene expression response of cancerous cells

to clinically relevant ribonucleases

4.1 Abstract

Pancreatic-type ribonucleases that evade the cytosolic ribonuclease inhibitor protein constitute a novel class of chemotherapeutic agents. These enzymes enter cancerous cells and destroy intracellular RNA, leading to cell death. Onconase, an amphibian ribonuclease, is in confirmatory Phase IIIb clinical trials and has been granted orphan-drug status for the treatment of malignant mesothelioma. A homologous human variant, QBI-139, is now in a Phase I clinical trial. Despite obvious similarities, mammalian ribonucleases and onconase differ in their substrate preferences, internalization efficiency and routing, conformational stability, and levels of catalytic activity. The extent to which these dissimilarities elicit different cellular responses is not well understood. Here, we use DNA microarrays and nucleic acid amplification techniques to investigate the transcriptional response of K-562 cells to clinically relevant ribonucleases. We find that onconase upregulates genes ATF3, IL-6, and TNFAIP3, and modifies genes associated with cytokine-cytokine interactions and the MAPK and JAK-STAT signaling pathways. We also observe increases in genes associated with apoptosis and the charging of tRNAs. Intriguingly, the most pronounced response in cells treated with QBI-139 is a relative increase of polyadenylated histone transcripts, many of which were chimeric histone mRNAs that were fused to unrelated RNA sequences encoded elsewhere in the genome.

4.2 Introduction

In the 1970's, early frog embryo extracts were found to possess antitumoral activity (Shogen and Yoan, 1973). Later work attributed this activity to onconase, a pancreatic-

type ribonuclease (Ardelt *et al.*, 1991). Onconase is cytostatic and cytotoxic towards tumor cells (Darzynkiewicz *et al.*, 1988; Rybak *et al.*, 1996; Juan *et al.*, 1998; Halicka *et al.*, 2000; Leland *et al.*, 2000; Lee and Raines, 2003; Rodriguez *et al.*, 2007) and, in mouse models, antagonizes xenograft tumor growth (Mikulski *et al.*, 1990a; Rybak *et al.*, 1996; Lee and Raines, 2003; Lee *et al.*, 2007). The enzyme is now in confirmatory Phase IIIb clinical trials and has been granted orphan-drug status as a second-line therapy for patients with malignant mesothelioma.

Onconase and other cytotoxic ribonucleases cause cell death by degrading cellular RNA. A necessary feature of these ribonucleases is the ability to evade the cytosolic ribonuclease inhibitor protein (RI) that serves as a sentry to protect intracellular RNA. RI-evasive bovine and human variants have been created and shown to display potent cytotoxicity (Leland *et al.*, 1998; Leland *et al.*, 2001; Rutkoski *et al.*, 2005; Johnson *et al.*, 2007a). Notably, QBI-139 is an RI-evasive variant of human pancreatic ribonuclease (RNase 1) that is in a Phase I clinical trial with patients having advanced, refractory, solid tumors.

Onconase and cytotoxic mammalian ribonucleases share many features typical of members of the RNase A superfamily (Beintema, 1987). These cationic enzymes catalyze RNA degradation, share a similar tertiary structure and key active site residues (Figure 4.1), and are remarkably stable. Additionally, the same general mechanism has been proposed to explain their cytotoxic effects (Figure 4.2). Nevertheless, important differences remain. The ribonucleolytic activity of onconase with common substrates is ~5 orders of magnitude lower than that for mammalian homologues (Boix *et al.*, 1996). Also, *in vitro*, onconase shows a unique preference for cleavage on the 5′ side of a

guanine nucleobase (Lee *et al.*, 2008; Lee and Raines, 2008), and tRNA is preferentially degraded *in cellulo* (Saxena *et al.*, 2001). Other evidence suggests that the cytotoxic effects of onconase may be due to degradation of small RNA substrates (Zhao *et al.*, 2008). Finally, important details differentiate the cellular entry of onconase and mammalian ribonucleases. Onconase binds to a broad array of cell-surface glycans, whereas RNase A, a bovine homologue, binds with only low affinity. Further, the internalization of mammalian ribonucleases, but not that of onconase, correlates with cell anionicity (Chao *et al.*, 2010).

To determine the extent to which these dissimilarities elicit a different biological response, we use DNA microarrays and nucleic acid-amplification techniques to investigate the gene expression response of cancerous cells to both onconase and QBI-139. We find distinct differences in the cellular response to an assault by these homologous cytotoxins.

4.3 Results and Discussion

4.3.1 Primary cellular response is due to degradation of intracellular RNA

To evaluate the ribonuclease-dependent gene expression response of K-562 cells, we added RNase 1, onconase, or QBI-139 to a final concentration of 0.15 μM for 24 h. Under these conditions, cell proliferation of onconase and QBI-139-treated cells (as measured by S-phase incorporation of [*methyl*-^{3}H]thymidine into cellular DNA) is ~80–90% of the PBS control (Figure 4.3), and ribosomal RNA is largely intact (data not shown). This ribonuclease concentration was arbitrarily chosen because a cellular

response is apparent in the cell proliferation assay after 24 h (Figure 4.3). After isolation of the RNA and cDNA synthesis, gene expression changes were investigated by analysis with DNA microarrays. The data show that cells treated with RI-evasive ribonucleases elicit a much more pronounced gene-expression response than do those treated with RNase 1. ANOVA-derived *p*-value versus fold-change scatter plots ("volcano plots") show that treatment with onconase or QBI-139 results in both larger fold changes and increased statistical significance relative to RNase 1 (Figure 4.4). The more dramatic transcriptional response of RI-evasive ribonucleases strongly suggests that the primary cellular response to clinical ribonucleases results from the degradation of intracellular RNA.

4.3.2 Cellular response to onconase

There is notable agreement between previous microarray results of onconase-treated malignant mesothelioma cells (Altomare *et al.*, 2010) and those reported here. In particular, three of the eight (37.5%) most highly onconase-regulated genes (>4-fold increase) in the earlier work were also differentially regulated by onconase in this study (>2-fold increase, p-value <0.05, Table 4.1). These genes have been implicated in tumor growth inhibition (ATF3) (Fan *et al.*, 2002; Lu *et al.*, 2006) and inflammation (IL-6, TNFAIP3) (Vereecke *et al.*, 2009; Nishimoto, 2010). Further, we note that protein interaction networks derived from the onconase-regulated genes (Figure 4.5) highlight important nodes that correspond to the MAPK signaling (MAP2K1/2, ERK, Ras), cytokine-cytokine receptor interactions (IL1, interferon, interferon α/β, interferon β, TNFAIP3, IL20RB), and JAK-STAT signaling pathways (STAT5a/b) that were

implicated previously in an onconase-dependent response (Altomare *et al.*, 2010). Network and gene ontology analyses also reveal that onconase-regulated genes are associated with apoptosis (p-value = 1.99×10^{-5}), and tRNA aminoacylation (p-value = 5.3×10^{-4}). It is unclear if there is any association between the upregulation of genes associated with tRNA aminoacylation (*e.g.*, tRNA synthetases) and the preferential cleavage of tRNA by onconase *in vivo*. The selective cleavage of charged tRNAs by onconase would, however, explain why onconase preferentially degrades tRNA in both cells and cells lysates but not *in vitro* with purified total RNA (Saxena *et al.*, 2001). Additionally, onconase treatment leads to a modest apparent increase in histone mRNA (see below).

4.3.3 Histone mRNAs and other differences between onconase- and QBI-139-treated cells

Onconase and QBI-139 elicited remarkably different transcriptional responses, as only one gene, JUN (jun oncogene), was differentially upregulated (>2-fold difference in gene expression, p-value <0.05) in both treatments (Table 4.1). Furthermore, network analyses of QBI-139 and onconase-regulated genes show that each ribonuclease produces a distinct cellular response (compare Figures 4.5 and 4.6). Most dramatically, 20 of the 26 genes that are differentially regulated by QBI-139 encode cell cycle-regulated histone proteins (Table 4.1 and Figure 4.7). This result was quite unexpected. While several replication-independent histone mRNAs are polyadenylated, cell cycle-regulated histone mRNAs generally lack poly(A) tails (Marzluff *et al.*, 2008), so their inclusion in our oligo(dT) primer-derived cDNA library was not anticipated. To a much lesser extent,

onconase and RNase 1 treatment also resulted in an apparent increase in histone mRNA expression (Figure 4.7).

4.3.4 Confirmation by quantitative PCR

Quantitative PCR was used to confirm the microarray data and probe further the puzzling histone mRNA results. For amplification, we selected genes that microarray analysis showed were upregulated in either QBI-139 (HIST1H1E and HIST1H2AE) or onconase-treated cells (DDIT4 and FNDC6). Quantitative PCR using cDNA samples generated with random primers confirmed the microarray results for the onconase-regulated genes, but showed no increased expression of HIST1H1E or HIST1H2AE mRNAs. Yet, with cDNA generated using an oligo(dT) primer, quantitative PCR not only confirmed the results of the onconase-regulated genes, but also showed a pronounced increase in histone mRNA in QBI-139-treated cells (see Figure 4.8). The ratio of non-polyadenylated to polyadenylated histone mRNA was estimated to be 16:1–50:1 by comparison of apparent histone mRNA expression in QBI-139 and onconase-treated cells relative to the control GAPDH mRNA. These data, combined with the microarray results, strongly suggest that treatment with QBI-139 leads to a significant increase in polyadenylated histone mRNA, which is, nonetheless, a small fraction of the overall histone mRNA population.

4.3.5 3′ rapid amplification of cDNA ends

To better understand the 3′ processing of polyadenylated histone mRNAs, we amplified the 3′ end of HIST1H1E, HIST1H2AB, and HIST1H2AE mRNAs using 3′

rapid amplification of cDNA ends (RACE). Surprisingly, 3′ RACE revealed that a significant number of the polyadenylated histone mRNAs were chimeric—the RNA sequence of the histone mRNA was fused to a different, unrelated RNA molecule encoded elsewhere in the genome (Figure 4.6). More specifically, the following RNAs from QBI-139-treated cells were fused to histone transcripts as identified by sequencing: RPLP1 (NM_001003.2, Chromosome (Chr.) 15), MRPL52 (NM_181306.2, Chr. 14), INTS4 (NM_033547.3, Chr. 11), NDUFB9 (NM_005005.2, Chr. 8), NASP (NM_172164.1, Chr. 1), LOC100128191 (NR_027157.1, Chr. 12), RPL41 (NM_021104.1, Chr. 12), and TIGD5 (NM_032862.3, Chr. 1). From both untreated and QBI-139-treated cells we found histone mRNAs fragments that were polyadenylated without any evidence of *trans*-splicing. Additionally, chimeric histone mRNAs were also identified from the PBS-treated control: HINT1 (NR_024611.1, Chr. 5), EIF4A1 (NM_001416.2, Chr. 17), MED25 (NM_030973.2, Chr. 19), TXNL1 (NM_004786.2, Chr. 18), HNRNPM (NM_005968.3, Chr. 19), OAZ1 (NM_004152.2, Chr. 19), LOC100130107 (XM_001718888.2, Chr. 15), and KHDRBS1 (NM_006559.1, Chr. 1).

4.3.6 Interpretation

Taken together, the data hint that exposure to QBI-139 leads to an increase in *trans*-spliced polyadenylated histone mRNAs. It is not known if this increase is histone-specific or if QBI-139 treatment leads to a global increase in *trans*-splicing. Since *trans*-splicing occurs at a relatively low level, the poly(A) tails of conventional mRNAs contribute far too much background noise to detect a global increase in *trans*-splicing using the facile detection methods that we use here. Furthermore, the data from the

untreated cells suggest that there is a low abundance of polyadenylated histone mRNAs under normal conditions.

The mechanism by which ribonuclease-dependent *trans*-splicing occurs is not clear. We are skeptical of spliceosome involvement, as these chimeric transcripts lack the traditional *cis* elements involved in spliceosome-mediated splicing (Walsh and Yang, 2005; Wang and Burge, 2008). It is tempting, however, to speculate that endonucleolytic cleavage of mRNA transcripts by QBI-139 results in RNA fragments that are subsequently joined by endogenous ligases. This mechanism is analogous to the nonspliceosomsal IRE1p- and *Methanococcus jannaschii* endoribonuclease-dependent splicing of the *HAC1* mRNA and bulge-helix-bulge-containing tRNAs (Gonzalez *et al.*, 1999; Deidda *et al.*, 2003). Several candidate RNA ligases have been identified in mammalian cells (Deidda *et al.*, 2003).

4.4 Conclusions

Here, we show that the gene expression response of K-562 cells to ribonucleases is due predominantly to the degradation of intracellular RNA. Also, our data generally confirm previous findings of the cellular response to onconase. The gene expression response to QBI-139 is, however, markedly different. Treatment with the RI-evasive mammalian ribonuclease may lead to an increase in chimeric histone mRNAs. Although the mechanism for this process is not well understood, the RNA-degrading ability of QBI-139 may lead to increased concentrations of mRNA fragments that are subsequently ligated within cells.

Recent work in *C. elegans* revealed the presence of polyadenylated histone mRNAs prompting speculation that histone polyadenylation may occur in higher eukaryotes as well (Mangone *et al.*, 2010). Our data here confirm that hypothesis, demonstrating the expression of polyadenylated cell-cycle-dependent histone mRNAs in human cells.

Finally, our work suggests that RI-evasive mammalian ribonucleases may be useful tools to increase the abundance of chimeric RNA transcripts and to help understand the mechanisms of *trans*-splicing. The isolation of chimeric histone mRNAs using oligo(dT) primers is facile, making histone mRNAs prime candidates for *trans*-splicing studies. We anticipate that this work will prompt a more in-depth investigation of whether histone mRNAs or the RNA fragments fused to the 3′ end of histone mRNA fragments are privileged *trans*-splicing substrates, or whether the proposed cleavage/ligation activity operates stochastically. Further research should also reveal whether this response is confined to particular cell types and establish the kinetics and concentration dependence of ribonuclease-induced histone *trans*-splicing.

4.5 Experimental

4.5.1 Materials

E. coli BL21(DE3) cells were from Novagen (Madison, WI). K-562 and DU145 cells were obtained from the American Type Culture Collection (Manassas, VA). Cell culture media and supplements were from Invitrogen (Carlsbad, CA) or ATCC. [*methyl*-^{3}H]Thymidine (6.7 Ci/mmol) was from Perkin–Elmer (Boston, MA). QBI-139 was a gift from Quintessence Biosciences (Madison, WI). TaqMan gene expression assays and PCR

Master Mix (No AmpErase) were from Applied Biosystems (HIST1H1E: Hs00271195_s1; HIST1H2AE: Hs00368307_s1; DDIT4: Hs00430304_g1; FNDC6: Hs01023484_m1; GAPDH: 4352934E). Oligo$(dT)_{12-18}$ primer was from Invitrogen (Carlsbad, CA). All other oligonucleotides were obtained from the Biotechnology Center of the University of Wisconsin–Madison. Phase Lock tubes (light, 1.5 mL) were from 5 PRIME (Gaithersburg, MD). All other chemicals used were of commercial reagent grade or better, and were used without further purification.

4.5.2 Instrumentation

Cellular DNA for the cytotoxicity assay was isolated using a PHD cell harvester (Cambridge Technology). A Microbeta TriLux liquid scintillation counter (Perkin–Elmer, Wellesley, MA) was used to quantify [*methyl*-^{3}H]thymidine incorporation. A Voyager-DE-PRO Biospectrometry Workstation (Applied Biosystems, Foster City, CA) at the University of Wisconsin-Madison Biophysics Instrumentation Facility was used for matrix-assisted laser desorption ionization time of flight (MALDI–TOF) mass spectrometry. RNA and cDNA concentrations were determined using a Nanodrop ND–1000 instrument. DNA sequences were determined with a 3730xl DNA Analyzer (Applied Biosystems, Carlsbad, CA) at the Biotechnology Center of the University of Wisconsin–Madison.

4.5.3 Ribonuclease production

Human RNase 1 and onconase were produced, purified, and quantified as described elsewhere (Leland *et al.*, 2001). The identity of each was verified by MALDI–TOF mass spectrometry.

4.5.4 Assay of cytotoxicity

The effect of ribonucleases on cell proliferation was determined by measuring [*methyl*-^{3}H]thymidine incorporation into the DNA of asynchronous log-phase K-562 cells. The assay was carried out as described previously (Leland *et al.*, 1998; Rutkoski *et al.*, 2005) with the following modifications. Cells were delivered to wells at an initial concentration of 1×10^5 cells/mL. After a 24-h incubation with the ribonucleases, cells were pulsed with radiolabeled thymidine for 4 h. Cellular DNA was recovered and [*methyl*-^{3}H]thymidine incorporation was measured by scintillation counting. Results show the percentage of [*methyl*-^{3}H]thymidine incorporation compared to PBS controls and represent the average of at least three measurements at each concentration. Values for IC_{50} were calculated as described previously (Rutkoski *et al.*, 2005).

4.5.5 Cell propagation

Cell culture medium was supplemented with fetal bovine serum and antibiotics (streptomycin, 100 μg/mL; penicillin, 100 U/mL). K-562 cells were propagated in RPMI 1640.

4.5.6 Microarray analysis

4.5.6.1 Isolation of RNA from cells exposed to ribonucleases

Ribonucleases were added to K-562 cells (25 mL, 1.4×10^6 cells/mL) to a final concentration of 0.15 μM and incubated at 37 °C in a humidified atmosphere containing 5% CO_2 (v/v). After 24 h, cells were harvested by centrifugation, and total RNA from PBS-, RNase1-, onconase-, and QBI-139-treated cells (one batch) was isolated using the RNeasy Mini Kit (QIAGEN, Germantown, MD). RNA from three batches was isolated on separate days. For all samples, both A_{260}/A_{280} and A_{260}/A_{230} were greater than 1.8. RNA integrity was verified by agarose electrophoresis (1% w/v).

4.5.6.2 First-strand cDNA synthesis

cDNA was produced using the Invitrogen SuperScript Double-Stranded cDNA synthesis kit. Briefly, oligo$(dT)_{12-18}$ primer (1 μL, 0.5 μg) was added to 10 μg RNA. After addition of water to a final volume of 11 μL, the sample was heated at 70 °C for 10 min. After cooling on ice, 4 μL 5X first-strand buffer, 2 μL 0.1 M DTT, and 1 μL 10 mM dNTP mix were added, and the resulting solution was heated to 42 °C for 2 min. Then, SuperScript II (400 U) was added, and the reaction mixture was incubated again at 42 °C for 1 h.

4.5.6.3 Second-strand cDNA synthesis

The following were added to each first strand cDNA synthesis reaction: 91 μL DEPC-treated water, 30 μL 5X second-strand buffer, 3 μL 10 mM dNTP mix, 1 μL (10 U) DNA ligase, 4 μL (40 U) DNA polymerase I, and 1 μL (2 U) RNase H. After incubation at 16 °C for 2 h, T4 DNA polymerase was added (10 U), and the reaction

mixture was incubated at 16 °C for an additional 5 min. RNA was degraded by incubating the reaction mixture at 37 °C with 1 μg of RNase A. cDNA was isolated by phenol:chloroform:isoamyl alcohol extraction using Phase Lock tubes. After ethanol precipitation, cDNA was resuspended in 20 μL water. cDNA was quantified using a NanoDrop ND–1000 instrument. For all samples, A_{260}/A_{280} and A_{260}/A_{230} were both greater than 1.8.

4.5.6.4 DNA labeling, hybridization and data extraction

DNA labeling, hybridization to Nimblegen HG18_60mer_expr arrays, data extraction, and pre-processing of hybridization signals were performed by Nimblegen (Madison, WI). All data manipulation was done with Partek Genomics Suite Software. Data were normalized by quantile normalization (Bolstad *et al.*, 2003), and gene calls were made using the RMA (robust multichip average) algorithm (Irizarry *et al.*, 2003). Ribonuclease-regulated genes were identified by applying a filter (>2-fold gene expression change and unadjusted p-value <0.05) to an ANOVA analysis.

4.5.6.5 Gene ontology and pathway analysis

Gene ontologies that were responsive to QBI-139 and onconase were identified using the gene ontology ANOVA feature of the Partek software suite. Pathway analyses (Figures 4.5 and 4.6) were generated by importing QBI-139- and onconase-responsive gene lists into Ingenuity Pathways Analysis web-based software analysis program.

4.5.7 Quantitative real-time PCR

4.5.7.1 RNA isolation

Ribonucleases were added to K-562 cells (25 mL, 1.4×10^6 cells/mL) to a final concentration of 0.15 μM and incubated at 37 °C in a humidified atmosphere containing 5% CO_2 (v/v). After 24 h, cells were harvested by centrifugation, and total RNA was isolated using the RNeasy Mini kit (QIAGEN, Germantown, MD). For all samples, both A_{260}/A_{280} and A_{260}/A_{230} were greater than 1.8.

4.5.7.2 cDNA synthesis for quantitative real-time PCR

cDNA was synthesized from 1.5 μg total RNA using the high capacity cDNA reverse transcription kit (Applied Biosystems) according to the manufacturer's protocol. For oligo(dT)-primed reverse transcription, 1 μg oligo$(dT)_{12-18}$ primer (Invitrogen) was used in place of the kit-supplied random primer.

4.5.7.3 Quantitative real-time PCR

All quantitative PCR reactions used TaqMan® technology and were processed according to the manufacturer's protocol on a 7500 Fast Real-Time PCR System instrument (Applied Biosystems). All samples were denatured (95 °C for 10 min) and then cycled 40 times between 95 °C (15 s) and 60 °C (1 min). Data acquisition was performed with Sequence Detection Software v.1.3 (Applied Biosystems, Foster City, CA). For each assay, four technical replicates for each of three biological replicates were run. Relative gene expression was calculated using the comparative C_T method

(Schmittgen and Livak, 2008), and error bars represent the standard error of the biological replicates.

4.5.8 3′ Rapid amplification of cDNA ends

The 3′ ends of histone genes were investigated using the classic 3′ rapid amplification of cDNA ends (RACE) protocol (Scotto-Lavino *et al.*, 2007). cDNA was generated from 5 μg total RNA (isolated as for quantitative PCR) using the Q_T primer (Scotto-Lavino *et al.*, 2007) to amplify only poly(A)-containing RNAs. The following gene-specific primers were used in consecutive amplification steps: HIST1H1E, ATGTCCGAGACTGCGCCTGCCG, GCCGCCGAGAAGACTCCCGTGAAG, and TCCGAGCTCATTACTAAAGCT; HIST1H2AB, TGCAGTTTCCTGTGGGCCGA, TATCTCGCGGCGGTGCTTGA; HIST1H2AE, TGCTGTTAGGAAGCCACTATGTCTG, AAGCCACTATGTCTGGACGTGGAAA. 3′ RACE was carried out as specified except (Scotto-Lavino *et al.*, 2007) that Pfu Turbo (Stratagene) or GoTaq (Promega) polymerases were used for amplification steps. The annealing temperature for all amplification steps was 60 °C. Following the last amplification step, DNA was isolated by using the Wizard SV gel and PCR clean-up system (Promega). DNA was then cloned into a pGEM-T Easy vector (Promega) and sequenced by using the following oligonucleotide primers: HIST1H1E, GGCGCGTCGGGTTCCTTCAA; HIST1H2AB, CATCGCGCAGGGTGGCGTTT, HIST1H2AE, CCTGGCAGCGGTGCTGGAATAT. Pfu Turbo-amplified DNA was "A-tailed" with GoTaq polymerase before cloning according to manufacturer's instructions (Promega).

Acknowledgements. We thank Brian Yandell, Allan Attie, Mark Keller, Aimee Broman, and Jean-Yves Sgro for experimental and statistical guidance. This work was supported by grants CA073808 and GM044783 (NIH). R.W.W. was supported by an NSF Graduate Research Fellowship and by Chemistry–Biology Interface Training Grant GM008505 (NIH).

Table 4.1 Genes with >2-fold change and *p*-values <0.05 relative to PBS controls.

QBI-139-responsive genes		*Onconase-responsive genes*	
Gene Symbol	*Gene description*	*Gene symbol*	*Gene description*
C10orf10	chromosome 10 open reading frame 10	ACSM1	acyl-CoA synthetase medium-chain family member 1
HIST1H1B	histone cluster 1, H1b	ADM2	adrenomedullin 2
HIST1H1D	histone cluster 1, H1d	ALDH1L2	aldehyde dehydrogenase 1 family, member L2
HIST1H1E	histone cluster 1, H1e	ARRDC4	arrestin domain containing 4
HIST1H2AB	histone cluster 1, H2ab	ATF3	activating transcription factor 3
HIST1H2AE	histone cluster 1, H2ae	CHAC1	cation transport regulator homolog 1
HIST1H2AH	histone cluster 1, H2ah	DDIT4	DNA-damage-inducible transcript 4
HIST1H2AM	histone cluster 1, H2am	EPAS1	endothelial PAS domain protein 1
HIST1H3B	histone cluster 1, H3b	FNDC6	interleukin 20 receptor beta
HIST1H3F	histone cluster 1, H3f	G0S2	G_0/G_1 switch 2
HIST1H3J	histone cluster 1, H3j	GDF15	growth differentiation factor 15
HIST1H4A	histone cluster 1, H4a	HECW2	HECT, C2 and WW domain containing E3 ubiquitin protein ligase 2
HIST1H4B	histone cluster 1, H4b	IGF1	insulin-like growth factor I
HIST1H4K	histone cluster 1, H4k	IL6	interleukin 6
HIST2H2AB	histone cluster 2, H2ab	INHBE	inhibin, beta E
HIST2H2AC	histone cluster 2, H2ac	JUN	jun oncogene
HIST2H3C	histone cluster 2, H3c	KLF10	Kruppel-like factor 10
HIST2H3A	histone cluster 2, H3a	KLF6	Kruppel-like factor 6
HIST2H4	histone cluster 2, H4a	KLHL4	kelch-like 4 (Drosophila)
ID2B	inhibitor of DNA binding 2B	LOC653746	similar to phosphoprotein associated with glycosphingolipid microdomains 1
ID3	inhibitor of DNA binding 3	MAGEA5	melanoma antigen family A, 5
JUN	jun oncogene	SLC6A9	solute carrier family 6 (neurotransmitter transporter, glycine), member 9
LOC200261	hypothetical protein LOC200261	SLC7A11	solute carrier family 7 member 11
BC017361	histone cluster 1, H4j	TNFAIP3	tumor necrosis factor, alpha-induced protein 3
AB088847	BPA-1 mRNA for brain peptide A1	TP53	tumor protein p53 (TP53), transcript variant 1
RP5-998N21.6	histone cluster 2, H3, pseudogene 2	ULBP1	UL16 binding protein 1
		UNC5B	unc-5 homolog B (*C. elegans*)
		VMD2	bestrophin 1

Figure 4.1 Crystalline structures of (A) onconase (PDB entry 1onc) (Mosimann *et al.*, 1994) and (B) human RNase 1 (PDB entry 1z7x) (Johnson *et al.*, 2007b). Key catalytic residues are shown in red. Images were generated with MacPyMOL software (DeLano Scientific, South San Francisco, CA).

Figure 4.1

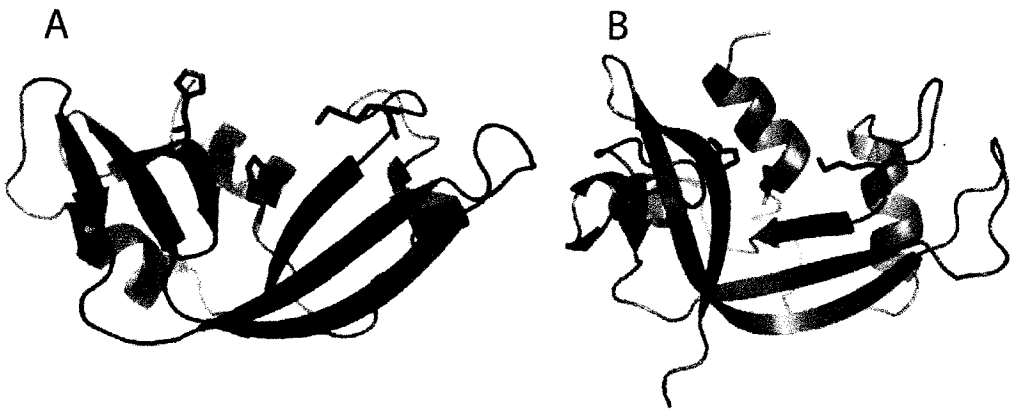

Figure 4.2 Mechanism of ribonuclease cytotoxicity. Ribonucleases bind to the cell surface, are internalized by endocytosis, and translocate across the lipid bilayer to enter the cytosol. RI-evasive RNases degrade intracellular RNA leading to cell death.

Figure 4.2

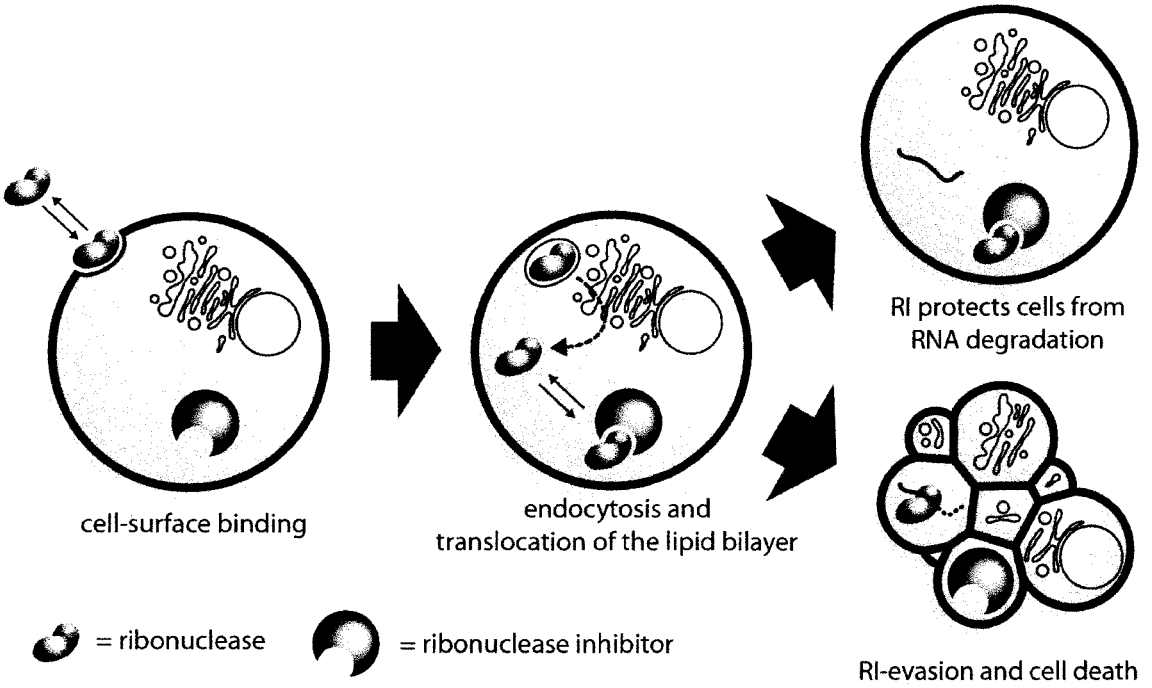
RI protects cells from
RNA degradation
cell-surface binding
endocytosis and
translocation of the lipid bilayer
= ribonuclease
= ribonuclease inhibitor
RI-evasion and cell death

Figure 4.3 Effect of ribonucleases on the proliferation of K-562 cells. Cells were incubated in the presence of ribonucleases for 24 h, followed by a 4 h pulse with [*methyl*-^{3}H]thymidine (0.20 μCi/well). Results show the percentage of [*methyl*-^{3}H]thymidine incorporation compared to PBS controls and represent the average of at least three measurements at each concentration.

Figure 4.3

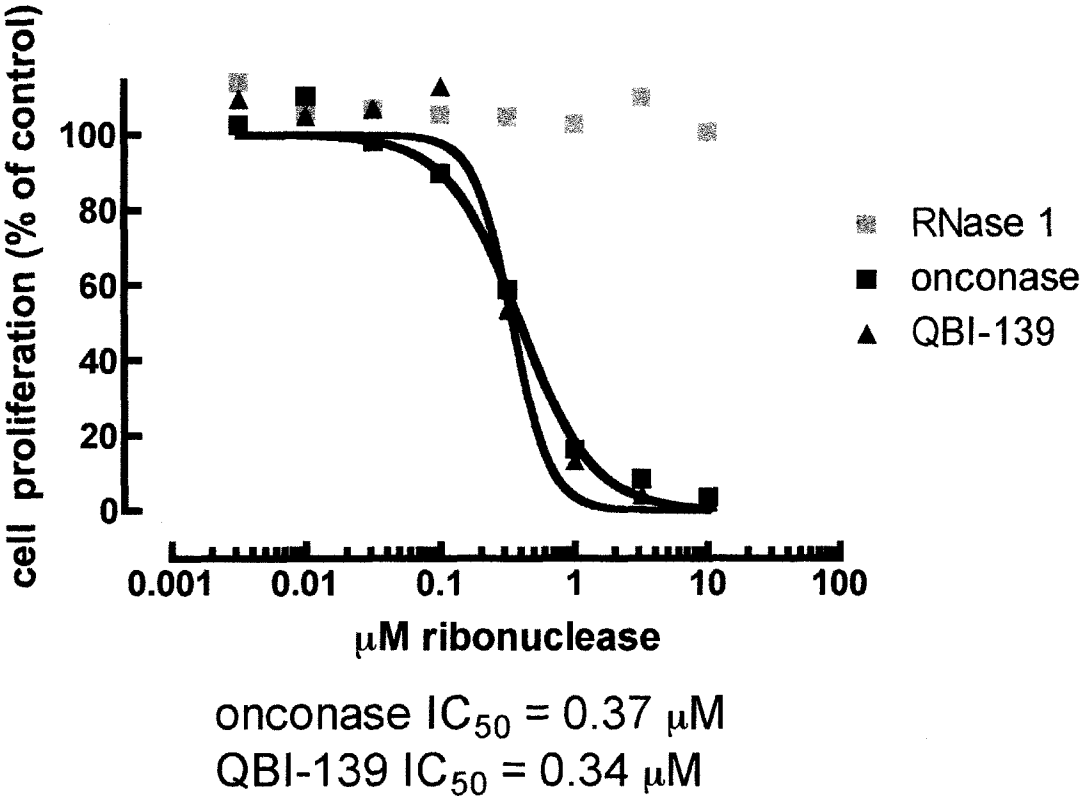
cell proliferation (% of control)
100
80
60
40
20
0
0.001
0.01
0.1
1
10
100
μM ribonuclease
RNase 1
onconase
QBI-139
onconase IC50 = 0.37 μM
QBI-139 IC50 = 0.34 μM

Figure 4.4 ANOVA-derived *p*-value versus fold-change scatter plots ("volcano plots") for ribonuclease-treated cells. Each data point corresponds to a specific gene probeset.

Figure 4.4

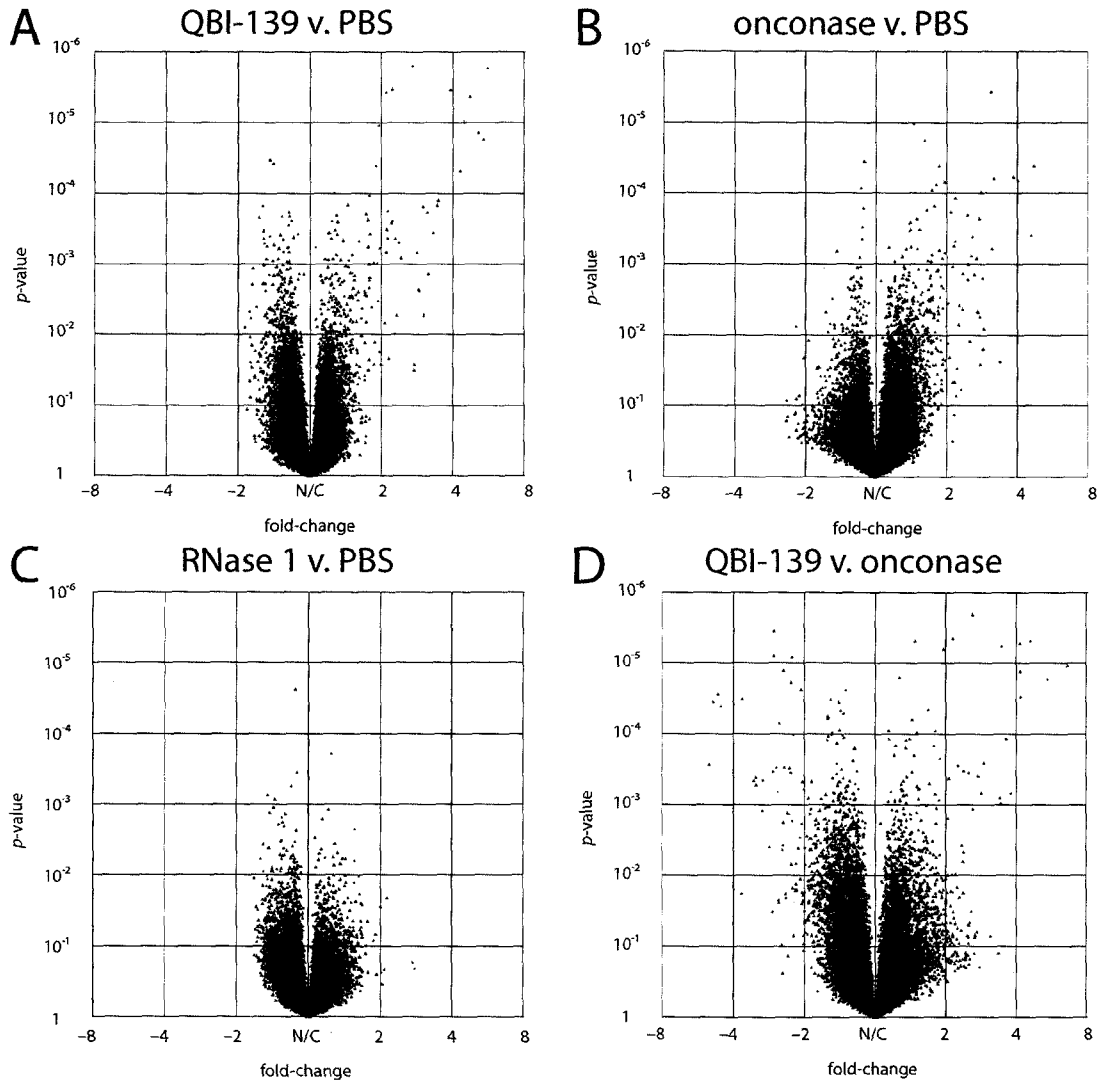
A
QBI-139 v. PBS
B
onconase v. PBS
C
RNase 1 v. PBS
D
QBI-139 v. onconase
p-value
fold-change
N/C
−8
−4
−2
2
4
8
1
10^{-1}
10^{-2}
10^{-3}
10^{-4}
10^{-5}
10^{-6}

Figure 4.5 Protein interaction network of genes differentially regulated by onconase. Red shapes denote genes that were upregulated >2-fold relative to the PBS control and were statistically significant (ANOVA-derived *p*-value <0.05). The diagram was generated by entering the onconase-responsive gene list (>2-fold upregulation and ANOVA-derived *p*-value <0.05) into Ingenuity Pathway Analysis software.

Figure 4.5

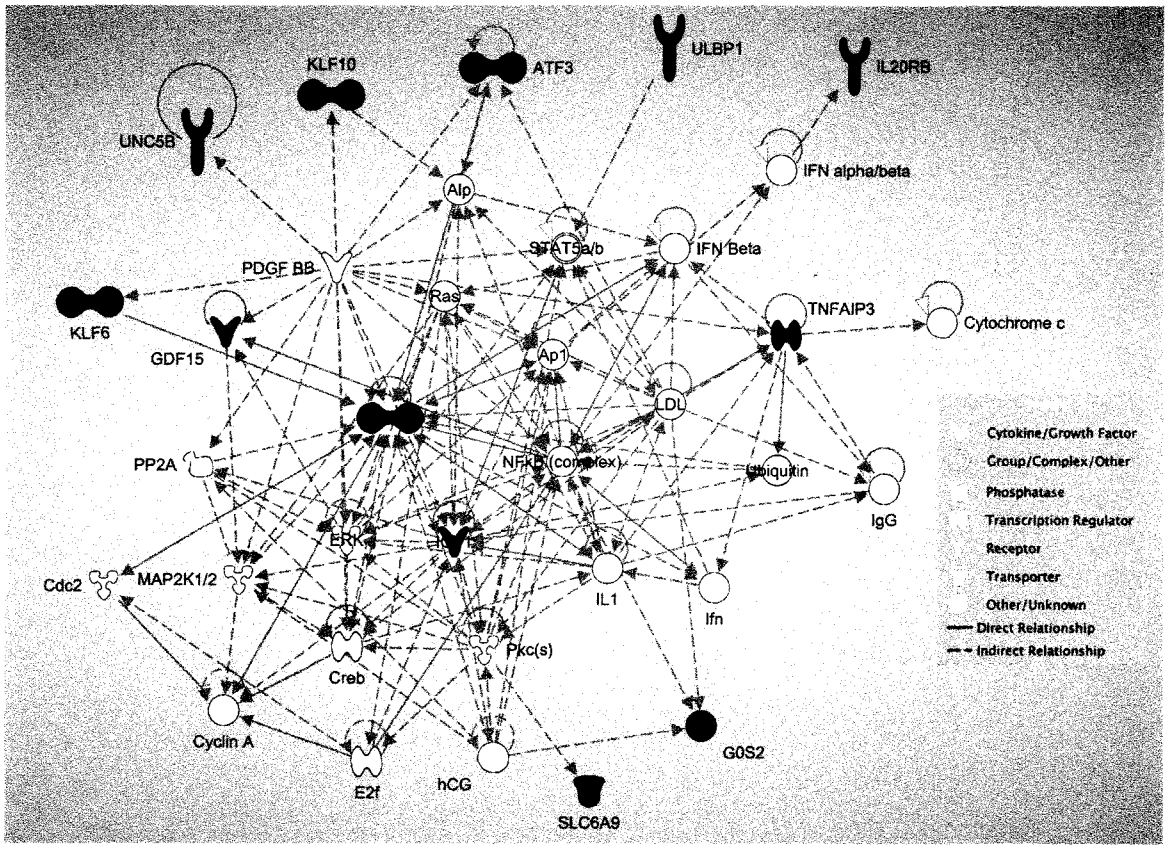
KLF10
ATF3
ULBP1
IL20RB
UNC5B
IFN alpha/beta
Alp
STAT5a/b
IFN Beta
PDGF BB
Ras
TNFAIP3
Cytochrome c
KLF6
GDF15
Ap1
LDL
PP2A
NFkB (complex)
Ubiquitin
IgG
ERK
Cdc2
MAP2K1/2
IL1
Ifn
Pkc(s)
Creb
Cyclin A
G0S2
E2f
hCG
SLC6A9
Cytokine/Growth Factor
Group/Complex/Other
Phosphatase
Transcription Regulator
Receptor
Transporter
Other/Unknown
Direct Relationship
Indirect Relationship

Figure 4.6 Protein interaction network of genes differentially regulated by QBI-139. Red shapes denote genes or gene families that were upregulated >2-fold relative to the PBS control and were statistically significant (ANOVA-derived *p*-value <0.05). The diagram was generated by entering the QBI-139-responsive gene list (>2-fold upregulation and ANOVA-derived *p*-value <0.05) into Ingenuity Pathway Analysis software.

Figure 4.6

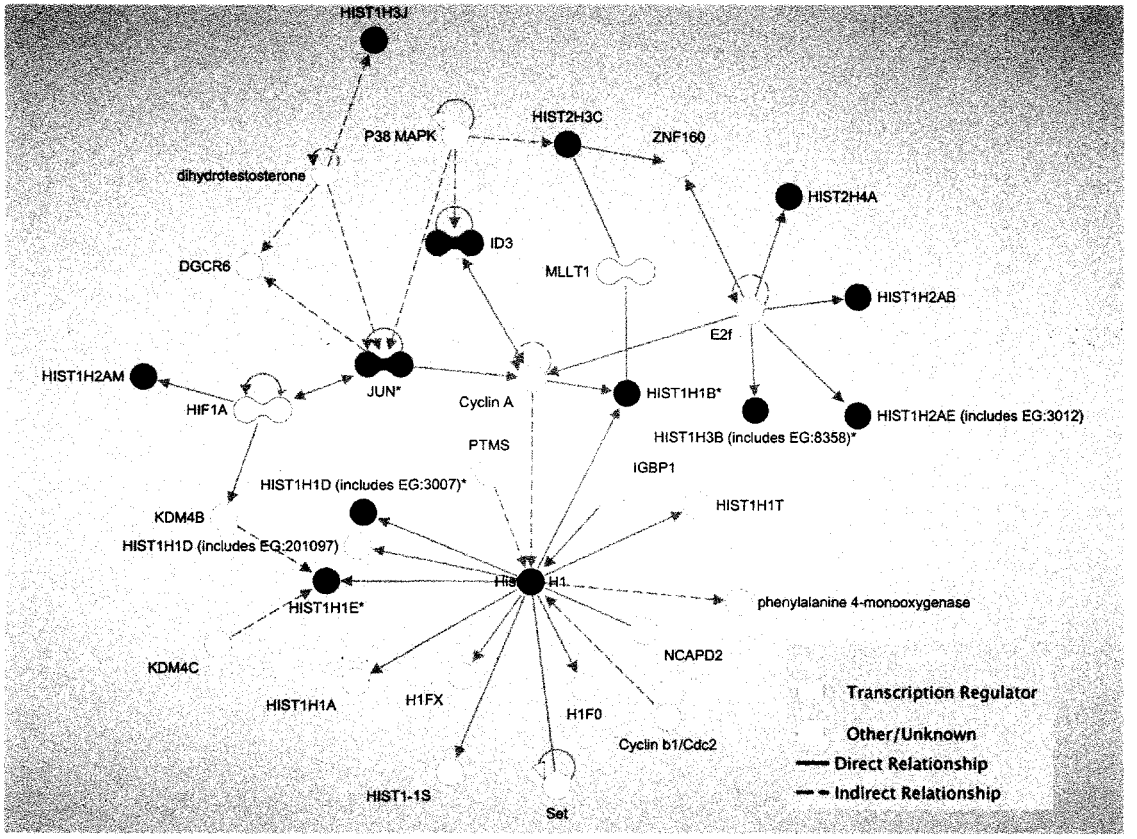
HIST1H3J
P38 MAPK
HIST2H3C
ZNF160
dihydrotestosterone
HIST2H4A
ID3
DGCR6
MLLT1
HIST1H2AB
E2f
HIST1H2AM
JUN*
Cyclin A
HIST1H1B*
HIF1A
HIST1H2AE (includes EG:3012)
HIST1H3B (includes EG:8358)*
PTMS
IGBP1
HIST1H1D (includes EG:3007)*
HIST1H1T
KDM4B
HIST1H1D (includes EG:201097)
HIST1H1E*
phenylalanine 4-monooxygenase
KDM4C
NCAPD2
HIST1H1A
H1FX
H1F0
Cyclin b1/Cdc2
HIST1-1S
Set
Transcription Regulator
Other/Unknown
Direct Relationship
Indirect Relationship

Figure 4.7 ANOVA-derived *p*-value versus fold-change scatter plots ("volcano plots") for ribonuclease-treated cells. Blue triangles represent histone mRNA probe sets.

Figure 4.7

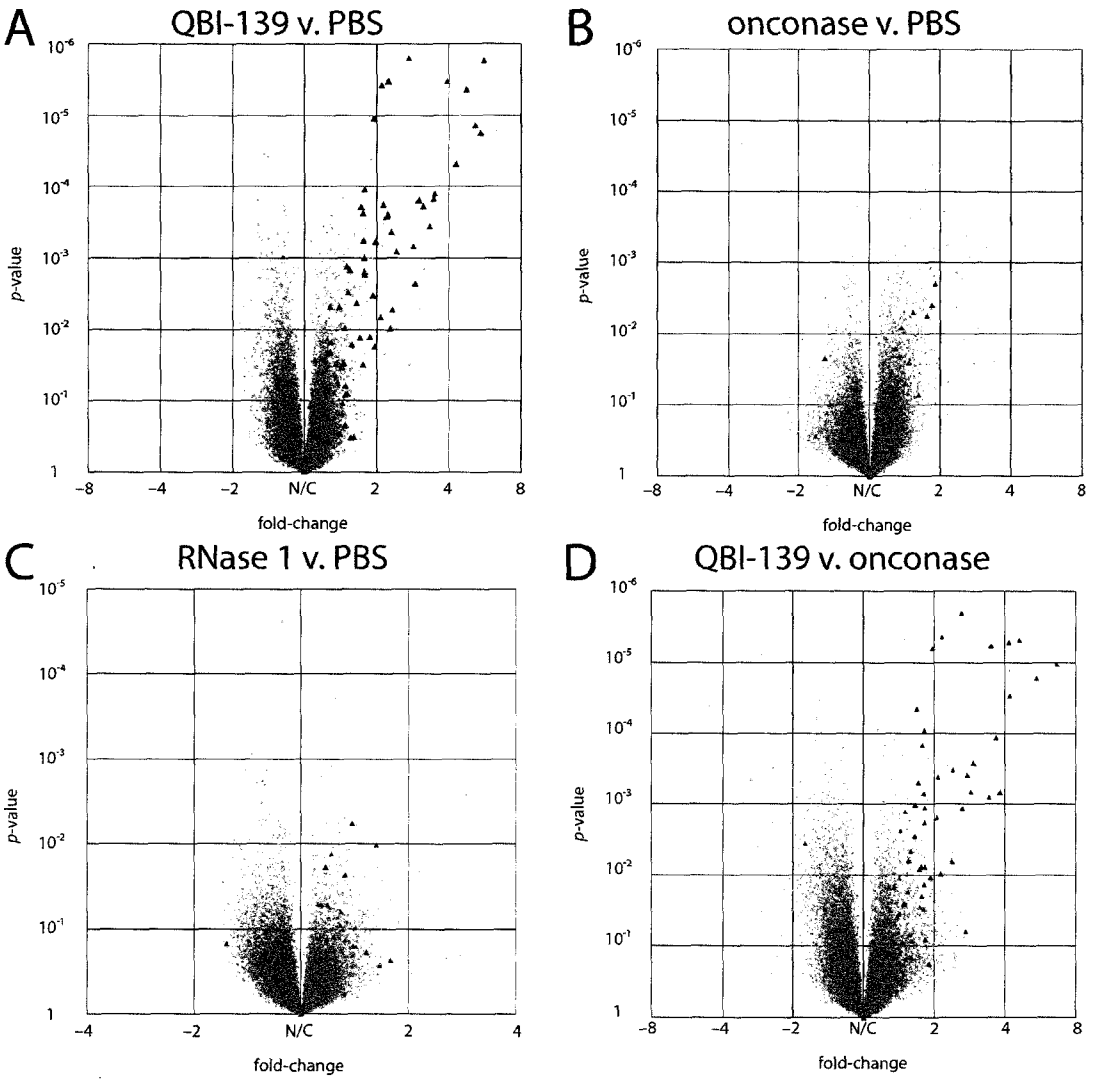
A
QBI-139 v. PBS
B
onconase v. PBS
C
RNase 1 v. PBS
D
QBI-139 v. onconase
p-value
fold-change
N/C

Figure 4.8 Quantitative real-time PCR from cDNA constructed using random and oligo(dT) primers. Microarray data from cDNA derived from oligo(dT) primers suggests that DDIT4 and IL-20 are upregulated in onconase-treated cells, while HIST1H1E and HIST1H2AE were upregulated in QBI-139-treated cells.

Figure 4.8

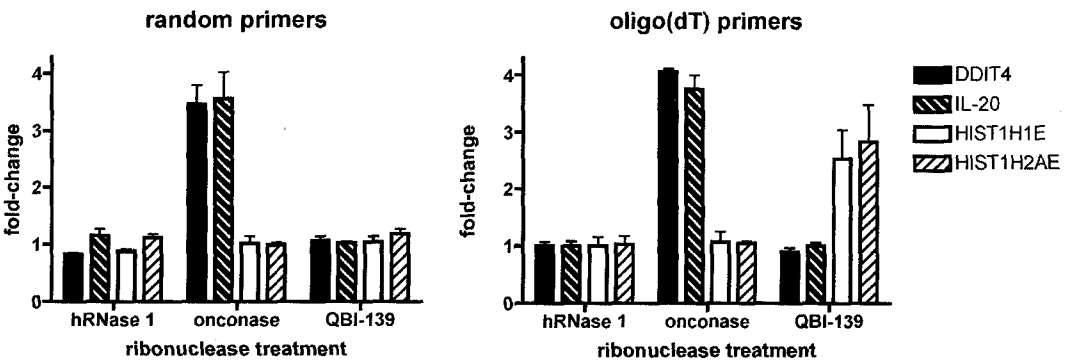
random primers
oligo(dT) primers
fold-change
0
1
2
3
4
hRNase 1
onconase
QBI-139
ribonuclease treatment
DDIT4
IL-20
HIST1H1E
HIST1H2AE

Figure 4.9 Sequences of cDNA derived from chimeric histone mRNAs as identified by 3′ RACE. RNA was isolated from PBS- and QBI-139-treated cells.

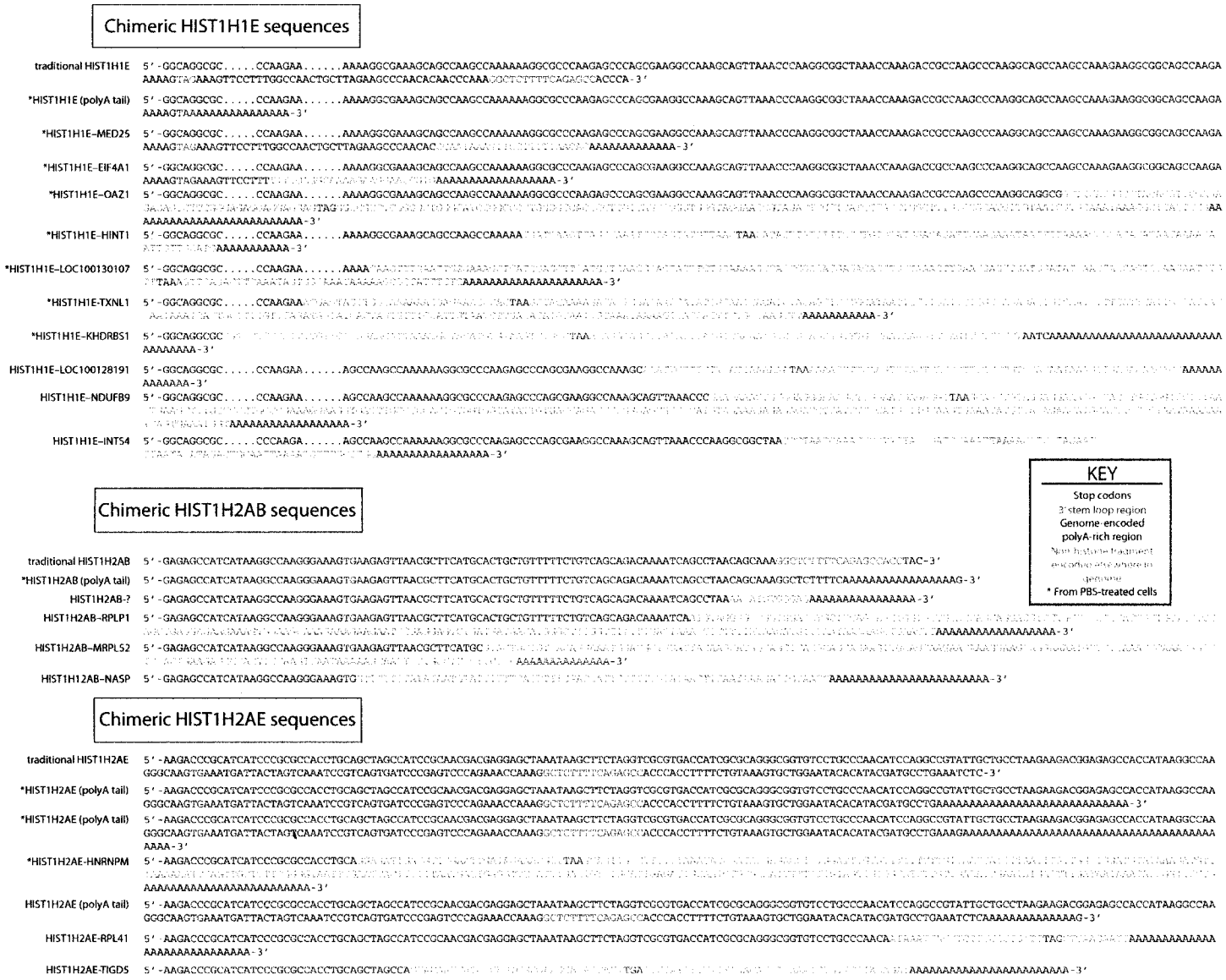
Chimeric HIST1H1E sequences
traditional HIST1H1E
*HIST1H1E (polyA tail)
*HIST1H1E–MED25
*HIST1H1E–EIF4A1
*HIST1H1E–OAZ1
*HIST1H1E–HINT1
*HIST1H1E–LOC100130107
*HIST1H1E–TXNL1
*HIST1H1E–KHDRBS1
HIST1H1E–LOC100128191
HIST1H1E–NDUFB9
HIST1H1E–INTS4
Chimeric HIST1H2AB sequences
traditional HIST1H2AB
*HIST1H2AB (polyA tail)
HIST1H2AB-?
HIST1H2AB–RPLP1
HIST1H2AB–MRPL52
HIST1H12AB–NASP
Chimeric HIST1H2AE sequences
traditional HIST1H2AE
*HIST1H2AE (polyA tail)
*HIST1H2AE (polyA tail)
*HIST1H2AE–HNRNPM
HIST1H2AE (polyA tail)
HIST1H2AE–RPL41
HIST1H2AE-TIGD5
KEY
Stop codons
3' stem loop region
Genome-encoded
polyA-rich region
Non-histone fragment
encoded elsewhere
in genome
* From PBS-treated cells

Figure 4.9

CHAPTER 5

Future directions

5.1 Additional utility of membrane-permeant affinity labels

In CHAPTER 2, we demonstrated the use of a urea–rhodamine affinity label that enables the facile, rapid labeling of a HaloTag® fusion protein in live cells.

The rapid labeling now possible with probe **1** should prove useful in pulse-chase experiments, which require differential labeling of temporally disparate pools of protein. Probe **1** may allow increased temporal resolution when used in conjunction with a cell-permeable red fluorophore that is already available commercially (HaloTag® TMRDirect™ Ligand, Promega).

Additionally, the utility of this probe can be expanded to include other affinity labeling systems. Because the synthesis of the urea–rhodamine label is modular, a separate bioreactive handle may be used in place of the chloroalkane. In particular, a diverse assortment of amines can be conjugated to probe **10** with ease.

This attribute may prove especially advantageous in the SNAP- and CLIP-tag labeling systems (Keppler *et al.*, 2004) that allow for two separate fusion proteins to be labeled in a single cell.

5.2 Further investigations of *trans*-splicing

In CHAPTER 4, we demonstrated that treatment of K-562 cells with QBI-139 results in an apparent increase of polyadenylated histone mRNAs. This observation may have been possible only because eukaryotic histone mRNAs are not usually polyadenylated (Marzluff *et al.*, 2008) (although there is evidence of polyadenylated histone mRNAs in *Caenorhabditis elegans* (Mangone *et al.*, 2010)) and thus a small increase in *trans*-splicing resulted in a relatively large increase of polyadenylated histones. Of note,

however, our experiments do not distinguish between a global increase in *trans*-splicing and a histone-specific increase.

RNA-seq (Wang *et al.*, 2009) is likely the best tool to distinguish between a histone-specific and a global increase in *trans*-splicing. RNA-seq could provide us with nucleotide resolution, whereas our microarray analysis is limited by the decreased resolution provided by hybridization techniques. These data may distinguish definitively between global and histone-specific changes.

If QBI-139 treatment results in a large increase in global *trans*-splicing, mammalian ribonucleases may become very useful reagents in *trans*-splicing experiments.

Interestingly, in K-562 cells, equal concentrations of QBI-139 and onconase did not elicit similar transcriptional responses, although they behave nearly identically in a cell-proliferation assay. The reasons for this disparity are unclear, but several experiments may shed additional light.

The different cellular responses to QBI-139 and onconase may be due to differing kinetics. That is, the cellular response to onconase at one timepoint may resemble more closely the cellular response to QBI-139 at a later point of time (or vice versa). Microarray, qPCR, and RNA-seq analysis of RNA harvested at various timepoints after treatment may help explain the existing disparity. Analogous experiments varying ribonuclease concentration may also provide increased clarity.

Also, it is not yet clear that all tumor cells will respond in the same fashion as K-562 cells. A repetition of the work in CHAPTER 4 with different cancer cell lines would provide important information about the generality of this response.

Likely, further research into the routing, translocation, and intracellular substrate specificity will likely be needed to explain fully the different cellular responses to onconase and QBI-139 treatment.

APPENDIX

Search for protein interaction partners

of ribonuclease inhibitor protein

A.1 Abstract

Ribonuclease inhibitor protein binds adventitiously internalized ribonucleases with 1:1 stoichiometry and renders them inactive. Although the role of ribonuclease inhibitor protein as an intracellular sentry is well established, several observations suggest additional biological roles. Here, I describe attempts to shed light on the biological role of ribonuclease inhibitor protein by determining additional protein interaction partners.

A.2 Introduction

Mammalian ribonuclease inhibitor protein (RI) is a 50-kDa cytosolic protein that binds secretory ribonucleases in a 1:1 ratio with very high affinity ($K_d \sim 10^{-15}$ M) and renders them inactive (Hofsteenge, 1997; Dickson *et al.*, 2005). RI is composed almost entirely of leucine-rich repeats (Kobe and Deisenhofer, 1994), which give it a remarkable horseshoe shape (Papageorgiou *et al.*, 1997). These repeats are known to foster protein–protein interactions by displaying large surface areas for protein binding (Kobe and Deisenhofer, 1994).

The biological role(s) of RI are not understood fully. Clearly, ribonuclease inhibitor protein acts as an intracellular sentry (Haigis *et al.*, 2003; Dickson *et al.*, 2005), protecting cytosolic RNA from degradation by adventitiously internalized secretory ribonucleases. This role, however, does not fully account for several observations. First, RI is found exclusively within cells, yet all known high affinity ligands for RI are secreted proteins. This paradox, in conjunction with the relatively high concentration (~4 μM, ~0.1% of cytosolic protein) of RI (Haigis *et al.*, 2003) within the cytosol (much higher than would be anticipated to merely inactivate adventitiously internalized

ribonucleases) suggests additional role(s) (Rutkoski and Raines, 2008). Moreover, RI is found in all cell types studied to date, even red blood cells, which are essentially devoid of RNA to protect (Nadano *et al.*, 1995; Moenner *et al.*, 1998). Furthermore, the interaction of RI with the neovascularization-inducing ribonuclease angiogenin is one of the tightest known interactions in all of biology (Chen and Shapiro, 1997), yet an anti-angiogenic role for ribonuclease inhibitor protein, although documented (Dickson *et al.*, 2009), is not well understood. Finally, RI has an uncommonly high percentage of cysteine residues and is quite susceptible to oxidative inactivation through cooperative disulfide bond formation (Fominaya and Hofsteenge, 1992; Kim *et al.*, 1999).

Several alternative/additional roles have been proposed to account for these observations. Some have advanced that RI monitors the oxidative state of a cell and/or protects it from oxidation (Blázquez *et al.*, 1996; Cui *et al.*, 2003; Monti *et al.*, 2007). Others have suggested that RI antagonizes angiogenesis (Dickson *et al.*, 2005; Dickson *et al.*, 2009). The presence of RI in erythrocytes has also led to the hypothesis that RI plays a role in the differentiation of red blood cells (Moenner *et al.*, 1998).

Clearly, further investigation is needed to decipher the true function(s) of RI within a cell. Determining the protein interaction partners of ribonuclease inhibitor protein may help answer important unanswered questions: Why has the K_d value of the RI·ribonuclease complex evolved to be so low? What is the fate of the bound complex? Is RI localized to a specific location within the cytosol? Why is RI so sensitive to oxidation? I anticipate that answers to these and related questions will both further basic science and help in the development of ribonuclease-based chemotherapeutic agents.

interest is fused to the DNA-binding domain of a transcription factor (known as the "bait" protein), and a library of potential interaction partners is fused to the activation domain of the transcription factor ("prey" protein).

A prey vector is then introduced into a yeast strain containing the bait vector. Binding of the prey protein to the bait protein brings together the activation and DNA-binding domains of the transcription factor and activates expression of a downstream reporter gene (Figure A.1).

I submitted the cDNA sequence of human RI to the Molecular Interaction Facility (MIF) at UW–Madison for a yeast two-hybrid screen (Table A.1). Human RI bait fused to the GAL4 DNA binding domain was screened against a combined brain/testes cDNA library (human library B). Four proteins were identified as putative interaction partners (Table A.1).

A.4 Experimental

A.4.1 Crosslinking with photo-leucine

L-Photo-leucine was synthesized according to a published procedure (Suchanek *et al.*, 2005). The amino acid was incorporated into HeLa cells by incubating 4 μM *L*-photo-leucine in DMEM devoid of leucine for 24 h. Cells were then placed in a photochamber and exposed to UV light for 20 min. RI was subsequently immunoprecipitated from HeLa cell lysates and then electrophoresed. After silver staining of the gel, isolated bands were submitted for trypsin digestion and mass-spectrometry. However no human

proteins were identified by mass spectrometry, perhaps due the large background of antibody proteins.

A.4.2 Yeast two-hybrid screen

A yeast two-hybrid (Y2H) screen (Fields and Song, 1989) was performed in the Molecular Interaction Facility (MIF) at the University of Wisconsin–Madison according to their protocols. MIF uses yeast strains developed by Phillip James (James *et al.*, 1996). A combined brain/testes human library is in pACT and pACT2 (Durfee *et al.*, 1993) or pGAD-T7Rec (Clonetech, Mountain View, CA) prey vectors.

DNA encoding the full-length sequence of the human ribonuclease inhibitor protein was cloned in-frame with the GAL4 DNA-binding domain of bait vector pBUTE (a kanamycin-resistant version of GAL4 bait vector pGBDUC1 (James *et al.*, 1996)). The resulting bait vector was sequenced to confirm an in-frame fusion, then transformed into mating type A of strain PJ694 and tested for autoactivation of the β-galactosidase reporter gene.

The Y2H screen was conducted using a human brain/testes cDNA library. Approximately 18 million clones were screened via mating. Controls included medium only, empty prey (activation domain) vector (pGADC1) (James *et al.*, 1996), prey construct expressing mouse epsin, prey construct expressing human Fbox3, and two premated interaction pairs: SH3:SOS and EH:Epsin. Following selection, nine yeast wells tested positive for interaction (via selection on histidine drop-out medium containing 1 mM 3-amino-1,2,4-triazole (3AT) and a β-galactosidase assay). Prey plasmids were re-transformed into the alpha mating type of PJ694 and validated in a

A.3 Results and Discussion

A.3.1 Crosslinking of RI-interaction partners with a photoactivatable leucine analogue

Since RI contains many leucine residues, I synthesized a photoactivatable leucine analogue (Suchanek *et al.*, 2005) that can be incorporated naturally into the proteins of live cells to enable identification of protein interaction partners by photocrosslinking. The photoactivatable amino acid was added to mammalian cells in culture medium devoid of leucine. Under such conditions, the amino acid escapes the stringent identity control of the mammalian translation machinery and is incorporated naturally into cellular proteins (Suchanek *et al.*, 2005). I then exposed the cells to UV light, which generates a reactive carbene that crosslinks protein interaction partners. Control experiments showed that the photo-leucine reagent crosslinks the dimerized EEA1 (Simonsen *et al.*, 1998; Suchanek *et al.*, 2005) protein by immunoblot.

In an attempt to identify proteins that interact with RI, I irradiated photo-leucine treated cells with UV light and then immunoprecipitated the RI. The immunoprecipitate was electrophoresed and silver stained. Although several bands were visible, attempts to identify the crosslinked proteins by mass spectrometry (in-gel digest) were unsuccessful. This reagent may, however, prove useful to confirm the interaction of RI with candidate interaction partners identified by other means.

A.3.2 Yeast two-hybrid screen with RI as bait

Yeast two-hybrid screening uses the modular nature of transcription factors to discover protein-protein interactions (Fields and Song, 1989). In general, the protein of

Table A.1 Putative protein-interaction partners of RI identified from a yeast two-hybrid screen.

Protein	Blast ID	Putative function
GABARAPL2	NM_007285.6, Homo sapiens GABA (A) receptor-associated protein-like 2	Marker of autophagy
Clusterin	NM_0018321.2, Homo sapiens clusterin (CLU), transcript variant 1, mRNA	Chaperone
RCC2	NM_018715.1, Homo sapiens regulator of chromosome condensation 2 (RCC2) mRNA	Guanine nucleotide exchange factor that helps kinetechore associate with microtubules
SCARF1	NM_003693.2, Homo sapiens scavenger receptor class F, member 1 (SCARF1)	Membrane receptor that internalizes low density lipoproteins

REFERENCES

Figure A.1 Yeast two-hybrid screen with RI as bait.

Advanced Chemical Development. www.acdlabs.com/physchemsuite. 29 April 2009

Allende, J. E. and Richards, F. M. (1962). The action of trypsin on ribonuclease S. *Biochemistry* **1**, 295-304.

Altomare, D. A., Rybak, S. M., Pei, J., Maizel, J., Cheung, M., Testa, J. and Shogen, K. (2010). Onconase responsive genes in human mesothelioma cells: implications for an RNA damaging therapeutic agent. *BMC Cancer* **10**, 1-12.

Amsberry, K. L. and Borchardt, R. T. (1990). The lactonization of 2'-hydroxyhydrocinnamic acid amides: a potential prodrug for amines. *J. Org. Chem.* **55**, 5867-5877.

Anfinsen, C. B. (1973). Principles that govern the folding of protein chains. *Science* **181**, 223-230.

Anfinsen, C. B., Haber, E., Sela, M. and White, F. H., Jr. (1961). The kinetics of formation of native ribonuclease during oxidation of the reduced polypeptide chain. *Proc. Natl. Acad. Sci. USA* **47**, 1309-1314.

Ardelt, W., Mikulski, S. M. and Shogen, K. (1991). Amino acid sequence of an anti-tumor protein from *Rana pipiens* oocytes and early embryos. *J. Biol. Chem.* **266**, 245-251.

Backer, M. V., Gaynutdinov, T. I., Aloise, R., Przekop, K. and Backer, J. M. (2002). Engineering S-protein fragments of bovine ribonuclease A for targeted drug delivery. *Protein Expr. Purif.* **26**, 455-461.

Backer, M. V., Patel, V., Jehning, B. T. and Backer, J. M. (2006). Self-assembled "Dock and Lock" system for linking payloads to targeting proteins. *Bioconjug. Chem.* **17**, 912-919.

Beintema, J. J. (1987). Structure, properties and molecular evolution of pancreatic-type ribonucleases. *Life Chem. Rep.* **4**, 333-389.

Beintema, J. J., Breukelman, H. J., Carsana, A. and Furia, A. (1997). Evolution of vertebrate ribonucleases: Ribonuclease A superfamily. In *Ribonucleases: Structures and Functions*, (eds G. D'Alessio and J. F. Riordan), pp. 245-269. New York: Academic Press.

Beintema, J. J., Hofsteenge, J., Iwama, M., Morita, T., Ohgi, K., Irie, M., Sugiyama, R. H., Schieven, G. L., Dekker, C. A. and Glitz, D. G. (1988a). Amino acid sequence of the nonsecretory ribonuclease of human urine. *Biochemistry* **27**, 4530-4538.

Beintema, J. J., Schüller, C., Irie, M. and Carsana, A. (1988b). Molecular evolution of the ribonuclease superfamily. *Prog. Biophys. Molec. Biol.* **51**, 165-192.

Benner, S. A. and Alleman, R. K. (1989). The return of pancreatic ribonucleases. *Trends Biochem. Sci.* **14**, 396-397.

Blake, C. C. F., Koenig, D. F., Mair, G. A., North, A. C. T., Phillips, D. C. and Sarma, V. R. (1965). Structure of hen egg-white lysozyme. *Nature* **206**, 757-761.

Blázquez, M., Fominaya, J. M. and Hofsteenge, J. (1996). Oxidation of sulfhydryl groups of ribonuclease inhibitor in epithelial cells is sufficient for its intracellular degradation. *J. Biol. Chem.* **271**, 18638-18642.

Boix, E., Wu, Y., Vasandani, V. M., Saxena, S. K., Ardelt, W., Ladner, J. and Youle, R. J. (1996). Role of the N terminus in RNase A homologues: Differences in catalytic activity, ribonuclease inhibitor interaction and cytotoxicity. *J. Mol. Biol.* **257**, 992-1007.

Bolstad, B. M., Irizarry, R. A., Astrand, M. and Speed, T. P. (2003). A comparison of normalization methods for high density oligonucleotide array data based on variance and bias. *Bioinformatics* **19**, 185-193.

Borchardt, R. T. and Cohen, L. A. (1972). Stereopopulation control. II. Rate enhancement of intramolecular nucleophilic displacement. *J. Am. Chem. Soc.* **94**, 9166-9174.

Bravo, J., Fernández, E., Ribó, M., de Llorens, R. and Cuchillo, C. M. (1994). A versatile negative-staining ribonuclease zymogram. *Anal. Biochem.* **219**, 82-86.

Brems, D. N. and Baldwin, R. L. (1984). Amid proton exchange used to monitor the formation of a stable alpha-helix by residues 3 to 13 during folding of ribonuclease S. *J. Mol. Biol* **180**, 1141-1156.

Cecchini, D. J., Ehrat, M. and Giese, R. W. (1986). Substrate–leash amplification of ribonuclease activity. *J. Am. Chem. Soc.* **108**, 7841-7843.

Chalfie, M. and Kain, S. R. (2006). Green Fluorescent Protein: Properties, Applications, and Protocols, 2nd ed. Hoboken, NJ: John Wiley & Sons.

Chalfie, M., Tu, Y., Euskirchen, G., Ward, W. W. and Prasher, D. C. (1994). Green fluorescent protein as a marker for gene expression. *Science* **263**, 802-805.

Chandran, S. S., Dickson, K. A. and Raines, R. T. (2005). Latent fluorophore based on the trimethyl lock. *J. Am. Chem. Soc.* **127**, 1652-1653.

parallel mating and selection assay with the human ribonuclease inhibitor protein bait and the empty bait vector. Four clones were positive, that is, they grew in interaction selection medium and exhibited β-galactosidase activity, and subsequently were identified by sequencing.

β-galactosidase activity was assayed in yeast culture lysed by the addition of yeast protein extraction reagent (Pierce Biotechnology, Rockford, IL) combined with chlorophenylred-β-D-galactopyranoside (Roche, Mannheim, Germany) as a substrate.

A.4.3 Attempts to confirm GABARAPL2-RI interaction

Preliminary immunoprecipitation experiments with HeLa and DU145 cell lysates were carried out with appropriate antibodies (rabbit anti-human ribonuclease inhibitor protein polyclonal antibody, Harlan Laboratories, Madison, WI; mouse anti-GABARAPL2 polyclonal antibody, Abnova, Taipei, Taiwan). These blots did not confirm the interaction, even when authentic GABARAPL2 protein was spiked into cell lysates.

Chao, T.-Y., Lavis, L. D. and Raines, R. T. (2010). Cellular uptake of ribonucleases. *Submitted for publication.*

Chen, C.-Z. and Shapiro, R. (1997). Site-specific mutagenesis reveals differences in the structural bases for tight binding of RNase inhibitor to angiogenin and RNase A. *Proc. Natl. Acad. Sci. USA* **94**, 1761-1766.

Cheruvu, N. P. and Kompella, U. B. (2006). Bovine and porcine transscleral solute transport: influence of lipophilicity and the Choroid-Bruch's layer. *Invest. Ophthalmol. Vis. Sci.* **49**, 333-341.

Cho, S., Beintema, J. J. and Zhang, J. (2005). The ribonuclease A superfamily of mammals and birds: Identifying new members and tracing evolutionary histories. *Genomics* **85**, 208-220.

Connelly, P. R., Varadarajan, R., Sturtevant, J. M. and Richards, F. M. (1990). Thermodynamics of protein – peptide interactions in the ribonuclease S system studied by titration calorimetry. *Biochemistry* **29**, 6108-6114.

Costanzi, J., Sidransky, D., Navon, A. and Goldsweig, H. (2005). Ribonucleases as a novel pro-apoptotic anticancer strategy: Review of the preclinical and clinical data for ranpirnase. *Cancer Invest.* **23**, 643-650.

Cui, X. Y., Fu, P. F., Pan, D. N., Zhao, Y., Zhao, J. and Zhao, B. C. (2003). The antioxidant effects of ribonuclease inhibitor. *Free Radic. Res.* **37**, 1079-1085.

D'Alessio, G., Di Donato, A., Mazzarella, L. and Piccoli, R. (1997). Seminal ribonuclease: The importance of diversity. In *Ribonucleases: Structures and Functions*, (eds G. D'Alessio and J. F. Riordan), pp. 383-423. New York: Academic Press.

Darzynkiewicz, Z., Carter, S. P., Mikulski, S. M., Ardelt, W. J. and Shogen, K. (1988). Cytostatic and cytotoxic effect of Pannon (P-30 Protein), a novel anticancer agent. *Cell Tissue Kinet.* **21**, 169-182.

De Groot, A. S. and Scott, D. W. (2007). Immunogenicity of protein therapeutics. *Trends Immunol.* **28**, 482-490.

Deidda, G., Rossi, N. and Tocchini-Valentini, G. P. (2003). An archael endoribonuclease catalyzes *cis*- and *trans*- nonspliceosomal splicing in mouse cells. *Nat. Biotechnol.* **21**, 1499-1504.

delCardayré, S. B. and Raines, R. T. (1994). Structural determinants of enzymatic processivity. *Biochemistry* **33**, 6031-6037.

delCardayré, S. B., Ribó, M., Yokel, E. M., Quirk, D. J., Rutter, W. J. and Raines, R. T. (1995). Engineering ribonuclease A: Production, purification, and characterization of wild-type enzyme and mutants at Gln11. *Protein Eng.* **8**, 261-273.

Dickson, K. A., Dahlberg, C. L. and Raines, R. T. (2003). Compensating effects on the cytotoxicity of ribonuclease A variants. *Arch. Biochem. Biophys.* **415**, 172-177.

Dickson, K. A., Haigis, M. C. and Raines, R. T. (2005). Ribonuclease inhibitor: Structure and function. *Prog. Nucleic Acid Res. Mol. Biol.* **80**, 349-374.

Dickson, K. A., Kang, D.-K., Kwon, Y. S., Kim, J. C., Leland, P. A., Kim, B.-M., Chang, S.-I. and Raines, R. T. (2009). Ribonuclease inhibitor regulates neovascularization by human angiogenin. *Biochemistry* **48**, 3804-3806.

Doscher, M. S. and Hirs, C. H. W. (1967). The heterogeneity of bovine pancreatic ribonuclease S. *Biochemistry* **6**, 304-312.

Dubos, R. J. and Thompson, R. H. S. (1938). The decomposition of yeast nucleic acid by a heat-resistant enzyme. *J. Biol. Chem.* **124**, 501-510.

Dunn, B. M., DiBello, C., Kirk, K. L., Cohen, L. A. and Chaiken, I. M. (1974). Synthesis, purification, and properties of a semisynthetic ribonuclease S incorporating 4-fluoro-L-histidine at position 12. *J. Biol. Chem.* **249**, 6295-6301.

Durfee, T., Becherer, K., Chen, P. L., Yeh, S. H., Yang, Y., Kilburn, A. E., Lee, W. H. and Elledge, S. J. (1993). The retinoblastoma protein associates with the protein phosphatase type-1 catalytic subunit. *Genes Dev.* **7**, 555-569.

Dyer, K. D. and Rosenberg, H. F. (2006). The RNase A superfamily: Generation of diversity and innate host defense. *Mol. Divers.* **10**, 585-597.

Ehrat, M., Cecchini, D. J. and Giese, R. W. (1986). Substrate–leash amplification with ribonuclease S-peptide and S-protein. *Clin. Chem.* **32**, 1622-1630.

Erlanson, D. A., Braisted, A. C., Raphael, D. R., Randal, M., Stroud, R. M., Gordon, E. M. and Wells, J. A. (2000). Site-directed ligand discovery. *Proc. Natl. Acad. Sci. USA* **97**, 9367-9372.

Fan, F., Jin, S., Amundson, S. A., Tong, T., Fan, W., Zhao, H., Zhu, X., Mazzacurati, L., Li, X., Petrik, K. L. *et al.* (2002). ATF3 induction following DNA damage is regulated by distinct signaling pathways and over-expression of ATF3 protein suppresses cells growth. *Oncogene* **49**, 7488-7496.

Fields, S. and Song, O. (1989). A novel genetic system to detect protein-protein interactions. *Nature* **20**, 245-246.

Findlay, D., Herries, D. G., Mathias, A. P., Rabin, B. R. and Ross, C. A. (1961). The active site and mechanism of action of bovine pancreatic ribonuclease. *Nature* **190**, 781-784.

Fominaya, J. M. and Hofsteenge, J. (1992). Inactivation of ribonuclease inhibitor by thiol–disulfide exchange. *J. Biol. Chem.* **267**, 24655-24660.

Futami, J., Tada, H., Seno, M., Ishikami, S. and Yamada, H. (2000). Stabilization of human RNase 1 by introduction of a disulfide bond between residues 4 and 118. *J. Biochem.* **128**, 245-250.

Gaidamakova, E. K., Backer, M. V. and Backer, J. M. (2001). Molecular vehicle for target-mediated delivery of therapeutics and diagnostics. *J. Controlled Release* **74**, 341-347.

Gaynutdinov, T. I., Myshkin, E., Backer, J. M. and Backer, M. V. (2003). Chimeric ribonuclease as a source of human adaptor protein for targeted drug delivery. *Protein Eng.* **16**, 771-775.

Gilmanshin, R., Van Beek, J. and Callender, R. (1996). Study of the ribonuclease S-peptide/S-protein complex by means of raman difference spectroscopy. *J. Phys. Chem* **100**, 16754-16760.

Goldberg, J. M. and Baldwin, R. L. (1998). Kinetic mechanism of a partial folding reaction. 1. Properties of the reaction and effects of denaturants. *Biochemistry* **37**, 2546-2555.

Gonzalez, T. N., Sidrauski, C., Dorfler, S. and Walter, P. (1999). Mechanism of non-spliceosomal mRNA splicing in the unfolded protein response pathway. *EMBO J.* **18**, 3119-3132.

Griffin, A., Adams, S. R., Jones, J. and Tsien, R. Y. (2000). Fluorescent labeling of recombinant proteins in living cells with FlAsH. *Methods Enzymol.* **327**, 565-578.

Gutte, B. and Merrifield, R. B. (1971). The synthesis of ribonuclease A. *J. Biol. Chem.* **246**, 1922-1941.

Haigis, M. C., Kurten, E. L. and Raines, R. T. (2003). Ribonuclease inhibitor as an intracellular sentry. *Nucleic Acids Res.* **31**, 1024-1032.

Halicka, H. D., Murakami, T., Papageorgio, C. N., Mittelman, A., Mikulski, S. M., Shogen, K. and Darzynkiewicz, Z. (2000). Induction of differentiation of leukaemic (HL-60) or prostate cancer (LNCaP, JCA-1) cells potentiates apoptosis triggered by onconase. *Cell Prolif.* **33**, 407-417.

Hearn, R. P., Richards, F. M., Sturtevant, J. M. and Watt, G. D. (1971). Thermodynamics of the binding of S-peptide to S-protein to form ribonuclease S'. *Biochemistry* **10**, 806-816.

Hirschmann, R., Nutt, R. F., Veber, D. F., Vitali, R. A., Varga, S. L., Jacob, T. A., Holly, F. W. and Denkewalter, R. G. (1969). Studies on the total synthesis of an enzyme. V. The preparation of enzymatically active material. *J. Am. Chem. Soc.* **91**, 507-508.

Hofsteenge, J. (1997). Ribonuclease inhibitor. In *Ribonucleases: Structures and Functions*, (eds G. D'Alessio and J. F. Riordan), pp. 621-658. New York: Academic Press.

Huang, S. T. and Lin, Y. L. (2006). New latent fluorophore for DT diaphorase. *Org. Lett.* **8**, 265-268.

Ioffe, I. S. and Otten, V. F. (1965). Rhodamine dyes and compounds related to them. XIV. Interconversion of the colorless and colored forms of rhodamine and rhodol. *Zh. Obshch. Khim* **1**, 333-336.

Irizarry, R. A., Hobbs, B., Collin, F., Beazer-Barclay, Y., D, Antonellis, K. J., Scherf, U. and Speed, T. P. (2003). Exploration, normalization, and summaries of high density oligonucleotide array probe level data. *Biostatistics* **4**, 249-264.

James, P., Halladay, J. and Craig, E. A. (1996). Genomic libraries and a host strain designed for highly efficient two-hybrid selection in yeast. *Genetics* **144**, 1425-1436.

Johnson, R. J., Chao, T.-Y., Lavis, L. D. and Raines, R. T. (2007a). Cytotoxic ribonucleases: The dichotomy of Coulombic forces. *Biochemistry* **46**, 10308-10316.

Johnson, R. J., McCoy, J. G., Bingman, C. A., Phillips, G. N., Jr. and Raines, R. T. (2007b). Inhibition of human pancreatic ribonuclease by the human ribonuclease inhibitor protein. *J. Mol. Biol.* **367**, 434-449.

Johnsson, K. (2009). Visualizing biochemical activities in living cells. *Nat. Chem. Biol.* **5**, 63-65.

Johnsson, N. and Johnsson, K. (2007). Chemical tools for biomolecular imaging. *ACS Chem. Biol.* **2**, 31-38.

Jones, W. (1920). The action of boiled pancreas extract on yeast nucleic acid. *J. Am. Physiol.* **52**, 203-207.

Juan, G., Ardelt, B., Li, X., Mikulski, S. M., Shogen, K., Ardelt, W., Mittelman, A. and Darzynkiewicz, Z. (1998). G1 arrest of U937 cells by onconase is associated with suppression of cyclin D3 expression, induction of p16INK4A, p21WAF1/CIP1 and p27KIP and decreased pRb phosphorylation. *Leukemia* **12**, 1241-1248.

Kartha, G., Bello, J. and Harker, D. (1967). Tertiary structure of ribonuclease. *Nature* **213**, 862-865.

Kato, I. and Anfinsen, C. B. (1969). On the stabilization of ribonuclease S-protein by ribonuclease S-peptide. *J. Biol. Chem.* **244**, 1004-1007.

Kelemen, B. R., Klink, T. A., Behlke, M. A., Eubanks, S. R., Leland, P. A. and Raines, R. T. (1999). Hypersensitive substrate for ribonucleases. *Nucleic Acids Res.* **27**, 3696-3701.

Kendrew, J. C. and Parrish, R. G. (1956). The crystal structure of myoglobin. III. Sperm-whale myoglobin. *Proc. Roy. Soc. London* **A238**, 305-324.

Keppler, A., Pick, H., Arrivoli, C., Vogel, H. and Johnsson, K. (2004). Labeling of fusion proteins with synthetic fluorophores in live cells. *Proc. Natl. Acad. Sci. USA* **101**, 9955-9959.

Kim, B.-M., Schultz, L. W. and Raines, R. T. (1999). Variants of ribonuclease inhibitor that resist oxidation. *Protein Sci.* **8**, 430-434.

Kim, J.-S. and Raines, R. T. (1993). Ribonuclease S-peptide as a carrier in fusion proteins. *Protein Sci.* **2**, 348-356.

Kim, J.-S. and Raines, R. T. (1994a). Peptide tags for a dual affinity fusion system. *Anal. Biochem.* **219**, 165-166.

Kim, J.-S. and Raines, R. T. (1994b). S-Peptide in protein fusion systems: History and significance. *inNovations* **1**, 5-6.

Klink, T. A. and Raines, R. T. (2000). Conformational stability is a determinant of ribonuclease A cytotoxicity. *J. Biol. Chem.* **275**, 17463-17467.

Klink, T. A., Woycechowsky, K. J., Taylor, K. M. and Raines, R. T. (2000). Contribution of disulfide bonds to the conformational stability and catalytic activity of ribonuclease A. *Eur. J. Biochem.* **267**, 566-572.

Kobe, B. and Deisenhofer, J. (1994). The leucine-rich repeat: A versatile binding motif. *Trends Biochem. Sci.* **19**, 415-421.

Kuila, K. and Lahiri, S. C. (2004). Comparison of the macroscopic molecular properties in understanding the structural aspects of mixed aquo-organic binary mixtures. *Z. Phys. Chem.* **218**, 803-828.

Kunitz, M. (1939). Isolation from beef pancreas of a crystalline protein possessing ribonuclease activity. *Science* **90**, 112-113.

Kunitz, M. (1946). A spectrophotometric method for the measurement of ribonuclease activity. *J. Biol. Chem.* **164**, 563-568.

Kunitz, M. and McDonald, M. R. (1953). Ribonuclease. *Biochem. Prep.* **3**, 9-19.

Lampidis, T. J., Castello, C., del Giglio, A., Pressman, B. C., Viallet, P., Trevorrow, K. W., Valet, G. K., Tapiero, H. and Savaraj, N. (1989). Relevance of the chemical charge of rhodamine dyes to multiple drug resistance. *Biochem. Pharmacol.* **38**, 4267-2471.

Lavis, L. D., Chao, T.-Y. and Raines, R. T. (2006a). Fluorogenic label for biomolecular imaging. *ACS Chem. Biol.* **1**, 252-260.

Lavis, L. D., Chao, T.-Y. and Raines, R. T. (2006b). Latent blue and red fluorophores based on the trimethyl lock. *ChemBioChem* **7**, 1151-1154.

Lavis, L. D. and Raines, R. T. (2008). Bright ideas for chemical biology. *ACS Chem. Biol.* **3**, 142-155.

Lee, I., Kalota, A., Gewirtz, A. M. and Shogen, K. (2007). Antitumor efficacy of the cytotoxic RNase, ranpirnase, on A549 human lung cancer xenografts of nude mice. *Anticancer Res.* **27**, 299-307.

Lee, I., Lee, Y. I., Mikulski, S. M. and Shogen, K. (2003). Effect of onconase +/- tamoxifen on ASPC-1 human pancreatic tumors in nude mice. *Adv. Exp. Med. Biol.* **530**, 187-196.

Lee, J. E., Bae, E., Bingman, C. A., Phillips, G. N., Jr. and Raines, R. T. (2008). Structural basis for catalysis by onconase. *J. Mol. Biol.* **374**, 165-177.

Lee, J. E. and Raines, R. T. (2003). Contribution of active-site residues to the function of onconase, a ribonuclease with antitumoral activity. *Biochemistry* **42**, 11443-11450.

Lee, J. E. and Raines, R. T. (2008). Ribonucleases as novel chemotherapeutics: The ranpirnase example. *BioDrugs* **22**, 53-58.

Leland, P. A., Schultz, L. W., Kim, B.-M. and Raines, R. T. (1998). Ribonuclease A variants with potent cytotoxic activity. *Proc. Natl. Acad. Sci. USA* **98**, 10407-10412.

Leland, P. A., Staniszewski, K. E., Kim, B.-M. and Raines, R. T. (2000). A synapomorphic disulfide bond is critical for the conformational stability and cytotoxicity of an amphibian ribonuclease. *FEBS Lett.* **477**, 203-207.

Leland, P. A., Staniszewski, K. E., Kim, B.-M. and Raines, R. T. (2001). Endowing human pancreatic ribonuclease with toxicity for cancer cells. *J. Biol. Chem.* **276**, 43095-43102.

Levine, M. N., Lavis, L. D. and Raines, R. T. (2008). Trimethyl lock: A stable chromogenic substrate for esterases. *Molecules* **13**, 204-211.

Los, G. V., Encell, L. P., McDougall, M. G., Hartzell, D. D., Karassina, N., Zimprich, C., Wood, M. G., Learish, R., Ohana, R. F., Urh, M. *et al.* (2008). HaloTag: A Novel Protein Labeling Technology for Cell Imaging and Protein Analysis. *ACS Chem. Biol.* **3**, 373-382.

Los, G. V. and Wood, K. (2007). The HaloTag: A novel technology for cell imaging and protein analysis. *Methods Mol. Biol.* **356**, 195-208.

Lu, D., Wolfgang, C. D. and Hai, T. (2006). Activating transcription factor 3, a stress-inducible gene, suppresses Ras-stimulated tumorigenesis. *J. Biol. Chem.* **281**, 10473-10481.

Machleidt, T., Robers, M. and Hanson, G. T. (2006). Protein Labeling with FlAsH and ReAsH. In *High Content Screening*, vol. 356, pp. 209-220: Humana Press.

Mangold, S. L., Carpenter, R. T. and Kiessling, L. L. (2008). Synthesis of fluorogenic polymers for visualizing cellular internalization. *Org. Lett.* **10**, 2997-3000.

Mangone, M., Manoharan, A. P., Thierry-Mieg, D., Thierry-Mieg, J., Han, T., Mackowiak, S. D., Mis, E., Zegar, C., Gutwein, M. R., Khivansara, V. *et al.* (2010). The landscape of *C. elegans* 3'UTRs. *Science* **329**, 432-435.

Markert, Y., Köditz, J., Mansfeld, J., Arnold, U. and Ulbrich-Hofmann, R. (2001). Increased proteolytic resistance of ribonuclease A by protein engineering. *Protein Eng.* **14**, 791-796.

Markland, F. S. and Smith, E. L. (1971). Subtilisins: Primary structure, chemical and physical properties. In *The Enzymes, Vol. 3*, (ed. P. D. Boyer), pp. 53-585. New York: Academic Press.

Marshall, G. R. and Feng, J. A. (D.J. Kuster). Back to the future: Ribonuclease A. *Biopolymers* **90**, 259-277.

Marshall, G. R., Feng, J. A. and Kuster, D. J. (2008). Back to the future: Ribonuclease A. *Biopolymers* **90**, 259-277.

Marzluff, W. F., Wagner, E. J. and Duronio, R. J. (2008). Metabolism and regulation of canonical histone mRNAs: life without a poly(A) tail. *Nature Rev. Genet.* **9**, 843-854.

Mei, Y., Yong, J., Liu, H., Shi, Y., Meinkoth, J., Dreyfuss, G. and Yang, X. (2010). tRNA binds to cytochrome c and inhibits caspase activation. *Mol. Cell* **37**, 668-678.

Merrifield, R. B. (1984). Solid phase synthesis. *Science* **232**, 341-347.

Michnick, S. W., Ear, P. H., Manderson, E. N., Remy, I. and Stefan, E. (2007). Universal strategies in research and drug discovery based on protein-fragment complementation assays. *Nat. Rev. Drug Discov.* **6**, 569-582.

Mikulski, S. M., Ardelt, W., Shogen, K., Bernstein, E. H. and Menduke, H. (1990a). Striking increase of survival of mice bearing M109 Madison carcinoma treated with a novel protein from amphibian embryos. *J. Natl. Cancer Inst.* **82**, 151-153.

Mikulski, S. M., Chun, H. G., Mittelman, A., Panella, T., Puccio, C. A., Shogen, K. and Costanzi, J. J. (1995). Relationship between response rate and median survival in patients with advanced non-small cell lung cancer: Comparison of ONCONASE® with other anticancer agents. *Int. J. Oncol.* **6**, 889-897.

Mikulski, S. M., Costanzi, J. J., Vogelzang, N. J., McCachren, S., Taub, R. N., Chun, H., Mittelman, A., Panella, T., Puccio, C., Fine, R. *et al.* (2002). Phase II trial of a single weekly intravenous dose of ranpirnase in patients with unresectable malignant mesothelioma. *J. Clin. Oncol.* **20**, 274-281.

Mikulski, S. M., Grossman, A. M., Carter, P. W., Shogen, K. and Costanzi, J. J. (1993). Phase I human clinical trial of ONCONASE (P-30 Protein) administered intravenously on a weekly schedule in cancer patients with solid tumors. *Int. J. Oncol.* **3**, 57-64.

Mikulski, S. M., Viera, A., Ardelt, W., Menduke, H. and Shogen, K. (1990b). Tamoxifen and trifluoperazine (Stelazine) potentiate cytostatic/cytotoxic effects of P-30 protein, a novel protein possessing anti-tumour activity. *Cell Tissue Kinet.* **23**, 237-246.

Mikulski, S. M., Viera, A., Darzynkiewicz, Z. and Shogen, K. (1992). Synergism between a novel amphibian oocyte ribonuclease and lovastatin in inducing

cytostatic and cytotoxic effects in human lung and pancreatic carcinoma cell lines. *Br. J. Cancer* **66**, 304-310.

Mikulski, S. M., Viera, A., Deptala, A. and Darzynkiewicz, Z. (1998). Enhanced *in vitro* cytotoxicity and cytostasis of the combination of onconase with a proteasome inhibitor. *Int. J. Oncol.* **13**, 633-644.

Milstein, S. and Cohen, L. A. (1972). Stereopopulation control. I. Rate enhancement in the lactonizations of *o*-hydroxyhydrocinnamic acids. *J. Am. Chem. Soc.* **94**, 9158-9165.

Moenner, M., Vosoghi, M., Ryazantsev, S. and Glitz, D. (1998). Ribonuclease inhibitor protein of human erythrocytes: Characterization, loss of activity in response to oxidative stress, and association with Heinz bodies. *Blood Cells Mol. Dis.* **24**, 149-164.

Monnè, L. (1935). Permeability of the nuclear membrane to vital stains. *Proc. Soc. Exp. Biol. Med.* **32**, 1197–1199.

Monti, D. M., Montesano Gesualdi, N., Matoušek, J., Esposito, F. and D'Alessio, G. (2007). The cytosolic ribonuclease inhibitor contributes to intracellular redox homeostasis. *FEBS Lett.* **581**, 930-934.

Moore, S. and Stein, W. H. (1973). Chemical structures of pancreatic ribonuclease and deoxyribonuclease. *Science* **180**, 458-464.

Morón, J. A. and Devi, L. A. (2007). Use of proteomics for the identification of novel drug targets in brain diseases. *J. Neurochem.* **102**, 306-315.

Mosimann, S. C., Ardelt, W. and James, M. N. G. (1994). Refined 1.7 Å X-ray crystallographic structure of P-30 protein, an amphibian ribonuclease with anti-tumor activity. *J. Mol. Biol.* **236**, 1141-1153.

Nadano, D., Yasuda, T., Takeshita, H. and Kishi, K. (1995). Ribonuclease inhibitors in human blood: Comparative studies on the inhibitors detected in erythrocytes, platelelts, mononuclear leukocytes and granulocytes. *Int. J. Biochem. Cell. Biol.* **27**, 971-979.

Nadig, G., Ratnaparkhi, G. S., Varadarajan, R. and Vishveshwara, S. (1996). Dynamics of ribonuclease A and ribonuclease S: Computational and experimental studies. *Protein Sci.* **5**, 2104-2114.

Ning, X., Guo, J., Wolfert, M. A. and Boons, G.-J. (2008). Visualizing metabolically-labeled glycoconjugates of living cells by copper-free and fast Huisgen cycloadditions. *Angew. Chem. Int. Ed.* **47**, 2253-2255.

Nishimoto, N. (2010). Interleukin-6 as a therapeutic target in candidate inflammatory diseases. *Clin. Pharamcol. Ther.* **87**, 483-487.

Notomista, E., Catanzano, F., Graziano, G., Dal Piaz, F., Barone, G., D'Alessio, G. and Di Donato, A. (2000). Onconase: An unusually stable protein. *Biochemistry* **39**, 8711-8718.

Papageorgiou, A., Shapiro, R. and Acharya, K. (1997). Molecular recognition of human angiogenin by placental ribonuclease inhibitor—an X-ray crystallographic study at 2.0 Å resolution. *EMBO J.* **16**, 5162-5177.

Park, C., Schultz, L. W. and Raines, R. T. (2001). Contribution of the active site histidine residues of ribonuclease A to nucleic acid binding. *Biochemistry* **40**, 4949-4956.

Parker, R. and Song, H. (2004). The enzymes and control of eukaryotic mRNA turnover. *Nat. Struct. Mol. Biol.* **11**, 121-127.

Pavlakis, N. and Vogelzang, N. J. (2006). Ranpirnase—an antitumour ribonuclease: Its potential role in malignant mesothelioma. *Expert Opin. Biol. Ther.* **6**, 391-399.

Plainkum, P., Fuchs, S. M., Wiyakrutta, S. and Raines, R. T. (2003). Creation of a zymogen. *Nat. Struct. Biol.* **10**, 115-119.

Potts, J. T., Jr., Young, D. M. and Anfinsen, C. B. (1963). Reconstitution of fully active RNase S by carboxypeptidase-degraded RNase S-peptide. *J. Biol. Chem.* **238**, 2593-2594.

Prasher, D. C., Eckenrode, V. K., Ward, W. W., Prendergast, F. G. and Cormier, M. J. (1992). Primary structure of the *Aequorea victoria* green-fluorescent protein. *Gene* **111**, 229-233.

Raines, R. T. (1998). Ribonuclease A. *Chem. Rev.* **98**, 1045-1065.

Raines, R. T., McCormick, M., Van Oosbree, T. R. and Mierendorf, R. C. (2000). The S·Tag fusion system for protein purification. *Methods Enzymol.* **326**, 362-376.

Ramos-Nino, M. E. and Littenberg, B. (2008). A novel combination: Ranpirnase and rosiglitazone induce a synergistic apoptotic effect by down-regulating FRA-1 and Survivin in cancer cells. *Mol. Cancer Ther.* **7**, 1871-1879.

Ratnaparkhi, G. S. and Varadarajan, R. (2001). Osmolytes stabilize ribonuclease S by stabilizing its fragments S-protein and S-peptide to compact folding-competent states. *J. Biol. Chem.* **276**, 28789-28798.

Richards, F. M. (1958). On the enzymic activity of subtilisin-modified ribonuclease. *Proc. Natl. Acad. Sci. USA* **44**, 162-166.

Richards, F. M. (1992). Linderstrφm-Lang and the Carlsberg Laboratory: The view of a postdoctoral fellow in 1954. *Protein Sci.* **1**, 1721-1730.

Richards, F. M. (1997). Whatever happened to the fun? An autobiographical investigations. *Annu. Rev. Biophys. Biomol. Struct.* **26**, 1-25.

Richards, F. M. and Vithayathil, P. J. (1959). The preparation of subtilisin-modified ribonuclease and the separation of the peptide and protein components. *J. Biol. Chem.* **234**, 1459-1465.

Richards, F. M. and Wyckoff, H. W. (1971). Bovine pancreatic ribonuclease. *The Enzymes* **IV**, 647-806.

Richards, F. M., Wyckoff, H. W. and Allewell, N. M. (1970). The origin of specificity in binding: A detailed example in a protein – nucleic acid interaction. In *The Neurosciences*, (ed. F. O. Schmitt), pp. 901-912. New York: Rockefeller University.

Riordan, J. F. (1997). Structure and function of angiogenin. In *Ribonucleases: Structures and Functions*, (eds G. D'Alessio and J. F. Riordan), pp. 445-489. New York: Academic Press.

Rodriguez, M., Torrent, G., Bosch, M., Rayne, F., Dubremetz, J.-F., Ribó, M., Benito, A., Vilanova, M. and Beaumelle, B. (2007). Intracellular pathway of Onconase that enables its delivery to the cytosol. *J. Cell Sci.* **120**, 1405-1411.

Rutkoski, T. J., Kurten, E. L., Mitchell, J. C. and Raines, R. T. (2005). Disruption of shape-complementarity markers to create cytotoxic variants of ribonuclease A. *J. Mol. Biol.* **354**, 41-54.

Rutkoski, T. J. and Raines, R. T. (2008). Evasion of ribonuclease inhibitor as a determinant of ribonuclease cytotoxicity. *Curr. Pharm. Biotechnol.* **9**, 185-199.

Rybak, S. M., Pearson, J. W., Fogler, W. E., Volker, K., Spence, S. E., Newton, D. L., Mikulski, S. M., Ardelt, W., Riggs, C. W., Kung, H. F. *et al.* (1996). Enhancement of vincristine cytotoxicity in drug-resistant cells by simultaneous treatment with onconase, an antitumor ribonuclease. *J. Natl. Cancer Inst.* **5**, 747-753.

Saxena, S. K., Sirdeshmukh, R., Ardelt, W., Mikulski, S. M., Shogen, K. and Youle, R. J. (2001). Entry into cells and selective degradation of tRNAs by a cytotoxic member of the RNase A family. *J. Biol. Chem.* **277**, 15142-15146.

Schmittgen, T. D. and Livak, K. J. (2008). Analyzing real-time PCR data by the comparative C_T method. *Nat. Methods* **3**, 1101-1108.

Schreier, A. A. and Baldwin, R. L. (1976). Concentration-dependent hydrogen exchange kinetics of ^{3}H-labeled S-peptide in ribonuclease S. *J. Mol. Biol.* **105**, 409-426.

Schreier, A. A. and Baldwin, R. L. (1977). Mechanism of dissociation of S-peptide from ribonuclease S. *Biochemistry* **16**, 4203-4209.

Scotto-Lavino, E., Du, G. and Frohman, M. A. (2007). 3' End cDNA amplification using classic RACE. *Nat. Protoc.* **1**, 2742-2743.

Sela, M., Anfinsen, C. B. and Harrington, W. F. (1957a). The correlation of ribonuclease activity with specific aspects of tertiary structure. *Biochim. Biophys. Acta* **26**, 502-512.

Sela, M., White, F. H., Jr. and Anfinsen, C. B. (1957b). Reductive cleavage of disulfide bridges in ribonuclease. *Science* **125**, 691-692.

Shaner, N. C., Steinback, P. A. and Tsien, R. Y. (2005). A guide to choosing fluorescent proteins. *Nat. Methods* **12**, 905-909.

Shogen, K. and Yoan, W. K. (1973). Antitumor activity in extracts of Leopard frog (*Rana pipiens*) embryos In *27th Annual Eastern Colleges Science Conference*. State College (PA).

Simonsen, A., Lippe, R., Christoforidis, S., Gaullier, J.-M., Brech, A., Callaghan, J., Toh, B.-H., Murphy, C., Zerial, M. and Stenmark, H. (1998). EEA1 links PI(3)K function to Rab5 regulation of endosome fusion. *Nature* **394**, 494-498.

Soellner, M. B., Nilsson, B. L. and Raines, R. T. (2006). Reaction mechanism and kinetics of the traceless Staudinger ligation. *J. Am. Chem. Soc.* **128**, 8820-8828.

Suchanek, M., Radzikowska, A. and Thielle, C. (2005). Photo-leucine and photo-methionine allow identification of protein-protein interactions in living cells. *Nat. Methods* **2**, 261-268.

Suhasini, A. N. and Sirdeshmukh, R. (2006). Transfer RNA cleavages by Onconase reveal unusual cleavage sites. *J. Biol. Chem.* **281**, 12201-12209.

TAMIR Biotechnologies, Inc. http://www.alfacell.com/press_release_archive.html. 22 July 2010

Taylor, H. C., Richardson, D. C., Richardson, J. S., Wlodawer, A., Komoriya, A. and Chaiken, I. M. (1981). "Active" conformation of an inactive semi-synthetic ribonuclease-S. *J. Mol. Biol.* **149**, 313-317.

Thompson, J. E., Kutateladze, T. G., Schuster, M. C., Venegas, F. D., Messmore, J. M. and Raines, R. T. (1995). Limits to catalysis by ribonuclease A. *Bioorg. Chem.* **23**, 471-481.

Thompson, J. E. and Raines, R. T. (1994). Value of general acid–base catalysis to ribonuclease A. *J. Am. Chem. Soc.* **116**, 5467-5468.

Thomson, J., Ratnaparkhi, G. S., Varadarajan, R., Sturtevant, J. M. and Richards, F. M. (1994). Thermodynamic and structural consequences of changing a sulfur atom to a methylene group in the M13Nle mutation in ribonuclease-S. *Biochemistry* **33**, 8687-8593.

Tsien, R. Y. (2009). Constructing and exploiting the fluorescent protein paintbox. *Angew. Chem. Int. Ed.* **48**, 5612-26.

Turcotte, R. F., Lavis, L. D. and Raines, R. T. (2009). Onconase cytotoxicity relies on the distribution of its positive charge. *FEBS J.* **276**, 4270-4281.

van de Waterbeemd, H. (2009). Physicochemical approaches to drug absorption. In *Drug Bioavailability: Estimation of Solubility, Permeability, Absorption, and Bioavailability, 2nd ed.*, (eds H. van de Waterbeemd H. Lennernas and P. Arturrson), pp. 71-100. Weinheim, Germany: Wiley–VHC.

Vasandani, V. M., Wu, Y.-N., Mikulski, S. M., Youle, R. J. and Sung, C. (1996). Molecular determinants in the plasma clearance and tissue distribution of ribonucleases of the ribonuclease A superfamily. *Cancer Res.* **56**, 4180-4186.

Velculescu, V. E., Madden, S. L., Zhang, L., Lash, A. E., Yu, J., Rago, C., Lal, A., Wang, C. J., Beaudry, G. A., Ciriello, K. M. *et al.* (1999). Analysis of human transcriptomes. *Nat. Genet.* **23**, 387-388.

Vereecke, L., Beyaert, R. and van Loo, G. (2009). The ubiquitin-editing enzyme A20 (TNFAIP3) is a central regulator of immunopathology. *Trends Immunol* **30**, 383-391.

Walsh, C. E. and Yang, Y. (2005). Spliceosome-mediated RNA *trans*-splicing. *Mol. Ther.* **12**, 1006-1012.

Wang, Z. and Burge, C. B. (2008). Splicing regulation: From a parts list of regulatory elements to an integrated splicing code. *RNA* **14**, 802-813.

Wang, Z., Gerstein, M. and Snyder, M. (2009). RNA-Seq: a revolutionary tool for transcriptomics. *Nature Rev. Genet.* **10**, 57-63.

Welker, E., Hathaway, L., Xu, G., Narayan, M., Pradeep, L., Shin, H. C. and Scheraga, H. A. (2007). Oxidative folding and N-terminal cyclization of onconase. *Biochemistry* **46**, 5485-5493.

Winkler, J., Urban, E., Losert, D., Wacheck, V., Pehamberger, H. and Noe, C. R. (2004). A novel concept for ligand attachment to oligonucleotides via a 2'-succinyl linker. *Nucleic Acids Res.* **32**, 710-718.

Wu, Y., Mikulski, S. M., Ardelt, W., Rybak, S. M. and Youle, R. J. (1993). A cytotoxic ribonuclease. *J. Biol. Chem.* **268**, 10686-10693.

Wyckoff, H. W., Hardman, K. D., Allewell, N. M., Inagami, T., Johnson, L. N. and Richards, F. M. (1967a). The structure of ribonuclease-S at 3.5 Å resolution. *J. Biol. Chem.* **242**, 3984-3988.

Wyckoff, H. W., Hardman, K. D., Allewell, N. M., Inagami, T., Tsernoglou, D., Johnson, L. N. and Richards, F. M. (1967b). The structure of ribonuclease-S at 6 Å resolution. *J. Biol. Chem.* **242**, 3749-3753.

Yatzeck, M. M., Lavis, L. D., Chao, T. Y., Chandran, S. S. and Raines, R. T. (2008). A highly sensitive fluorogenic probe for cytochrome P450 activity in live cells. *Bioorg. Med. Chem. Lett.* **18**, 5864-5866.

Youle, R. J. and D'Alessio, G. (1997). Antitumor RNases. In *Ribonucleases: Structures and Functions*, (eds G. D'Alessio and J. F. Riordan), pp. 491-514. New York: Academic Press.

Zaikova, T. O., Rukavishnikov, A. V., Birrell, G. B., Griffith, O. H. and Keana, J. F. W. (2001). Synthesis of fluorogenic substrates for continuous assay of phosphatidylinositol-specific phospholipase C. *Bioconjug. Chem.* **12**, 307-313.

Zhao, H., Ardelt, B., Ardelt, W., Shogen, K. and Darzynkiewicz, Z. (2008). The cytotoxic ribonuclease onconase targets RNA interference (siRNA). *Cell Cycle* **7**, 3258-3261.

Zheng, X. L., Kitamoto, Y. and Sadler, J. E. (2009). Enteropeptidase, a type II transmembrane serine protease. *Front. Biosci.* **E1**, 242-249.

Zuckermann, R. N. and Schultz, P. G. (1988). A hybrid sequence-selective ribonuclease S. *J. Am. Chem. Soc.* **110**, 6592-6594.